QUAD-RIDGE HORN ANTENNA WITH ELLIPTICALLY SHAPED SIDEWALLS FOR USE AS A REFLECTOR FEED FOR RADIO ASTRONOMY

by

Ockert Botha Jacobs

Submitted in partial fulfilment of the requirements for the degree

Master of Engineering (Electronic Engineering)

in the

Department of Electrical, Electronic and Computer Engineering
Faculty of Engineering, the Built Environment and Information Technology

UNIVERSITY OF PRETORIA

September 2011

SUMMARY

QUAD-RIDGE HORN ANTENNA WITH ELLIPTICALLY SHAPED SIDEWALLS FOR USE AS A REFLECTOR FEED FOR RADIO ASTRONOMY

by

Ockert Botha Jacobs

Supervisor:	Prof J.W. Odendaal
Co-Supervisor:	Prof J. Joubert
Department:	Electrical, Electronic and Computer Engineering
University:	University of Pretoria
Degree:	Master of Engineering (Electronic Engineering)
Keywords:	Quad-ridge horn antenna, dual polarization, radio astronomy, reflector antenna feed, method of moments, wideband.

Reflector antennas used for radio astronomy require feeds that use the reflector surface as efficiently as possible while maintaining low noise levels. The specifications of new radio astronomy telescopes under development such as MeerKAT and the square kilometre array calls for feeds that have wide frequency bandwidths. The antennas traditionally used as reflector feeds, corrugated horns, are incapable of achieving the required bandwidth. Thus new feeds have to be developed that are capable of achieving high efficiencies and low noise over a large frequency bandwidth.

A quad-ridge horn antenna is developed that is more suitable for use as a reflector feed antenna. Quad-ridge horn antennas are dual-polarized and can obtain wide bandwidths. A disadvantage of using a quad-ridge horn as a reflector feed is that the radiation pattern changes as a function of frequency. The geometry of the quad-ridge horn antenna is investigated to determine which features of the antenna can be used to control the radiation pattern. The use of elliptically shaped sidewalls is proposed. Elliptically shaped sidewall quad-ridge horn antennas are shown to have improved radiation patterns that are more constant as a function of frequency compared to conventional quad-ridge horn antennas. A prototype of such an antenna, with the design based on the results of the parametric study, is presented. The antenna is well matched to the source and has excellent radiation patterns over a wide bandwidth. Good agreement between measured and simulated results is obtained.

OPSOMMING

KWAD-RIF HORING ANTENNE MET ELLIPTIES-GEVORMDE SYWANDE VIR GEBRUIK AS ‘N REFLEKTOR VOER IN RADIO-ASTRONOMIE

deur

Ockert Botha Jacobs

Promotor:	Prof J.W. Odendaal
Mede-promotor:	Prof J. Joubert
Departement:	Elektriese, Elektroniese en Rekenaar Ingenieurswese
Universiteit:	Universiteit van Pretoria
Graad:	Meestersgraad in Ingenieurswese (Elektroniese Ingenieurswese)
Sleutelwoorde:	Kwad-rif horing-antenna, dubbele polarisasie, radio-astronomie, reflektor-antenna voer, metode van momente, wyeband.

Voer-antennas vir radio-astronomie reflektor-antennas moet die reflektor-oppervlak optimaal benut en lae ruisvlakke handhaaf. Nuwe radio-astronomie teleskope wat tans ontwikkel word, soos die MeerKAT en die SKA, benodig voer-antennas wat oor breë bandwydtes funksioneer. Die voer-antenna wat tradisioneel gebruik word, die geriffelde horing-antenne, kan nie oor sulke groot bandwydtes funksioneer nie. Breë bandwydte voer-antennes wat die oppervlakte van die reflektor optimaal benut en lae ruisvlakke handhaaf, moet dus ontwikkel word.

‘n Kwad-rif horing-antenne word ontwikkel wat meer geskik is as ‘n reflektor voer-antenna. Kwad-rif horing-antennas is dubbel-gepolariseer en kan oor groot bandwydtes funksioneer. ‘n Nadeel van kwad-rif horing-antennas is dat die stralingspatroon as ‘n funksie van frekwensie verander. Die geometrie van die antenna word parametries ondersoek om vas te stel watter onderdele van die antenna gebruik kan word om die stralingspatroon te beheer. Die gebruik van sywande wat ellipties gevorm is, word voorgestel. Dit word gedemonstreer dat antennas met ellipties-gevormde sywande stralingspatrone het wat minder varieer as ‘n funksie van frekwensie as konvensionele kwad-rif horing antennas. ‘n Prototipe met ‘n ontwerp wat gegrond is op die resultate van die parametriese studie, word voorgelê. Die prototipe is goed aangepas en het baie goeie stralingspatrone oor ‘n breë bandwydte. Gesimuleerde en gemete resultate van die antenna stem goed ooreen.

ACKNOWLEDGEMENT

I would like to acknowledge the support of the EMSS group, not only did they provide me with financial support but also gave me valuable opportunities to learn during time spent at EMSS Antennas, EMSS-SA, EMSS Consulting and Antenna Magus.

I am grateful to my supervisors, Prof. J.W. Odendaal and Prof. J. Joubert, for all the guidance and the opportunities they created. I would also like to thank Mr. L. Naude of the Compact Antennna Test Range.

My family and parents supported and encouraged me throughout. I want to especially thank my brother for his help, support and valuable advice.

I thank the Lord for the opportunity and ability to complete this work.

TABLE OF CONTENTS

1. INTRODUCTION

1.1 Background and motivation

The Square Kilometre Array (SKA) is an international project that aims at developing an imaging radio telescope 50 times more sensitive than its predecessors [1]. This enhanced sensitivity will be used to observe further back in time than previously possible. The instrument will enable the investigation of scientific questions that will enhance our understanding of the universe.

The development of the SKA presents a wide range of challenges and achieving this level of sensitivity requires the development of new technology. Reflector antennas are typically used for radio astronomy at higher frequencies. Parabolic reflector antennas can operate over an extremely wide frequency band, being limited in operation at the low frequency end by the size of the reflector and at the high frequency end by the accuracy with which the reflector surface can be constructed [2]. The reflector antenna performance is determined mainly by the performance of the feed antenna that is used [3].

A typical feed antenna used for radio astronomy is the hybrid mode horn (corrugated horns are commonly used). These antennas can achieve very high sensitivity, but have limited frequency bandwidths [2], are difficult to manufacture (especially at higher frequencies) and tend to be very heavy. A reflector telescope typically employs a number of frequency scaled versions of these horns to cover the total frequency band of the system [4]. As a large number of feed horns have to be used, the cost of the instrument is increased. In addition the telescope can be used to observe only a limited band of frequencies at a time due to the limited bandwidth of the feed antennas. This increases the time required for broadband observations. The SKA aims at using antennas with wider bandwidths thereby reducing the number of feed antennas required. This can not only reduce the cost of the instrument, but also make it more suitable for experiments that require the simultaneous observation of multiple frequencies. Wide band feeds also allow the observation of short pulses.

The development of a wideband feed capable of achieving high sensitivity has thus been a very active field of research. Although many wideband antennas exist, the requirements of radio astronomy make many of these antenna types unsuitable. One of the most important

specifications for the SKA is that the antenna be dual-polarized. Other important considerations include a return loss better than 15 dB [2], very low insertion losses (a loss of 0.1 dB can increase the system noise by approximately 6 K [5]), good isolation between the two polarizations and low cross-polarization. The use of a reflector antenna imposes additional constraints, specifically achieving the highest possible efficiency while limiting the spill-over noise temperature. As the goal of the SKA is to achieve a specified sensitivity (effective collection surface divided by system noise figure) achieving greater efficiency and reducing noise for a single telescope significantly reduces the cost of the project as fewer telescopes are required. These requirements are discussed in detail in Chapter 2.

Wideband feeds that have been proposed for radio astronomy include a non-planar log periodic antenna that is used for the Allen Telescope Array (ATA) [5, 6], the Eleven antenna which is an arrangement of stacked folded dipoles above a ground plane [7 – 10], a similar Quasi Self-Complementary (QSC) antenna which is a log periodic array above a ground plane [11 – 13] and modified quad-ridge horn antennas [14, 15].

All the above antennas have strengths and weaknesses with regard to achieving the specifications. The non-planar log periodic antenna is a frequency independent antenna and has a wide bandwidth and good radiation pattern stability [5, 16]. The main disadvantage of this type of antenna is movement of the phase centre as a function of frequency [17]. This causes defocusing loss if used in a reflector antenna. The Eleven and QSC antenna solved the shifting phase centre by the addition of a ground plane [7] – which made the antenna difficult to match [10]. The Eleven and QSC antennas are also difficult to manufacture. Current commercial quad-ridge horn antennas have not been designed to operate as radio astronomy antennas and are thus not adequately matched [18]. These quad-ridge horn designs often opt to achieve much larger frequency bandwidths, typically at the expense of low frequency matching. Quad-ridge Ortho-Mode Transducers (OMTs) have seen extensive use for radio astronomy applications and have demonstrated that transitions between coaxial line to quad-ridge waveguide can achieve low return loss, good isolation between ports and low insertion loss [19]. A problem associated with quad-ridge horn antennas is that the radiation pattern changes as a function of frequency [18, 20]. Quad-ridge horns are aperture antennas – as the frequency increases, the size of the aperture in wavelengths increases, reducing the beamwidth [21, 22]. This is also observed

as an increase in boresight gain as a function of frequency. The smaller beamwidths at higher frequencies result in reduced aperture efficiency when used as a feed for reflector antennas.

Given the advantages and disadvantages of these feed antennas it was decided to develop a quad-ridge horn antenna, to obtain a feed more suitable to radio astronomy. Comparison of current commercial quad-ridge horn antennas to results achieved using OMTs in radio astronomy indicated that the feed section of quad-ridge horn antennas could be made suitable for radio astronomy. The aspect of the antenna performance that was of greatest concern was the radiation pattern of the antenna. Little work has been done on this aspect of the antenna's performance. Studies on quad-ridge horns typically focus on improving the impedance bandwidth of the antenna or on preventing the occurrence of higher order modes at higher frequencies.

Studies that aimed at improving the radiation patterns have used resistive cards to obtain greater pattern symmetry and reduced side lobes [22]. This is not an option for radio astronomy as this will increase loss which will result in increased system noise temperature – or by using a dielectric lens to improve efficiency [23] which cannot improve the frequency variation of the patterns. A shaped waveguide horn antenna that has radiation patterns that are to a large extent frequency independent has been demonstrated [24]. Applying this principle to quad-ridge horns could offer a method to improve the radiation patterns of this antenna type.

The antenna will be investigated with the aim of achieving a bandwidth of at least 4:1. The antenna is intended as an incremental development towards a feed capable of being used for the MeerKAT antenna array. The current specifications of the MeerKAT array calls for a bandwidth of 5:1 (500 MHz to 2.5 GHz) with later possible extension to a bandwidth of more than 10:1 (700 MHz to 10 GHz) [25]. The specifications relevant to the feed antenna are shown in Table 1.1 [25].

Table 1.1. The current MeerKAT reference design specifications and possible alternative specifications.

Specification	Current	Alternative
Lower Frequency	500 MHz	700 MHz
Upper Frequency	2.5 GHz	10 GHz
Optical Configuration	Symmetric prime focus	Offset or symmetric Gregorian
Aperture Efficiency	0.7	0.7
T_{sys} (K)	30 K	25 K
Polarization Isolation	20 dB	25 dB

1.2 Scope and objectives

This study will focus on developing a quad-ridge horn antenna with the objective of obtaining a wideband reflector feed suitable for radio astronomy. The development thus has to take into account radio astronomy as well as reflector feed antenna considerations. The specific objectives of the study are detailed in the points that follow.

- A primary objective is to develop an accurate numerical model to predict the performance of quad-ridge horn antennas. The appropriate numerical analysis technique will be selected based on the geometry and composition of quad-ridge horn antennas. The numerical model will be validated by comparing measured and simulated results.
- A parametric study of the numerical model will be used to identify parameters of the quad-ridge horn antenna that primarily affect the beamwidth. Parameters with a large effect on the beamwidth will be investigated further with the objective of determining whether these parameters can be used to improve the radiation patterns. The range of beamwidths that can be achieved will be investigated. Parameters that have little effect on the radiation pattern of the antenna will also be investigated to ensure adequate return loss, low insertion loss and low coupling between orthogonal polarizations.
- A major objective is the design and implementation of a prototype quad-ridge horn antenna with improved radiation patterns. The prototype radiation and impedance characteristics will be measured. The measured results of the prototype will also be used to validate the numerical model. The performance of the antenna when used as a feed for a reflector will be comprehensively evaluated. Other aspects of the

antenna performance, such as conductive loss, will be evaluated to determine whether the antenna would be suitable for use in radio astronomy.

1.3 Original contribution

The original contribution of the study lies in attempting to overcome the disadvantages of a quad-ridge horn antenna when used as a reflector antenna feed for radio astronomy applications. Important contributions are listed below.

- A parametric study is presented that identifies features of a quad-ridge horn antenna that affect the radiation pattern and how these features can be manipulated to obtain radiation patterns more suited for radio astronomy reflector antenna feeds. Previous studies on quad-ridge horns have mainly focussed on extending the impedance bandwidth of the antenna with little regard to the radiation patterns.
- A quad-ridge horn antenna with elliptically shaped sidewalls is proposed as a reflector antenna feed. Elliptically shaped sidewall quad-ridge horn antennas are compared to conventional quad-ridge horn antennas and are shown to have radiation patterns that are more constant with frequency, closer to being rotationally symmetrical and with lower side lobes. Such a comparison was the subject of a paper published by the author [26]. This type of antenna is analysed to determine the range of beamwidths that can be obtained. A simple design approach is presented that allows these antennas to be designed for a wide range of beamwidths.
- The performance of the quad-ridge horn antenna with elliptically shaped sidewalls is comprehensively evaluated. Existing studies on quad-ridge horns neglect various performance measures that are of importance in radio astronomy and reflector antennas. The performance measures that are most often neglected are the phase centre variation, the conductive loss and cross-polarization in the 45° plane. These are all calculated and presented. Efficiencies of the antenna when used as a reflector antenna feed are also presented. This gives a clear indication of the performance that can be expected of the antenna when used as a reflector antenna feed as well as highlighting possible shortcomings of the feed in its current form.

1.4 Overview of the dissertation

This chapter provided some brief background information, listed the scope and objectives of the study and presented the original contribution made by the study. The rest of the dissertation is organized as indicated below:

Chapter 2 presents background on radio astronomy, reflector antennas and reflector antenna feeds that are typically used. The specifications for an antenna arising from radio astronomy requirements are discussed, which revolve primarily around maximising efficiency while minimising system noise. Reflector feed antenna requirements are also discussed. As a reflector antenna with maximum aperture efficiency over a wide frequency band is required, a feed antenna pattern with a constant beamwidth and sharp cut-off beyond the dish edge would be necessary. The reflector feed antennas that have been used in the past are discussed as well as more recent attempts at wide band feed antennas. The quad-ridge horn antenna is identified as a possible candidate for a wide band feed.

Chapter 3 discusses existing methods for analysing quad-ridge horn antennas. Method of Moments (MoM) is identified as being suitable for analysis of the antenna. The quad-ridge horn antenna is discussed. The antenna is divided into two sections, the coaxial-to-waveguide transition and the waveguide to free-space transition. The implementation of each part of the two sections in the commercial MoM code FEKO is discussed.

Chapter 4 presents a parametric investigation of the geometry features of a quad-ridge horn antenna. The investigation focuses on identifying the geometry features that primarily affect the radiation pattern of the antenna. A quad-ridge antenna is investigated to determine how the impedance characteristics of the antenna can be improved and the radiation patterns manipulated to yield patterns more suitable for feeding a reflector antenna. Elliptically shaped sidewall quad-ridge horn antennas are shown to have reasonably constant radiation patterns and that the antenna can be designed for a wide range of beamwidth levels.

Chapter 5 details the design of a quad-ridge horn antenna for a specific reflector antenna requirement. The design is based on the information obtained from the parametric study. The electromagnetic design of the antenna to obtain the specified beamwidth and

impedance specifications is discussed. The mechanical implementation of the antenna design is presented.

Chapter 6 presents the performance evaluation of the prototype antenna. Measured and simulated results are compared to validate the simulated results. Deviations between measured and simulated results are investigated. Measured results of interest are presented and include the reflection and transmission S-parameters, the coupling between ports, principal as well as 45° plane radiation patterns both co- and cross-polarization, boresight gain and measured beamwidths. Some performance measures are estimated from simulated results, such as conductive loss. The performance of the antenna in a sample prime-focus reflector antenna system is evaluated. The position of the phase centre is calculated.

Chapter 7 concludes the dissertation. The chapter includes a short summary of the contribution made as well as suggestions for future work and improvements to this type of antenna.

2. BACKGROUND OF RADIO ASTRONOMY REFLECTOR FEED ANTENNA DEVELOPMENT

2.1 Introduction

In 1932 Karl Jansky was attempting to determine the source of noise experienced on transatlantic radio telecommunication circuits when he observed faint noise that seemed to emanate from the direction of the Milky Way [27]. This marked the first time radio signals from a non-terrestrial origin could be discerned from background noise. Attempts had been made before Jansky's discovery to detect radio signals of extra-terrestrial origin, specifically from the sun, but had failed due to receiver systems that were not sensitive enough [28]. This highlights that radio astronomy is driven by advances in technology. Before 1932 the state of technology was not sufficiently advanced and observations of faint radio signals failed due to receivers lacking the necessary sensitivity.

Jansky did not continue his observations and the first observations targeted solely at the radio sky were done by Grote Reber. Reber built a 9.45 m diameter parabolic reflector antenna for his observations [28, 29]. The parabolic reflector antenna has since become one of the antenna types that is most associated with radio astronomy. Only after the Second World War did radio astronomy truly come of age. The remarkable advances in microwave technology as well as the abundance of surplus wartime equipment enabled astronomers to make observations of increasing accuracy that led to discoveries of astronomical phenomena that were previously hidden to optical astronomy.

Higher sensitivity can be obtained by having a larger antenna aperture area and utilising the aperture more effectively. The size of a single large reflector is limited by practical considerations. The largest reflector that has been constructed thus far is the 305 m spherical dish at Arecibo [27, 28]. Concepts for radio telescopes under development utilise an array of a large number of smaller parabolic reflector to obtain large collection areas [25]. The large number of smaller antennas has the ability to resolve the position of a given radio source with greater accuracy as their ability to resolve different sources is determined by the distance between them. The technique used is called interferometry. This has been the approach most often used in the recent past as it is much more cost effective compared

to a single large reflector antenna. Examples of such antenna arrays are the Allen Telescope Array (ATA) and the Very Large Array (VLA) [6].

The project that has been driving the recent development of the technology behind radio astronomy will also use the array approach to obtain a radio astronomy antenna that has an effective collecting surface of one square kilometre. This project is aptly named the Square Kilometre Array (SKA) and aims at improving on the sensitivity of the best current radio telescope by a factor of 50 [1]. Such a large improvement requires the collection area of the antenna to be increased as well as an improvement in the individual antennas. One of the critical aspects of this technological development is the reflector feed antenna.

In the sections that follow the requirements of radio astronomy antennas and reflector feed antennas will be discussed. Commonly used radio astronomy reflector antennas are mentioned. A discussion of wideband feeds that have recently been developed is presented. The advantages and disadvantage of these wideband feed antennas are compared.

2.2 Radio astronomy

Knowledge of the characteristics required from a radio astronomy antenna is necessary for the antenna development. The most important metric used to characterize radio astronomy antennas is the A_{eff}/T_{sys} factor. This is a measure of the sensitivity of the radio telescope and should be as high as possible. A_{eff} defines the effective collection surface of the antenna while T_{sys} represents the noise present in the system. Other important considerations include the polarization of the antenna, the side lobe level and of increasing importance, the frequency bandwidth of the antenna-receiver system.

2.2.1 Interpreting A_{eff}/T_{sys}

The effective area of an aperture type antenna (A_{eff}) is related to the size of the physical aperture by the antenna efficiency (η_{ant}) [30].

$$\eta_{ant} = \frac{A_{eff}}{A_p} \tag{2.1}$$

The aperture efficiency (η_{ap}) is the ratio between the maximum directivity (D) of the antenna and the standard directivity (D_{std}), where the standard directivity is the maximum directivity possible for a given physical aperture. This ratio can typically be related to the physical aperture using the relations below (provided the aperture is large enough in terms of wavelength) ─

$$D_{std} = \frac{4\pi}{\lambda^2} A_p \tag{2.2}$$

$$\eta_{ap} = \frac{D}{D_{std}} \tag{2.3}$$

where A_p is the physical aperture area and λ the wavelength [30]. The difference between the aperture and antenna efficiency is the radiation efficiency which can be defined as the ratio of the total power radiated by the antenna to the power accepted by the antenna from an input – this is the ratio between the directivity and the gain [30]. Including the radiation efficiency in the aperture efficiency gives a relation between the gain of an antenna and the effective area as shown below.

$$\eta_{ant} = \eta_{ap} \times \eta_{rad} \tag{2.4}$$

$$G = \eta_{rad} \times D = \eta_{ant} \frac{4\pi}{\lambda^2} A_p \tag{2.5}$$

Using equations 2.1 and 2.5 the effective area of the telescope can thus be determined from the gain of the system. Maximizing the gain of a reflector antenna also maximizes the effective area. It should be noted that the terms used here, such as aperture- or antenna efficiency are often used by authors to represent different quantities. The IEEE definitions were used for these efficiencies. As authors often uses these terms to denote other efficiencies the calculation of efficiency factors will be preceded by a discussion as to the definition of the efficiency calculated as well as its significance in terms of reflector performance.

The system noise temperature (T_{sys}) represents the equivalent noise introduced into the entire system. Some of the main contributors are the receiver and the antenna noise temperatures. The noise temperature can be reduced by cooling the receiver to cryogenic temperatures. This reduces the thermal noise introduced by the Low Noise Amplifiers

(LNA) and transmission lines. Transmission line loss can be quantified as noise temperature. The noise power is expressed as an equivalent noise temperature. A line with a loss of 0.1 dB contributes approximately 6-7 K noise [5, 31]. Low conductive losses for the antenna are essential to reduce the noise contribution. As the system noise temperature goal at higher frequencies can be as low as 30 K, transmission line loss can be a major contributor to system noise if adequate care is not taken to reduce the length and loss of transmission lines. The input reflection coefficient should be at least -15 dB with -20 dB preferable [2] to reduce losses due to mismatch.

The antenna also contributes to the noise temperature. All objects with temperatures that are above absolute zero radiate noise. The equivalent antenna temperature can be defined as the temperature the antenna radiation resistance has to be raised to, to produce the same noise power as the antenna. If the antenna is in a perfectly absorbing cavity (a blackbody) the noise temperature of the antenna is equal to the temperature of the cavity [3, 28].

The area that the antenna observes, influences the noise temperature of the antenna. The noise temperature of the sky is typically very low (especially above 250 MHz) and can be in the order of a few Kelvins rising to between 100 to 150 K at the horizon while the noise temperature of the ground can be approximated by an average noise temperature of 300 K [32]. Pointing the feed antenna towards an object with a high noise temperature can introduce unacceptably high levels of noise into the receiver system. Preventing the antenna from radiating towards the ground is thus an important consideration to reduce overall system noise. In addition radar absorbent materials at room temperature cannot be used in radio astronomy antenna design as it could contribute significantly to the antenna noise temperature. The noise temperature of an antenna can be determined as below [32]

$$T_A = \frac{\int_0^{2\pi}\int_0^{\pi} T_B(\theta,\phi)G(\theta,\phi)sin\theta d\theta d\phi}{\int_0^{2\pi}\int_0^{\pi} G(\theta,\phi)sin\theta d\theta d\phi} \tag{2.6}$$

where T_A is the antenna temperature, G the power pattern and T_B the observed brightness temperature. The pattern of the antenna multiplied by the brightness distribution is integrated over a full solid angle and divided by the integral of the pattern over a full solid angle to obtain the noise temperature.

2.2.2 Effect of side lobes

An ideal directive antenna pattern would radiate solely in a narrow beam with no radiation elsewhere. Unfortunately this is not the case for practical antennas [28]. The radiation patterns of practical antennas often have side lobes. Low side lobes are crucial to radio astronomy applications. The presence of side lobes make it difficult to accurately measure small radio sources close to large sources. The side lobes introduce ambiguity as to which source is observed. Another scenario, in which side lobes can interfere with measurements, is if a source is being tracked across the sky. The signals from weak sources often have to be integrated over extended periods of time to obtain a signal discernible from the noise (the noise is a zero mean signal). The side lobes can introduce error signals as the source is tracked across the sky that might not necessarily be zero mean. Signals emanating from communication satellites can be avoided with the main beam, but might be picked up by side lobes.

2.2.3 Polarization

Some sources of radiation observed are often said to be un-polarized, or randomly polarized, and the orthogonal polarizations are not correlated (such as thermal radiation). If such a source is observed by a linearly polarized antenna only half the power (in a time average sense) is received. Other sources of interest are polarized and their orthogonal polarizations are statistically correlated. Characterizing the polarization of such a source requires a dual polarized antenna. One of the key science projects that require dual polarization is the study of magnetic fields, where a magnetic field alters the polarization of an electromagnetic wave passing through it. Study of this phenomenon requires that the polarization of the wave be known accurately [1]. Characterisation of the polarization of weak sources thus requires dual polarized antennas to have good polarization purity [28].

2.2.4 Frequency bandwidth

Initial radio astronomy observations were made at a single frequency to simplify the development of receivers and amplifiers. As receiver and antenna technology improved later telescopes employed antennas with larger bandwidths. This enabled more observations to be made in a smaller space of time. Observation over very large bandwidths requires a number of feeds, each of which can cover only a portion of the

spectrum to be observed. This increases the time required for observations. Recent development focussed on creating feeds that operate over even larger bandwidths in an attempt to minimize the number of antennas required and increase the speed of observations [6].

2.3 Reflector antennas

Reflector antennas are typically used for radio astronomy applications due to the high gain that can be achieved with these antennas. There are various types of reflector antennas with the most prominent being the parabolic reflector. Parabolic reflector antennas produce a pencil beam (very high gain) with low side lobes and good cross-polarization [33], all of which are desirable for radio astronomy applications.

If a plane wave is incident on the parabolic reflector surface the wave will be reflected to a single point named the focus point. A parabolic dish can be completely defined by the diameter of the dish and the position of the focal point.

There are various types of parabolic antennas, the most common being the prime focus, Cassegrain and Gregorian configurations (the other configurations can be represented as an equivalent prime focus configuration [3, 32 34]). A prime focus has the antenna feed located at the focal point of the parabolic reflector A Cassegrain has a hyperboloid sub reflector close to the focus point that allows the feed to be positioned at the base of the main reflector while the Gregorian has an ellipsoidal sub reflector [32]. Offset Gregorian configurations are also used, specifically for the ATA array [6] and for more recent reference designs for the MeerKAT [25].

If placed at the focal point of the reflector the antenna and the struts that support it will block some of the antenna collection surface. This is called blockage and can be calculated as a percentage of the surface that is obscured. Reducing the amount of blockage results in a more efficient utilization of the reflector surface area and can reduce side lobes [33]. Feed antennas thus have to be small and have a low weight to enable the use of smaller supporting struts. The accessibility of the receiver also factors into the choice of reflector configuration. Prime focus reflector antennas have an antenna mounting point that is difficult to reach. Antenna maintenance and replacement would thus be much more

difficult. This becomes an important consideration if the receiver is cooled, as cryogenically cooled receivers require frequent maintenance. The feed mounting point of Cassegrain antennas are much more accessible.

The different geometries have advantages and disadvantages that have to be traded off against each other [32]. The design of the KAT-7 [35] and the initial design for the MeerKAT both employed prime focus configurations although later MeerKAT designs calls for offset Gregorian configurations which reduce blockage. As this reference design is not completed and subject to change, this study was not based on a specific configuration. As all configurations can be reasonably accurately approximated by an equivalent prime focus feed [34] the basic principles of designing for a prime focus antenna feed were used.

2.3.1 Frequency bandwidth

Reflectors function over frequency ranges that are only determined by their size (low frequency limit) and the accuracy with which the surface can be manufactured (upper frequency limit). As such the limiting factor for the bandwidth of the antenna is the bandwidth of the feed [2].

2.3.2 Polarization

The reflector can contribute to the cross-polarization of the antenna. The contribution of the reflector is a maximum in the 45° planes and a minimum in principal planes [3]. The shape of the reflector also influences the amount of cross-polarization – a shallow reflector with a large F/D ratio results in reduced cross-polarization. A commonly used maximum peak level for cross-polarization is -30 dB [3], although in some cases a level of -20 dB can also be acceptable [2]. The feed antenna typically contributes a great deal more to cross-polarization than the reflector.

2.3.3 Edge taper

The ideal reflector feed antenna would illuminate only up to the edge of the reflector and nowhere else. Such a source cannot be realised and has to be approximated by physical

sources. An important parameter of the feed antenna is the edge taper. The feed taper is defined as how much the radiation pattern has fallen from the boresight value to the value at the edge of the reflector. The edge taper includes the spherical spreading loss. The distance from the focal point to the reflector is greater at the edge of the reflector than at the centre, leading to additional spreading loss [3, 33]. The difference in these distances is determined by the F/D ratio of the parabolic reflector. The edge taper is determined by [3]:

$$ET = -20\,log\left[G_f(\theta_0)\right] - 20log\left[\frac{1+cos\theta_0}{2}\right] \tag{2.7}$$

θ_0 is the reflector half angle (determined from the F/D ratio of the reflector) and G_f the normalized feed pattern. Figure 2.1 shows a parabolic reflector and how a plane wave incident on the aperture plane is focussed to a single point, the feed taper is also indicated on a radiation pattern.

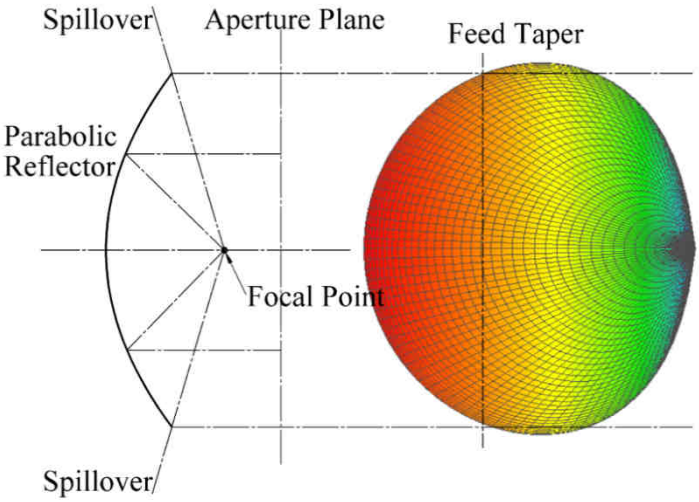

Figure 2.1. A parabolic reflector and a radiation pattern, indicating the effect of the radiation pattern on spill-over and aperture taper efficiency.

Efficient use of the reflector requires a uniform illumination across the surface, a wide radiation pattern with a low edge taper is ideal (high edge illumination). This is at odds with the reduction of spill-over which requires as little as possible radiation past the edges of the reflector, to reduce spill-over a narrow radiation pattern with a high edge taper is required [32]. Spill-over is especially bad for radio astronomy applications as it increases the system noise temperature due to radiation past the dish edge picking up noise from the ground [33]. This results in a compromise between the efficient use of the surface,

quantified by the illumination efficiency and the amount of spill-over that can be tolerated before too much noise is introduced into the system. The edge taper represents this compromise and is typically between 10 and 15 dB [32, 33].

2.3.4 Reflector antenna efficiencies

The efficiency of the feed of a reflector antenna system is often split into a number of sub-efficiencies. The antenna, radiation and aperture efficiency has already been mentioned. As the use of terms denoting efficiency is often not consistent, the efficiencies are defined in detail below.

One method often used to calculate reflector antenna efficiencies is to only use the principal plane patterns of the feed antenna and to assume the pattern is rotationally symmetric (or occasionally the pattern in the 45° plane). This simplification results in simpler equations (integration over only a single dimension is required) and is often necessary as radiation patterns are typically measured only in the principal planes [36] – as measuring three dimensional patterns are time-consuming and expensive. This approach can be inaccurate for patterns that are not perfectly rotationally symmetric. Furthermore the cross-polarization in the principal planes is often the minimum cross-polarization which can result in cross-polarization efficiency being under-estimated. Due to this, both the principal plane approach and the full 3D integrals will be considered and compared. Although full 3D radiation patterns are not often available for measured results electromagnetic simulation allows these patterns to be calculated accurately. The efficiency factors discussed in this section include spill-over, polarization, taper, phase and the combination of these factors, aperture efficiency.

Although the edge taper provides a convenient value for expressing the level of spill-over that can be tolerated, it can also be misleading. A radiation pattern with very large side lobes, or shoulders, just past the dish edge can result in a great deal more spill-over than expected for a given edge taper. A sharp drop in radiation past the dish edge is thus required. The spill-over efficiency can be calculated by dividing the power illuminating the reflecting surface by the power of the total field radiated by the feed antenna as shown below [30, 33, 36].

$$\eta_s = \frac{\int_0^{2\pi}\int_0^{\theta_0}(|F_{co}(\theta,\phi)|^2 + |F_{cross}(\theta,\phi)|^2)sin\theta d\theta d\phi}{\int_0^{2\pi}\int_0^{\pi}(|F_{co}(\theta,\phi)|^2 + |F_{cross}(\theta,\phi)|^2)sin\theta d\theta d\phi} \quad (2.8)$$

The integration is with respect to the feed antenna pattern axes (in other words at the focal point), F_{co} denotes the co-polarization and F_{cross} the cross-polarization radiation pattern. The integral of the pattern incident on the reflector (integration only up to the edge of the reflector) is divided by the integral of the entire pattern.

The antenna spill-over noise temperature is another metric often used to describe spill-over. This can be determined by integrating the normalized power pattern with the observed source brightness (temperature) distribution. For spill-over noise temperature only the section of the pattern that does not intersect the reflector is considered [28]. The direction in which the reflector points can change and the amount of sky and earth the feed antenna would observe past the dish edge would thus vary. Typical brightness temperatures for various elevations of a reflector antenna have been determined and can be used to determine the antenna spill-over noise temperature [37]. An alternative approach is to use an approximation and assume a uniform brightness temperature with a temperature value reflecting an average value of the observed brightness distribution.

The polarization efficiency can be defined as the ratio between the power of the co-polar field incident on the reflector to the total power incident on the reflector, this is calculated as below [36]. It can be seen that the integration for the numerator and the denominator is done only up to the edge of the reflector.

$$\eta_{pol} = \frac{\int_0^{2\pi}\int_0^{\theta_0}(|F_{co}(\theta,\phi)|^2)sin\theta d\theta d\phi}{\int_0^{2\pi}\int_0^{\theta_0}(|F_{co}(\theta,\phi)|^2 + |F_{cross}(\theta,\phi)|^2)sin\theta d\theta d\phi} \quad (2.9)$$

The taper efficiency is a measure of how the amplitude taper of the feed pattern reduces the gain of the antenna compared to a uniform illumination. It is sometimes referred to as the illumination efficiency of the antenna [36] (although it should be noted that in [30] aperture efficiency and illumination efficiency are used interchangeably). The integral is derived from integration over the aperture of the reflector antenna where a coordinate transformation has been applied to allow the use of spherical coordinates.

$$\eta_t = \frac{16F^2}{\pi D^2}\left(\frac{\left(\int_0^{2\pi}\int_0^{\theta_0}|F_{co}(\theta,\phi)|tan\frac{\theta}{2}d\theta d\phi\right)^2}{\int_0^{2\pi}\int_0^{\theta_0}|F_{co}(\theta,\phi)|^2 sin\theta d\theta d\,\phi}\right) \tag{2.10}$$

Where D is the reflector diameter and F is the focal length, integration is again done only up to the reflector edge. The final efficiency factor is the phase efficiency. This efficiency depends on the position of the feed relative to the focal point of the antenna as well as the phase taper of the feed pattern. It is assumed that the feed can be accurately positioned on a line perpendicular to the aperture plane and coincident with the reflector centre. As the reflector is symmetric defocusing would be due to axial movements of the phase centre – towards or away from the reflector. The phase efficiency can then be calculated using the equation below.

$$\eta_p = \frac{\left|\int_0^{2\pi}\int_0^{\theta_0} F_{co}(\theta,\phi)tan\frac{\theta}{2}d\theta d\phi\right|^2}{\left(\int_0^{2\pi}\int_0^{\theta_0}|F_{co}(\theta,\phi)|tan\frac{\theta}{2}d\theta d\,\phi\right)^2} \tag{2.11}$$

These factors can be combined to give the aperture efficiency (also called the feed efficiency) [36], the feed efficiency can also be calculated directly:

$$\eta_{ap} = \eta_s\eta_{pol}\eta_t\eta_p = \frac{cot^2\left(\frac{\theta_0}{2}\right)}{\pi}\frac{\left|\int_0^{2\pi}\int_0^{\theta_0} F_{co}(\theta,\phi)tan\frac{\theta}{2}d\theta d\phi\right|^2}{\int_0^{2\pi}\int_0^{\pi}(|F_{co}(\theta,\phi)|^2+|F_{cross}(\theta,\phi)|^2)sin\theta d\theta d\phi} \tag{2.12}$$

If the radiation efficiency of the antenna can be calculated, the effective area of the antenna can be determined (although for a well-designed feed the radiation efficiency should be close to unity). This of course excludes such elements as aperture blockage due to the feed itself or supporting struts or the surface roughness of the reflecting surface. These are primarily effects due to the construction of the reflector itself and are not considered in this study (expect for the aperture size of the feed in a prime focus system contributing to aperture blockage and the weight of the antenna affecting the size of the struts required).

2.3.5 Rotationally symmetric pattern

Radiation patterns that are not rotationally symmetrical do not have equal edge tapers in all planes and can have greater spill-over in one plane than another if used in a symmetric reflector. Unbalanced principal plane patterns can also introduce additional cross-polarization [3]. A simple measure of the rotational symmetry of a radiation pattern can be obtained by comparing the principal plane patterns. If these are equal it is a good indication that the radiation pattern is rotationally symmetric.

2.3.6 Defocusing loss

Another important consideration arising from the need to use a reflector antenna is the reduction in gain due to phase errors as a result of defocusing. The phase efficiency has already been mentioned. This efficiency, however, has two components – the phase taper of the feed and the position of the phase centre of the feed. The situation where the phase centre is not located on the focal point of the reflector results in defocusing loss [32].

Positioning the phase centre of the antenna on the focal point of the reflector antenna mitigates the phase error due to defocusing. The phase centre of an antenna is a reference point from which the radiation seems to occur. If the phase of the radiation on a spherical surface is the same at all points on the sphere, the centre of the sphere is the phase centre. Essentially plotting the phase of the antenna against the angle of observation should yield a constant phase. A phase centre can approximately be identified for some types of feeds, most feeds, however, do not have a spherical phase front or the phase front can be approximated as spherical over only a limited solid angle.

A number of methods can be used to determine the location of a phase centre. One approach is to approximate the phase centre position as the point from which the phase is closest to being constant on a spherical surface, in a least squares sense [38]. As many antennas have phase patterns that are only locally spherical this is typically calculated over a limited solid angle. Other approaches are more suited to measurements and estimate the phase centre using graphical techniques such as plotting the phase against the cosine of the observation angle and using an estimate of the slope of the resulting plot to approximate the phase centre location [39].

Another, much more general, definition that will be used in this study, is that the phase centre is the point that minimizes the defocusing loss of the antenna [38]. This is especially appropriate for reflector antenna feeds and results in an unambiguous phase centre location that ensures maximum phase efficiency for a given reflector size.

Broadband antennas typically have some variation in the phase centre location as the frequency changes. If the variation is not severe the feed can likely be mounted for a phase centre near the centre of the band with little loss in efficiency. Some antennas, however, show significant phase centre variation as a function of frequency. This is especially true of structures such as log periodic dipole arrays or non-planar log periodic antennas [17] where the active region (the area from which the antenna appears to radiate) moves as a function of frequency [16]. If such an antenna is mounted at the focus point of a parabolic reflector defocusing loss will occur over some parts of the bandwidth. The ATA uses a linear focus actuator to position the antenna correctly depending on the frequency band being used [6], focussing the feed. This is not an optimal solution as the entire bandwidth of the antenna is not available for a single observation without significant defocusing loss at the band edges. An antenna with a phase centre that is fixed, or very nearly so, with frequency would be greatly preferable.

2.4 Reflector antenna feeds

2.4.1 Dipole antenna feeds

Some of the simplest antennas used for a reflector feed are variations of dipole antennas. A reflective ground plane is introduced just behind the dipole antenna (in the form of a circular metal disc) to produce a directional antenna. The resulting radiation pattern is not rotationally symmetrical and results in low aperture efficiency if used to feed a parabolic reflector.

The pattern can be improved by introducing a beam forming ring [40]. This results in higher aperture efficiency, low cross-polarization and reduced side lobes. If the reflector antenna is designed to resonate (resonance occurs between the reflector and the ground plane) the gain can also be improved [41]. This antenna has a convenient structure that is

easy to manufacture and the coaxial cable used to feed the antenna can also be used to support the structure, reducing blockage.

An alternative approach is to use two dipole antennas separated by half a wavelength and 0.15 wavelengths above the ground plane. The dipoles are excited by the same source (in phase) and produce a rotationally symmetrical radiation pattern [8]. Another advantage of this configuration is that the phase centre of the antenna is located on the ground plane. Both these antennas can be designed to be dual polarized. Unfortunately these antennas are limited in the bandwidth they can achieve by the requirement to use dipoles and can achieve a maximum bandwidth of only between 10 and 20%. This narrow band has limited the use of these antennas. The concepts these antennas are based on can be used to obtain improved antennas as has been done for the Eleven antenna [7] (also known as the Chalmers feed).

2.4.2 Horn antennas

Arguably the most widely used feed for radio astronomy reflector antennas is, however, the horn antenna [32]. Pyramidal (single polarization) or conical horns are used. Such horn antennas have high gain, very good pattern symmetry and can have low cross-polarization [32]. They cannot be used over a very broad bandwidth due to the fact that the antenna beamwidth decreases as a function of frequency [42]. In addition these antennas are usually fed by waveguides and have limited single mode (TE_{10} for pyramidal and TE_{11} for conical horns) bandwidth. Waveguides are limited to a relative bandwidth of less than 2:1 [43].

2.4.3 Corrugated horns

Hybrid mode horns have been developed to improve the cross-polarization, the aperture efficiency as well as the bandwidth of horn antennas and have been used widely for radio astronomy applications [3]. One type of hybrid mode horn is the conical corrugated horn.

The corrugations in the side of the horn enforce boundary conditions that allow both TE_{11} and TM_{11} modes to occur and propagate at the same velocity [3]. Several quarter wavelength deep corrugations per wavelength are required to enforce these boundary

conditions [3]. Over the frequency range for which the modes are well balanced the corrugated horn can be matched well, have a near constant beamwidth and very low cross-polarization. An example of such a horn is shown in Figure 2.2.

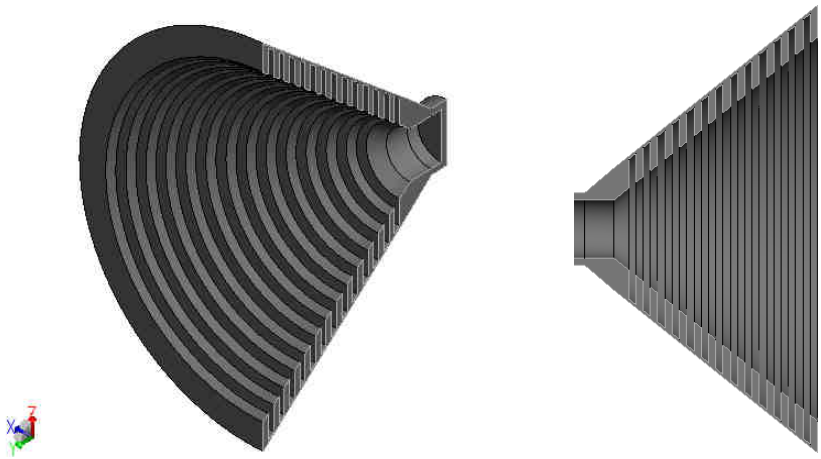

(a) (b)

Figure 2.2. An example of a corrugated horn antenna, (a) isometric view with a cutplane and (b) side view.

Reduction in the size of these antennas is possible, using compact corrugated horns. These antennas utilize a profiled horn instead of a linear taper [44]. Various types of profiles have been experimented with, such as exponential, sinusoid and tangential inner profiles [45]. Bandwidths of up to 2.4:1 have been reported for this type of antenna when used with reflectors [44]. The bandwidth limit is due to the fact that the phase centre and beamwidth of this type of antenna show some variation as a function of frequency as well as the physical size of the corrugations.

Two important parts of the corrugated horn antenna are the mode converter and the Ortho-Mode Transducer (OMT). The mode converter has to convert the TE_{11} waveguide mode to the balanced HE_{11} mode required for the horn antenna. The OMT is the device that couples the two orthogonal polarizations into the waveguide that feeds the horn. An example of such a transducer is two orthogonal dipoles fed by Marchand baluns [35]. A more common OMT is the coaxial to quad-ridge transition, the quad-ridge section is in turn transitioned to the waveguide used to feed the horn antenna [19, 46].

The quad-ridge OMTs can achieve very low return loss and good isolation between orthogonal ports [19]. Loading waveguides with ridges increases the available bandwidth

[47]. The bandwidth is limited by the need to transition to the corrugated horn. The process of designing these transitions has been well documented. Great care has to be taken when designing these transitions to prevent trapped modes that cause sharp resonances in the return loss. The trapped modes can occur due to unwanted higher order modes being excited by small asymmetries in the structure. Since the ridges are tapered to transition from ridged waveguide to normal waveguide at a point on the transition the higher order modes become evanescent and reflect, causing a resonance [48]. Trapped modes can be prevented from occurring by careful design of the waveguide transition, using an offset feed [48] or a modified backshort that uses shorting pins instead of a solid back wall [49].

As the frequency departs from the point where the corrugations are a quarter wavelength deep, the cross-polarization in the side lobes increases [43] which imposes additional bandwidth limitations. These horns are very heavy and expensive to manufacture [50].

2.4.4 Dielectric horns

Another type of hybrid mode horn is the dielectric horn. By loading the inside of a metal conical horn with two dielectric cores, one of a low permittivity in a layer above the metal and a second with a higher permittivity in the centre the HE_{11} mode can be supported [50]. This antenna is much simpler to design and analyse than the corrugated horn, has a lower weight and is cheaper to manufacture [50]. In addition much larger bandwidths have been reported when the horn is profiled and special low permittivity dielectrics are used. A bandwidth of up to 5:1 has been reported [51]. These improvements, however, comes at a cost. The horn has loss associated due to the dielectric, which increases system noise [50]. Due to this the dielectric horn antenna is not typically used for radio astronomy applications despite the advantages it has over the corrugated horn antenna.

The problem of loss also limits the use of antennas that use solid dielectric structures, with no metal exterior except at the feed. Although wideband feeds of this type have been developed [52] they are not intended for use in radio astronomy and use radar absorbent materials in their construction. A further practical consideration that limits the development of antennas that use dielectric materials is the need to cool the antenna to cryogenic temperature. A near-perfect vacuum is required to limit heat transfer and enable low temperatures to be achieved. Many dielectric materials are not suitable for use in a

vacuum. In addition, if different materials in close contact are to be cooled, the large changes in temperatures that would be encountered could cause damage to components if the materials that are used do not have closely matched thermal expansion coefficients. This could be difficult to achieve if various dielectric materials and metals have to be used in the same assembly.

2.5 Wide band feed antennas

The broad bandwidth requirement of the SKA has led to the development of various modern reflector antenna feeds. In addition to these feeds there have been attempts to adapt existing wide band reflector feeds to be more suitable for radio astronomy applications. These modern feeds typically have a much wider bandwidth than the traditional corrugated feed horns, but suffer from various disadvantages. The most notable of these feeds include the Eleven antenna, a quasi self-complementary (QSC) feed, the non-planar log periodic feed used for the ATA and quad-ridged horns.

Focal plane arrays have also been proposed as feeds for the SKA. Such a feed has the advantage that it has a much larger field of view compared to a single wide band feed. This allows for increased observation speed as multiple beams can be formed using the correct phasing. The combination of the beams can also be performed off-line if the output from each of the phased array elements is recorded. There are, however, significant disadvantages. The phased array introduces additional performance degradation in the form of crossover losses and beam degradation as a function of frequency [53]. The large number of amplifiers and phase matched lines that would have to be cryogenically cooled would also be prohibitively expensive in a system as large as the SKA [54]. For lower frequencies this is not as great a problem and using a large number of antennas (not necessarily reflector antennas) to form a phased array, is being considered for the SKA [54]. The antenna types that are used for reflector feed arrays are typically orthogonal Vivaldi antennas due to the large bandwidth of the elements and the ease with which they can be manufactured [55, 56].

2.5.1 Non-planar log periodic feed

Log periodic antennas are structures that can obtain radiation patterns and input impedances that are largely independent of frequency for relative bandwidths greater than 10:1 [16]. Due to its shape the performance of the antenna is periodic as a function of the logarithm of frequency [32, 33]. If the antenna is properly designed the variations in performance is slight. As the frequency is increased the area where the antenna appears to radiate from (also called the active region) moves towards the smaller elements (closer to the feed) [57]. The planar log periodic antenna as shown in Figure 2.3(a) has the disadvantage that its radiation pattern is bidirectional. This would make it unsuitable for parabolic reflector antennas.

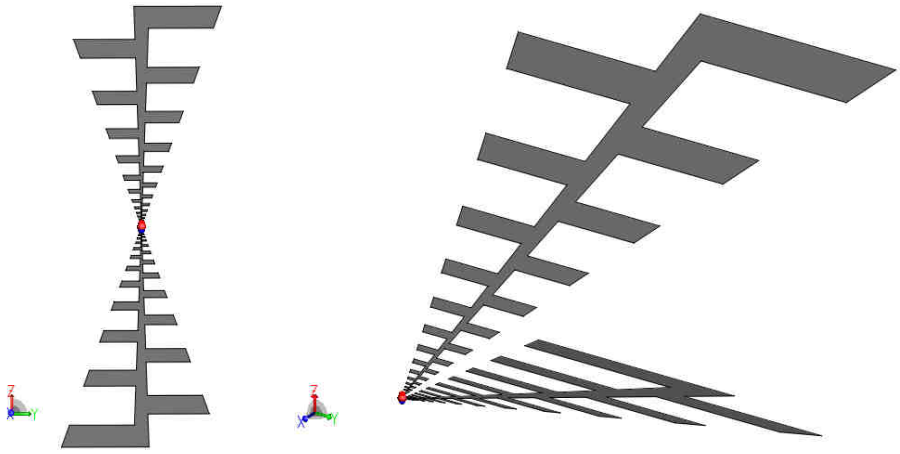

(a) (b)

Figure 2.3. (a) A planar log periodic structure and (b) the same structure in a non-planar configuration.

This effect can be overcome by inclining the two arms of the antenna as shown in Figure 2.3(b) to form a non-planar log-periodic antenna. The radiation pattern is directed towards the smallest element [3]. This type of structure is used for the ATA [6]. A log-periodic dipole array (LPDA) is based on the same principle. Two of these structures are arranged orthogonally to obtain dual polarization.

This configuration gives very stable radiation patterns as a function of frequency as well as good impedance matching [5]. Various parameters such as the type of element used (such as trapezoidal, saw tooth or circular), the width of the central support, the angle between the two arms and the growth rate (the width of the elements in relation to the previous

element) can be used as design parameters to achieve the necessary performance from the antenna [5].

The antenna has some disadvantages, most significantly a poor front to back ratio and the fact that the phase centre moves significantly as a function of frequency. The antenna also has a large aspect ratio. This phase centre movement is especially problematic as it prevents the antenna from being used over a large instantaneous bandwidth without gain loss at the edges of the bandwidth. An additional disadvantage is the position of the feed of the antenna. Positioning a cooled low noise amplifier at the feed point requires a housing immediately behind the antenna which can affect the antenna performance. Finally, using the antenna for higher frequencies would be problematic due to the manufacturing tolerances required to produce the high frequency radiating elements so close together [6].

2.5.2 Quasi self-complementary feed

A self-complementary antenna is a structure for which a rotation of 90 degrees would result in the same structure if the metallization and free space are exchanged [58]. It can be shown that in general the input impedance of a self-complementary antenna is a constant independent of frequency [59]. The quasi self-complementary feed is essentially a non-planar log-periodic antenna positioned over a ground plane. The ground plane anchors the phase centre which negates the main disadvantage of the non-planar log-periodic antenna [11]. An example of such a feed is shown in Figure 2.4.

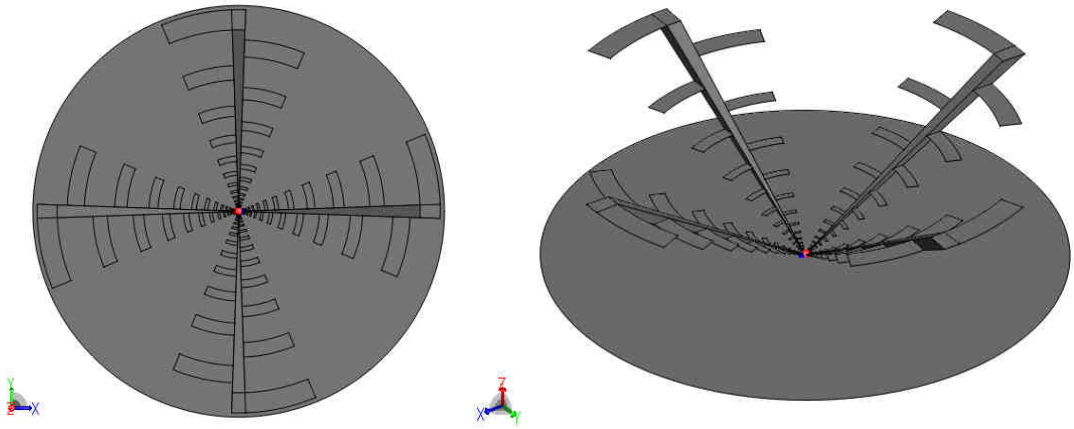

(a) (b)

Figure 2.4. An example of a quasi self-complementary feed with ground plane, (a) top view and (b) isometric view.

The maximum bandwidth reported is 10:1 [12]. The input impedance can be reasonably well matched. The shape and position of the arms can be optimised to obtain the best input matching and to reduce cross-polarization [11, 58]. The antenna is very compact though it has a high input impedance of approximately 270 Ω [12]. The beamwidth and radiation patterns of the antenna show little variation as a function of frequency [13]. The impedance matching and high cross-polarization of this feed are the main disadvantages that would have to be addressed before the antenna can be used as an efficient radio astronomy feed. Sinuous antennas in this configuration have also been proposed if circular polarization is required [60]. An alternative approach for this type of antenna has been proposed previously. Instead of using a ground plane a shaped reflector with a planar log-periodic antenna can be used as shown in Figure 2.5.

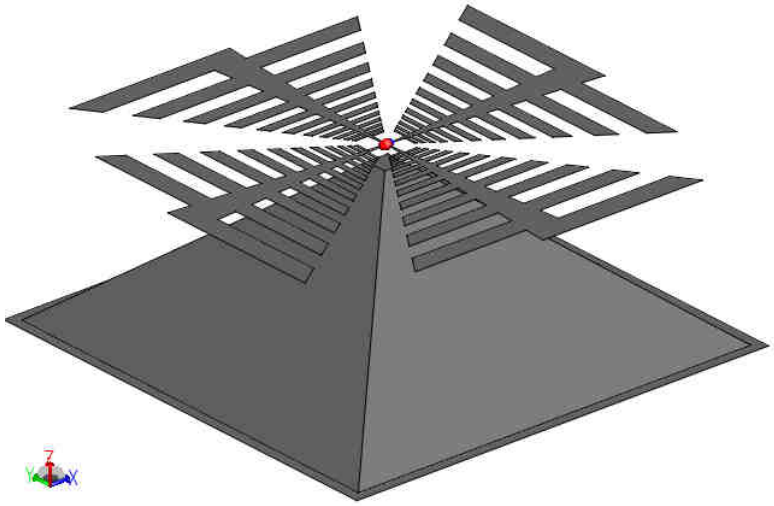

Figure 2.5. A planar log periodic antenna with a shaped ground plane.

This configuration has been used for spiral antennas [61]. More recently it has been proposed as a radio astronomy feed with a log periodic radiating element instead of a spiral antenna (dual linear instead of circular polarization) [62]. The reflector is designed to be about a quarter of a wavelength from the radiating element (a pyramidal reflector is used). This converts the bidirectional pattern to a directional pattern with little phase centre variations. The results obtained are similar to the quasi self-complementary feed. This approach, however, seems to offers little advantage over the QSC feed.

2.5.3 Eleven feed

The Eleven feed utilizes the fact that two dipoles that are positioned above a ground plane can produce a rotationally symmetrical radiation pattern [8]. The bandwidth of this configuration is extended by using multiple dipoles that are separated log periodically. This functions best with folded dipoles where the feed gap of each dipole is connected to the previous dipole [7]. The antenna is designed to be integrated with a balanced to unbalanced transformer. An example of a wire-grid linear polarized Eleven antenna is shown in Figure 2.6. Dual polarization can be obtained by adding another group of dipoles orthogonally. The antennas are constructed using printed circuit boards.

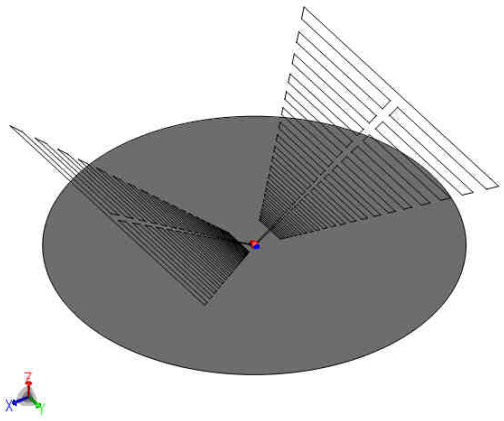

Figure 2.6. An example of a model of an Eleven feed. Only a single polarization is shown

The antenna has a rotationally symmetric radiation pattern, an 11:1 bandwidth, is compact and the phase centre is positioned on the ground plane over the frequency range. The main disadvantage of this antenna is the poor impedance matching of between -6 dB and -8 dB [58]. Another issue is the loss associated with the printed circuit board used to support the antenna elements. Recent efforts have been focussed on improving the input impedance. Using an optimization process the return loss was improved from -6 dB to -8 dB [9] and with a more sophisticated genetic algorithm this was further improved to -10 dB [10].

2.5.4 Quad-ridge horn antenna

The bandwidth of a waveguide, which is typically less than 2:1, can be extended by loading the inside of the waveguide with ridges [47]. Loading the waveguide with ridges lowers the cut off frequency of the dominant mode. This increases the bandwidth of such a

waveguide [63]. The same principle is used to extend the bandwidth of horn antennas. This led to the development of the double ridged horn antenna [64].

These horn antennas have very wide bandwidths and have been extensively used for applications where linear polarization is required [65]. The design and development of these horns have been greatly enhanced by the development of computational electromagnetic methods that can numerically analyse these antennas and predict their performance. It has been demonstrated that ridge waveguide horns can be very accurately analysed using commercial Method of Moments (MoM) software such as FEKO [66].

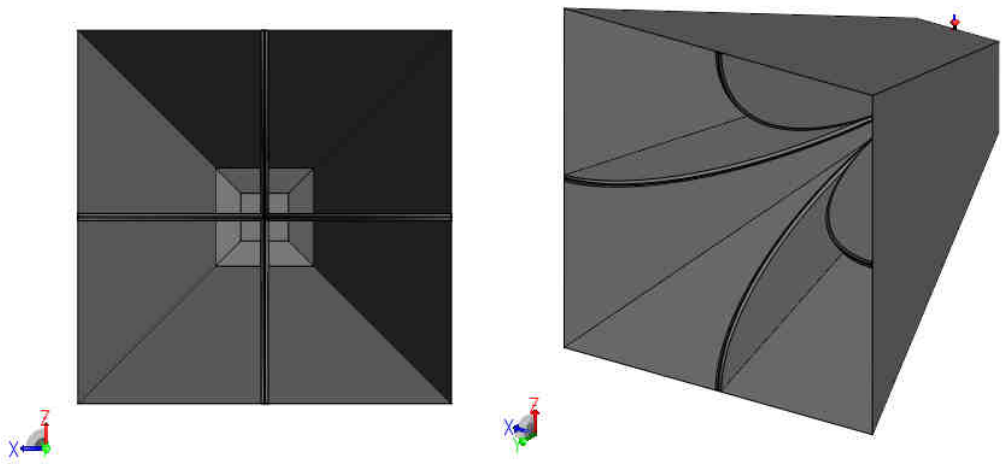

(a) (b)

Figure 2.7. An example of a quad-ridge horn antenna with a square aperture, (a) front view and (b) isometric view.

Quad-ridged horn antennas can be used if dual polarization is desired – an example of one is shown in Figure 2.7. Quad-ridged horns have been used as reflector antenna feeds [67] and commercial horns have been adapted for use as radio astronomy reflector feed antennas [14]. Quad-ridge horn antenna beamwidth decreases as a function of frequency (the gain increases) [22]. This effect can be exploited to create a reflector antenna with a constant beamwidth – as the beamwidth of the feed is inversely proportional to frequency it illuminates a smaller section of the reflector as the frequency is increased, creating essentially a smaller aperture at higher frequencies. This leads to an electrical (effective) aperture size that is close to being constant with frequency [42].

Radio astronomy calls for efficient use of the reflector surface to maximise sensitivity, for this purpose a constant illumination and hence constant beamwidth is required. The radiation patterns of quad-ridge horn antennas can have large side lobes, especially for open boundary type horns [18, 22]. The radiation patterns also tend not to be rotationally symmetric [22]. Quad-ridge horns are often not well matched over the entire bandwidth, as the design goals are typically set for maximum bandwidth with Voltage Standing Wave Ratio (VSWR) goals as high as 3:1 [18]. Aperture efficiency can be improved somewhat by the addition of a dielectric lens [22, 68]. Quad-ridge OMTs have shown that coaxial to quad-ridge waveguide transitions can be well matched over smaller bandwidths.

Recent investigation into quad-ridge horn antennas with shaped sidewalls has confirmed that these antennas can be made more suitable for radio astronomy applications [15]. This is also the only study that focuses on the same goal as the current study – to improve the quad-ridge horn for use as a wideband reflector antenna feed.

The return loss of the antenna is reported as better than 10 dB from 1.9 GHz to 19 GHz and better than 15 dB from 2.5 to 11 GHz. Patterns are not presented but from the efficiencies in a shaped reflector it can be inferred that the patterns deteriorate above 10 GHz (the aperture efficiency start to drops off). The antenna was designed using CST microwave studio, primarily a time domain solver and was manufactured using a spin process. The antenna used as starting point was an ETS Lindgren open boundary quad-ridge horn antenna [14, 17]. The antenna also added features such as mode suppressors and aperture matching to the basic antenna design. The profile used to shape the antenna is not mentioned.

The current study will focus on improving the radiation patterns – and obtaining a constant beamwidth – as opposed to optimizing for a specific reflector antenna configuration. In addition the study will investigate the effect of geometry changes on the quad-ridge horn antennas and determine the effect it has on the performance. This will aid in future antenna designs as the areas of the antenna that affects specific performance characteristics can be identified and adapted to deliver improved designs. It will also initially focus on a narrower bandwidth to attempt to obtain improved performance.

2.6 Summary

The characteristics required of a radio astronomy antenna have been outlined. Briefly stated this entails maximising the gain while reducing the noise inherent to the system. Aspects such as polarization purity and the reduction of side lobes are also crucial.

Due to these requirements reflector antennas are most often used for radio astronomy telescopes. The performance of reflector antennas is determined primarily by the feed of the antenna. The reflector also adds its own requirements with regards to the optimal use of the aperture versus the reduction of spill-over and aspects such as phase efficiency.

Satisfying all these requirements is challenging but has been achieved in the past to a satisfactory degree using antennas such as corrugated horns. New requirements on the bandwidth of antennas, however, rule out the use of these antennas. Achieving greater bandwidth has been the focus of a great deal of development work. The most prominent developments that are being investigated are the non-planar log-periodic antenna used for the ATA, a quasi self-complementary antenna, the Eleven antenna and quad-ridged horn antennas.

These antennas highlight the different approaches that have been used to obtain broad band performance. The ATA and QSC employ frequency independent elements. The Eleven antenna used an existing concept (two dipoles above a ground plane) and scaled it in a log periodic fashion to obtain a broad band antenna while the quad-ridged horn uses ridges in a waveguide to lower the cut off frequency and extend the bandwidth.

The primary disadvantage of the non-planar log periodic antenna, a shifting phase centre, is linking directly to the method of operation of the antenna and techniques to overcome it are limited to physically moving the antenna. Both the Elven feed and the QSC feed have proved difficult to match due to the presence of the ground plane introducing reflections, sophisticated optimization techniques have resulted in only small improvements [10]. The antennas also seem to be difficult to manufacture for a cryogenically cooled environment.

Quad-ridge horn antennas show great potential for improved performance. Quad-ridge OMTs have been used extensively in radio astronomy and indicates that the return loss can

be greatly improved. The radiation pattern could also be improved by investigating the effect of shaping the antenna similar to what has been done with waveguide horn antennas [15, 24]. Recent developments have highlighted that these antennas can be made more suitable as feeds for radio astronomy [15, 26]. Further investigation into the effects of changes to the antenna geometry could aid in developing feeds suitable for use as a wideband radio astronomy reflector antenna feed.

This study will attempt to address the drawbacks of the quad-ridge horn antenna as a radio astronomy reflector antenna feed. Specifications have been identified that are of importance to radio astronomy and reflector antenna feeds and that will be considered in the study of the quad-ridge horn antenna. These are summarized in Table 2.1.

Table 2.1. The specifications of the antenna that will be considered

Specification	Description
Bandwidth	4:1 0.75 GHz to 3 GHz
Input Impedance	50 Ω Although higher impedances are often preferred by LNA designers (typically 100 Ω) 50 Ω will enable a prototype to be manufactured using existing connectors.
Port Isolation	-30 dB
Input Reflection	-15 dB
Polarization	Dual polarization should be achieved
Pattern Rotational symmetry	Will be evaluated by comparison of the principal plane patterns- obtaining more symmetric pattern if possible.
Beamwidth	Constant beamwidth is required. The goal is to limit the variation in the 10 dB beamwidth. The range of beamwidths that can be achieved needs to be determined
Conductive Loss	The conductive loss of the antenna will be calculated to determine additional noise that can be expected.
Cross-Polarization	The cross-polarization of the feed antenna will be calculated.
Phase centre variation	The phase centre variation will be determined
Illumination efficiency	A prototype design will be evaluated with a reflector antenna to determine the aperture taper and spill-over efficiency achieved.

3. QUAD-RIDGE HORN ANTENNA MODELLING

3.1 Introduction

The numerical method chosen to model the quad-ridge horn antenna and the selection of the method will be discussed in this chapter. This chapter will investigate quad-ridge horn antenna geometries that have been proposed in literature. A quad-ridge horn can be broadly divided into two sections, a coaxial to waveguide transition and a waveguide to free-space transition. The method used to model each of these features will be discussed.

3.2 Modelling method

Mode matching methods are often used to analyse quad-ridge waveguides. These were not considered, as a model capable of predicting the radiation characteristics as well as the impedance characteristics of the antenna was required. General-purpose methods were thus used to analyse the quad-ridge horn antenna.

The three most widely used general-purpose methods are discussed in this section, the Finite Element Method (FEM), the Finite Difference Time Domain method (FDTD) and the Method of Moments (MoM) [69]. Commercial software packages are available that use these methods namely HFSS, CST (uses a finite integration technique, similar to FDTD [69]) and FEKO [70]. These software packages also include graphical Computer Aided Design (CAD) interfaces. The purpose of the discussion is to outline reasons for the choice of modelling method and the commercial software.

3.2.1 Finite element method

The FEM uses either of two approaches, namely variational analysis or weighed residuals to obtain an approximation to the solution of the differential equation formulation of Maxwell's equation. The resulting set of linear equations that have to be solved result in a sparse matrix. The calculated fields are represented on a finite triangular (surfaces) or tetrahedral (volumetric) mesh, although more complex mesh elements can also be employed [69]. The FEM is mostly used in frequency domain formulation. The

commercial software HFSS employs FEM. FEM is also used for analysis in other disciplines such as structural analysis and thermodynamics.

The advantages of FEM are that it can easily accommodate inhomogeneous geometries and materials and scales better with frequency than MoM [69]. The method can also be used to simultaneously analyse the electromagnetic, thermal and structural solutions. An example of this is the analysis of a high power resonator. Such coupled software can be used to determine how much the resonant frequency changes due to the resonant cavity deforming as a result of thermal expansion.

Disadvantages of the FEM is that it does not include the radiation condition – for open regions, such as horn antennas, an artificial absorbing boundary or hybridization with MoM is required. This leads to some inefficiency compared to MoM for conductive radiators. The FEM also requires a volumetric mesh, which can become complex for analysis of three dimensional geometries [69].

3.2.2 Finite difference time domain

The FDTD is a time domain based code. For FDTD no matrix is set up and solved. Instead the approximation is more direct. The problem is discretised in a grid staggered in space and time. The partial differential equations are approximated by finite differences and are solved using the boundary and initial conditions [69]. This amounts to finding the value of the fields at subsequent time steps. The mesh has to be terminated in a perfectly matched layer when modelling structures that radiate into free space.

An advantage of the time domain approach of FDTD is that wideband data can be calculated with a single solver run – as opposed to frequency domain methods which has to calculate a solution for each frequency. The method can also handle material inhomogeneity. The method scales reasonably well with frequency [69].

Disadvantages include the volumetric mesh required for three dimensional problems, which can be very memory intensive. If a regular mesh is used there can also be an error where curved surfaces are approximated by a staircase type of mesh. This effect can be overcome by using non-orthogonal grids. The method also does not include the radiation

condition which requires the use of perfectly matched layers. For radiating structures that consist entirely of conductive materials the MoM is more efficient [69].

3.2.3 Method of moments

MoM typically discretized the problem into wire segments and surface patches (volumetric meshes are not often used due to computational cost). The equivalent surface current on each of these elements is calculated. This is done by setting up a matrix equation representing the interaction of the mesh elements using the Greens function. Applying the boundary conditions and solving the resulting linear equations gives an approximation of the current on each mesh element. The MoM is mostly used as a frequency domain method [69]. FEKO is an example of software that uses MoM [70].

The advantages of MoM include that it is very efficient for radiating structures that consists of conductive surfaces. Only the surfaces are meshed and the method includes the radiation condition. The fact that the current density is calculated allows other parameters, such as conductive loss, to be derived easily [69].

Disadvantages are that the MoM cannot handle material inhomogeneity as well as FEM or FDTD – a volumetric mesh is required. Homogenous materials can be modelled using the Surface Equivalence Principle (SEP). The MoM is a frequency domain technique and the solution has to be recalculated for each frequency, in addition the method does not scale well with frequency [69].

3.2.4 Conclusion

The MoM was chosen to model the quad-ridge horn antenna. As the antenna is a radiator that consists primarily of highly conductive surfaces the MoM would be most appropriate. MoM handles such problems very efficiently, as only the surfaces have to be meshed. Although later simulations also include the dielectric in the SMA connector this could be modelled using SEP. Although MoM does not scale very well with frequency, the bandwidth of the antenna was small enough to still allow simulations to be completed in a reasonable time. This was also a factor in the choice between MoM and FDTD. As the

current data is directly available MoM can also easily calculate the conductive loss of the antenna.

The commercial software package FEKO, was chosen to model the antenna. The software allows CAD modelling of the antenna in three dimensions. The software also has an optimised implementation of MoM that can be run in parallel. Access to a full version of the software was available. The software also includes the Fast Moment Method (FMM) which offers greater efficiency for large (high frequency) problems, although the model was not substantial enough to take advantage of this. It has been demonstrated that ridge horns can be accurately modelled using this software [66]. The software also offers asymptotic techniques such as Physical Optics (PO) which is used to analyse electrically large objects – such as reflector antennas. Hybrid MoM-PO for analysis of the antenna with a reflector is possible with this software.

3.3 Coaxial to quad-ridge waveguide transition

The quad-ridge horn antenna is divided into two sections, the coaxial to quad-ridge waveguide transition and the transition from waveguide to free space. Both of these sections consist of a number of parts, each of which is discussed with regard to typical implementation and how they are modelled in FEKO.

3.3.1 Quad-ridge waveguide

Loading a waveguide with ridges increases the single mode bandwidth by lowering the cut-off frequency of the dominant mode [71]. Using quadruple ridges, dual polarization is achieved. These waveguides are typically used in three different geometries, square, diagonal or circular. These geometries along with dimensions are shown in Figure 3.1 [47].

This type of ridge waveguide has been analysed using various methods such as the magnetic field integral equation [47], mode matching [72] and FEM. The cut-off frequency and single mode bandwidths of various ridge geometries have been calculated, approximations of the impedance of quad-ridge waveguide have also been presented [47].

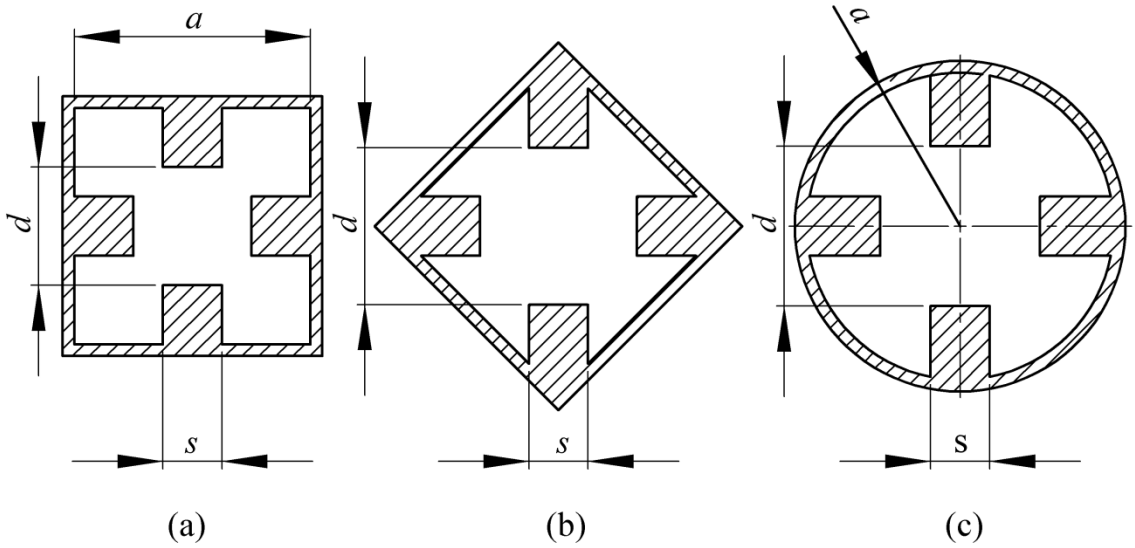

Figure 3.1. Quad-ridge waveguide geometry cross-section, (a) square, (b) diagonal and (c) circular.

The single mode bandwidth of a quad-ridge waveguide is much smaller than that of a double ridge waveguide. The TE_{11} mode (in square quad-ridge waveguide) cut-off frequency is very close to the TE_{10} mode (the fundamental mode). If the TE_{11} mode is not excited a very large single mode bandwidth can be obtained (the next higher order mode cut-off is at a much higher frequency) [47]. Waveguide symmetry has to be maintained to achieve this.

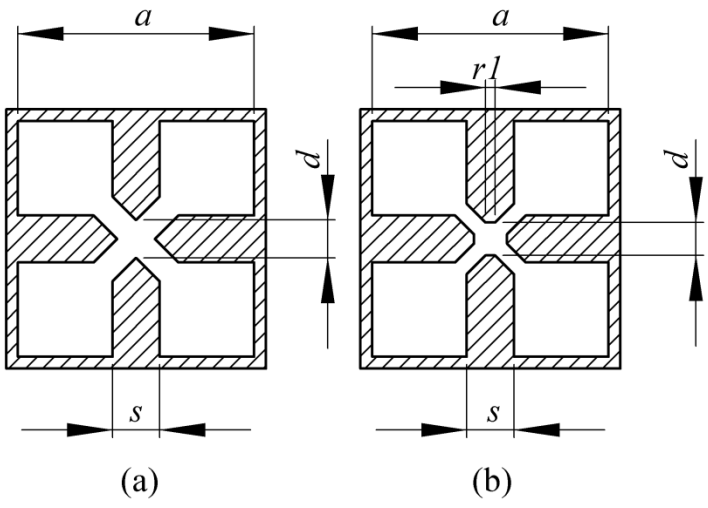

Figure 3.2. Quad-ridge waveguide cross-section chamfering, (a) completely chamfered and (b) Partially chamfered.

For low impedance (such as 50 Ω required for a match to a coaxial line) and wide bandwidths a very narrow ridge gap (*d* as in Figure 3.1) is required. A small enough gap

can often be achieved only by chamfering the ridges [72]. Two different methods for chamfering the ridges are shown in Figure 3.2 [72, 73].

The waveguide with partially chamfered ridges in Figure 3.2(b) was used. The choice was based on mechanical considerations. The ridges do not have sharp edges, which can be difficult to manufacture. Feed pins have to be connected to the ridges – this is much easier with a flat section than for a sharp ridge, which would have to be counter-bored to allow a hole to be tapped.

An analysis of quad-ridge waveguide with partially chamfered ridges using a hybrid mode-matching boundary element method has been presented [72]. Results were only presented for a limited set of parameters and were limited to reporting the bandwidth that could be achieved with these parameters. Initial analysis of a waveguide section was thus done in CST (where arbitrary waveguide ports are possible) to obtain a basic design for the quad-ridge waveguide. The initial design dimensions could then be used in the full antenna model and be adapted to provide adequate bandwidth and the correct impedance when used in conjunction with the transition from coaxial line and the backshort. Quad-ridge horn antenna designs are often adapted from double-ridge horn designs. Design equations of double-ridge waveguide are, however, not suitable for designing these types of quad-ridge waveguide as the modes are significantly perturbed by the proximity of the orthogonal pair of ridges.

3.3.2 Coaxial to waveguide transition

Quad-ridge horns are typically fed using coaxial transmission lines. The transmission lines are standard 50 Ω lines. The size of the ridges in the quad-ridge waveguide determine the size of the connector and coaxial cables that can be used, as the coaxial line has to pass through the ridge and be connected to the ridge on the opposite side of the waveguide. The ridge width thus places an upper limit on the size of the coaxial cable outer.

The method most often used is to drill a hole through one ridge, with either the metal of the ridge serving as the outer conductor or allowing the coaxial line to be inserted through this. A simple transition is shown in Figure 3.3.

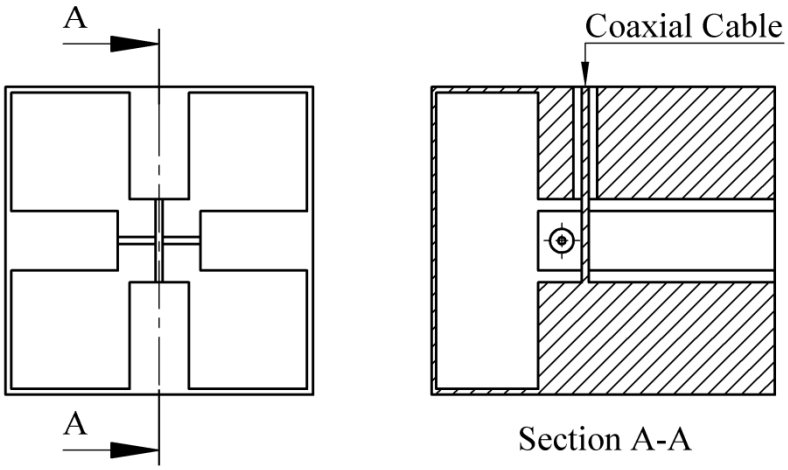

Figure 3.3. A simple coaxial to quad-ridge transition, (a) front and (b) cross-section view.

A disadvantage of this method is that the two orthogonal ports cannot cross the gap between the ridges at the same location. Bended probes that allow the transitions to occur at the same distance from the backshort have been proposed, but were not considered due to the difficulty associated with manufacturing such small features [74]. The result of this is that the two ports have slightly different reflection coefficients as the distances from the backshort to the feed pins are slightly different. An alternative feed method consists of using four ports, each feeding into the back face of the ridge with the input combined by a 180° hybrid. The exact mechanical arrangement of how this is achieved has not been shown [22]. With this feed arrangement the feed pins no longer cross the ridge gap. This has an additional advantage that the impedance required from the waveguide to match the coaxial line is 100 Ω, which is easier to realise using quad-ridge waveguide as the ridges can be further apart.

The centre conductor of the coaxial transmission line can be fixed to the ridge using a number of different methods. The conductor can either be press-fitted, using a collet to hold the centre conductor in position [66] or the conductor can be threaded and screwed into the bottom ridge [46]. Some coaxial lines have very small inner conductors on which it would be extremely difficult to cut thread. These lines can be attached to the ridge by drilling a hole in the bottom ridge just smaller than the dielectric. The coaxial line outer conductor is stripped away and the centre conductor and dielectric are inserted into this hole. The depth of the hole can also be used to adjust the impedance matching of the antenna [73].

3.3.3 Coaxial line model

The coaxial transmission line was modelled using two methods in FEKO. Initial models used a wire to approximate the centre conductor of the coaxial line with a delta gap source in the centre of the wire. A more detailed model was created that included the coaxial transmission line and the details of the transition into the waveguide, a final model also included the transition from SMA to an airline using SEP to model the dielectric.

These models required the creation of a coaxial waveguide. FEKO allows cylindrical structures to be created. When the cylinders are meshed, inconsistent meshing results can sometimes be obtained (although a mesh smoothing feature has been introduced in later versions of the software that improved on this aspect). Depending on the mesh size used the model is meshed differently and the geometry of the meshed cylinder can vary along the length of the line.

This was addressed by modelling the coaxial line as an octagonal or a 16 sided structure to force the meshing routine to mesh in a homogenous fashion across the length of the coaxial line. The round, 16 sided and 8 sided coaxial line models are shown in Figure 3.4 for comparison.

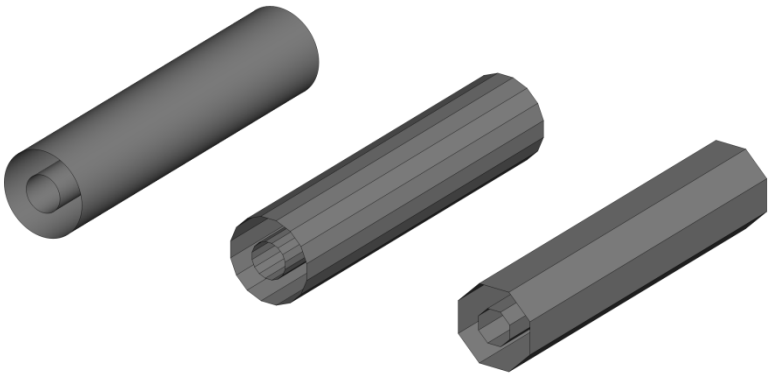

Figure 3.4. Coaxial transmission line FEKO model representations, round, 16 sided and 8 sided.

The resulting mesh was much more even along the length of the coaxial line and gave much more consistent results for different mesh sizes compared to the round model. Examples of meshing achieved for the different models are shown in Figure 3.5.

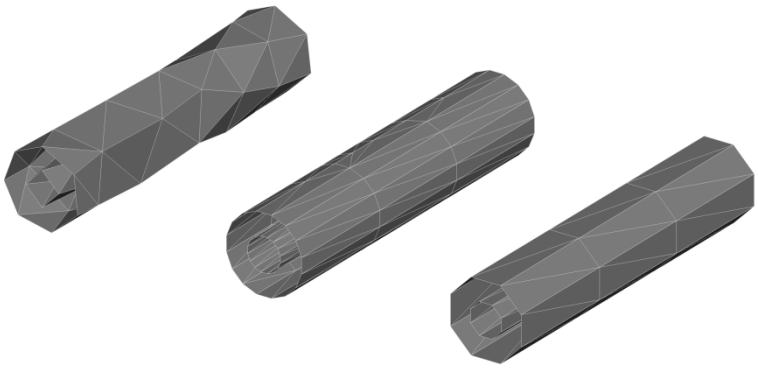

Figure 3.5. Coaxial transmission line model mesh, round, 16 sided and octagonal.

The fundamental mode was excited in a coaxial transmission line using a waveguide port. This port requires adequate definition of the coaxial face onto which it is to be applied. Coarse meshing could also lead to the face onto which the port had to be placed not being adequately represented. This can be remedied by specifying a smaller mesh size close to the port, although this gives an inhomogeneous mesh and typically requires more triangles than the octagonal coaxial line. The electric near field in the coaxial line for an octagonal and 16 sided mesh is compared in Figure 3.6 to show that these methods resulted in the excitation of a TEM mode in the transmission line. The octagonal model was mostly used due to the smaller number of triangles required to mesh the geometry, while still providing a good approximation to a TEM mode.

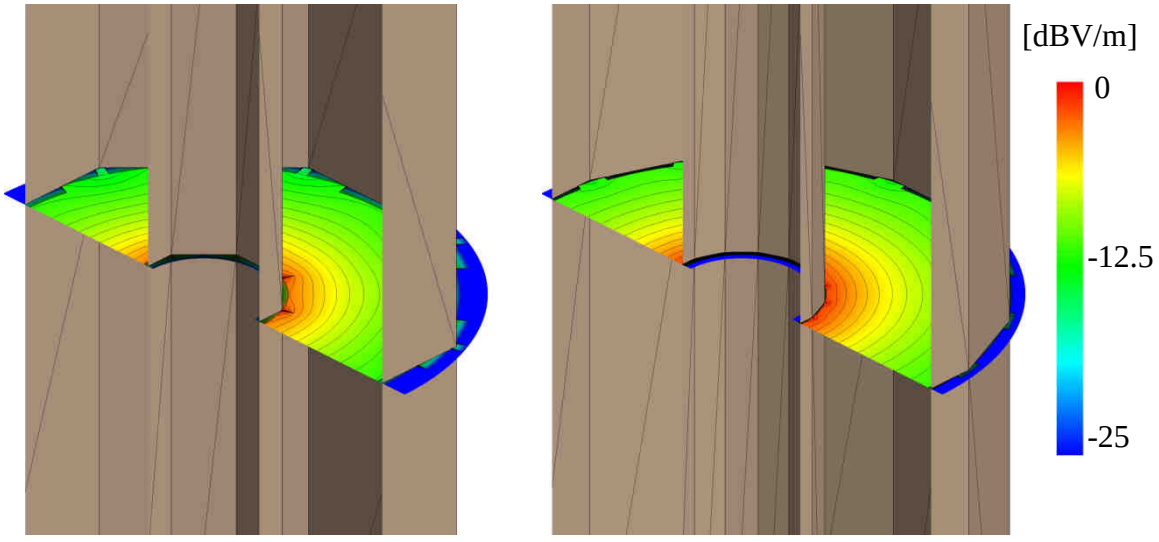

(a) (b)

Figure 3.6. The normalised electric field inside, (a) an octagonal and (b) sixteen sided approximation of coaxial transmission line to illustrate the TEM mode excited in the transmission line.

3.3.4 Backshort

The backshort is used to ensure propagation occurs in only one direction, while keeping reflections to a minimum to ensure a low input reflection coefficient. The backshort design has to prevent any modes from propagating past the end of the ridges, towards the back plate.

The geometry of the backshort is most often found by means of experimentation. Early studies utilized a plunger as a backshort instead of a fixed metal wall to experimentally determine the optimum distance from the feed position to the back plate [73]. The designs are often based on approaches that have been developed for double ridge horn antennas [79] and are then adapted to quad-ridge waveguide. Full wave simulation allowed more extensive experimentation with the backshort and has resulted in some modifications to the geometries of simple backshorts in an attempt to improve the Voltage Standing Wave Ratio (VSWR) [20]. A number of the configurations that have been proposed for quad-ridge horns and OMTs are shown in Figure 3.7.

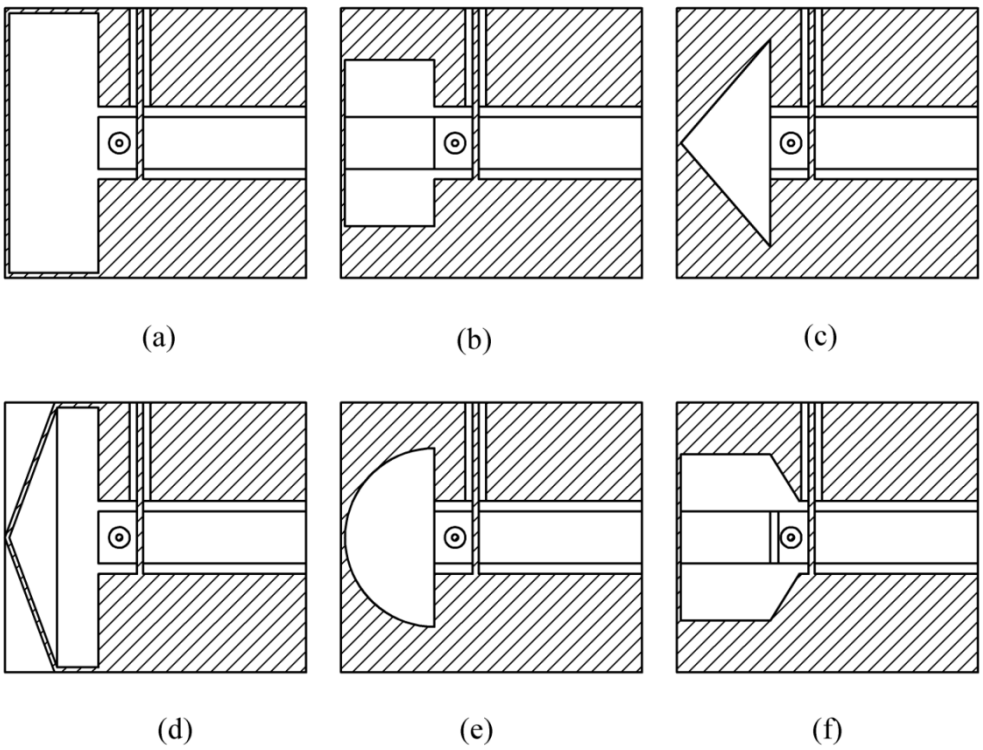

Figure 3.7. Example of types of backshorts used for coaxial to waveguide transitions. (a) Simple backshort [76, 78], (b) Stepped backshort [73], (c) Triangular backshort [19], (d) Pyramidal/Conical backshort [74], (e) Hemispherical backshort [18, 20] and (d) Stepped backshort with angles cut into the ridges [73].

3.4 Waveguide to free space transition

3.4.1 Ridge profile

The purpose of the ridge profile is to provide a transition from the impedance of the waveguide (close to 50 Ω) to that of free-space, 377 Ω [73, 75, 76, 77, 78]. An exponential impedance taper in the form of equation 3.1 and 3.2 is often used. This impedance taper has been used for double ridged horn antennas [79] and has since been adopted for quad-ridge horns as well.

$$Z = Z_0 e^{kx} \quad ; \quad 0 \leq x \leq \frac{l}{2} \tag{3.1}$$

$$Z = 377 + Z_0\left(1 - e^{k(l-x)}\right) \quad ; \quad \frac{l}{2} \leq x \leq l \tag{3.2}$$

Z_0 is the characteristic impedance of the transmission line (waveguides do not have a characteristic impedance – approximations to this impedance have to be made [46]), l is the length, k is a constant and x is the position on the ridge. This allows the required impedance on various positions of the ridge to be determined. From the impedance the required ridge gap can be calculated. This method relies on the calculation of the characteristic impedance of quad-ridge waveguides, some approximations to this impedance has been published for some waveguide geometries [47]. It has been found experimentally that adding a linear taper to the exponential taper resulted in improved VSWR, especially for low frequency [64]. Other ridge profiles have simply been an exponential taper of the ridge separation to a required aperture size (not an impedance taper), with which good results have also been obtained [20]. As the addition of a linear section resulted in such an improvement in VSWR it was decided to study the effect of various ridge profiles to determine if further improvements could be made. The effect of different ridge profiles on the radiation patterns was also investigated.

The exponential impedance taper assumes that the quad-ridge structure is simply a transmission line that has to be matched. This ignores the fact that changes to the structure of the waveguide can result in changes to how waves propagate in the quad-ridge waveguide. If the transition is too sudden higher order modes can propagate – leading to deterioration in high frequency VSWR and radiation pattern, while a too gradual transition

can result in low frequencies being at or below cut-off resulting in deterioration in low frequency VSWR.

The ridge profiles were implemented in FEKO either as a fitted spline where the points that define the curve are calculated in Matlab (utilizing enough points to ensure an accurate representation) and imported into FEKO or directly in FEKO as an analytical curve [70]. This ensured an accurate and smooth representation of the profiles allowing a homogenous mesh. Chamfering the ridges was also investigated – whether to have chamfered ridges from the waveguide to the aperture or whether, and how to transition from chamfered to un-chamfered ridges.

3.4.2 Sidewalls

The sidewalls refer to the flared section of the horn antenna. It is a transition from the waveguide to the aperture of the antenna. Typical sidewalls are a simple linear transition. Quad-ridge horn antennas have been proposed that have no sidewalls. These horns are called open-boundary quad-ridge horns [18]. The removal of the sidewalls was based on a double ridge horn antenna design. Double ridge horn antennas can show pattern deterioration for high frequencies – this has been addressed by removing the sidewalls, this double ridge design was used as the basis of a quad-ridge horn to obtain dual polarization. The open boundary horns also have patterns that vary as a function of frequency and typically have larger side lobes [18], compared to similar horn antennas. The sidewalls were investigated as they have a large effect on the radiation pattern. Shaping the sidewalls to obtain a more constant beamwidth was also considered given the effect this had on TEM and waveguide horn antennas [24, 80]. The shaped sidewalls were implemented in FEKO using analytical curves. Recent investigation into shaped sidewall quad-ridge horn antennas showed promise as reflector antenna feeds [15, 26].

3.5 Summary

The methods that could be used to perform the analysis of the quad-ridge horn antenna were discussed. The MoM, and the commercial code FEKO were chosen to model the antenna. This should result in an efficient model as the antenna model consists of

conductive surfaces and the frequency band of interest is 4:1. FEKO also includes other, asymptotic methods, such as physical optics, that can be used to analyse the performance of reflector antennas.

The make-up of a quad-ridge horn antenna and the approaches to designing these antennas have been discussed. The methods that are used to model each geometry feature were also presented. The antenna model is validated by comparing measured and simulated results as presented in Chapter 6.

4. ANTENNA PARAMETRIC STUDY

4.1 Introduction

The goal of this parametric study is to gain an understanding of the effect of each parameter on the impedance and radiation characteristics of the antenna. The parameters that primarily affect the radiation pattern, with little effect on the other aspects of the antenna performance are identified. The parametric study investigates how these parameters can be used to control the beamwidth and the range of beamwidths that can be achieved. Furthermore the parametric study also provides information on how the antenna geometry can be manipulated to improve the impedance matching and increase the frequency bandwidth of the antenna.

The parametric study uses a basic model of a quad-ridge horn antenna. The geometry of this model is described and dimensions are provided. The sets of parameters that are investigated are listed below.

- Orthogonal feed pin separation. The separation between the feed pins is investigated to determine the effect this parameter has on the isolation between the two ports and whether the ports have similar impedance and radiation characteristics.
- Waveguide parameters. These are the parameters of the quad-ridge waveguide and include the ridge width, ridge gap and waveguide size. It is demonstrated that these parameters strongly affect the antenna impedance characteristics.
- Backshort parameters. The distance to the backshort and steps in the backshort are investigated. These parameters have a large effect on impedance characteristics and can help to control higher order mode propagation.
- Ridge profile. The ridge profile type (elliptical and exponential) and transition are investigated. It is shown that this parameter affects both radiation pattern and impedance characteristics.
- Sidewalls. A quad-ridge horn antenna with elliptically shaped sidewall is proposed. The antenna is compared with straight and open-boundary quad-ridge horns. The most suitable geometry for the shaped sidewall antenna is determined. Beamwidth control using elliptically shaped sidewalls is investigated.

- Phase error. The phase error across the aperture of an elliptically shaped quad-ridge horn is compared to a quad-ridge horn with straight sidewalls.

The parameters investigated are described in each section with a sketch of the model geometry to show the position of the parameter. The results expected are discussed. Simulated results are shown and the significance of the results discussed. The S-parameters for each parameter change is shown along with the boresight gain. In addition the beamwidths are also shown. The 3 dB as well as the 10 dB beamwidths are shown in cases where significant beamwidth changes were observed while only the 10 dB beamwidths are shown for parameter changes that resulted in little or no beamwidth variation.

The beamwidth was chosen as a measure of how the radiation patterns were affected. Another possibility was to directly calculate the efficiencies of the antenna when used as a feed for a reflector. This had a few drawbacks. Firstly the size of reflector (the edge half angle) strongly influences the efficiencies of the feed antenna. The size of the reflector that will be used for future radio astronomy projects are still subject to change. This method would be most suitable for an antenna design where the feed antenna is to be optimized to work with a specific size reflector antenna – for the parametric study it adds another parameter that is not related to the antenna design and can make the results difficult to interpret. A feed with a low efficiency for a specific reflector might still be able to achieve very high efficiencies for a different reflector configuration.

The beamwidths give a good indication of how the radiation pattern changes as a function of frequency. It can also give an indication as to the presence of side lobes or shoulders in the pattern – these can be seen as sudden changes in the beamwidth as a function of frequency. Side lobes that are observed in the 10 dB beamwidth are undesirable as they would be close to a dish edge for a desired edge taper and could result in high spill-over.

4.2 Basic quad-ridge horn antenna model

A quad-ridge horn antenna model was developed to use for the parametric study. The development of the model gave an indication as to which parameters and limits should be used for the study and would provide meaningful results. This model was designed to be matched reasonably well. A sketch of the model indicating design detail is shown in Figure

4.1. The horn length and aperture width was 400 mm, the backshort distance 18.57 mm and the waveguide size (*a*) 100 mm. The model was created in FEKO and was fully parametric. The geometry of the antenna used for the parametric study was pyramidal, although many of the conclusions drawn in this chapter are also applicable to quad-ridge horn antennas with circular geometry.

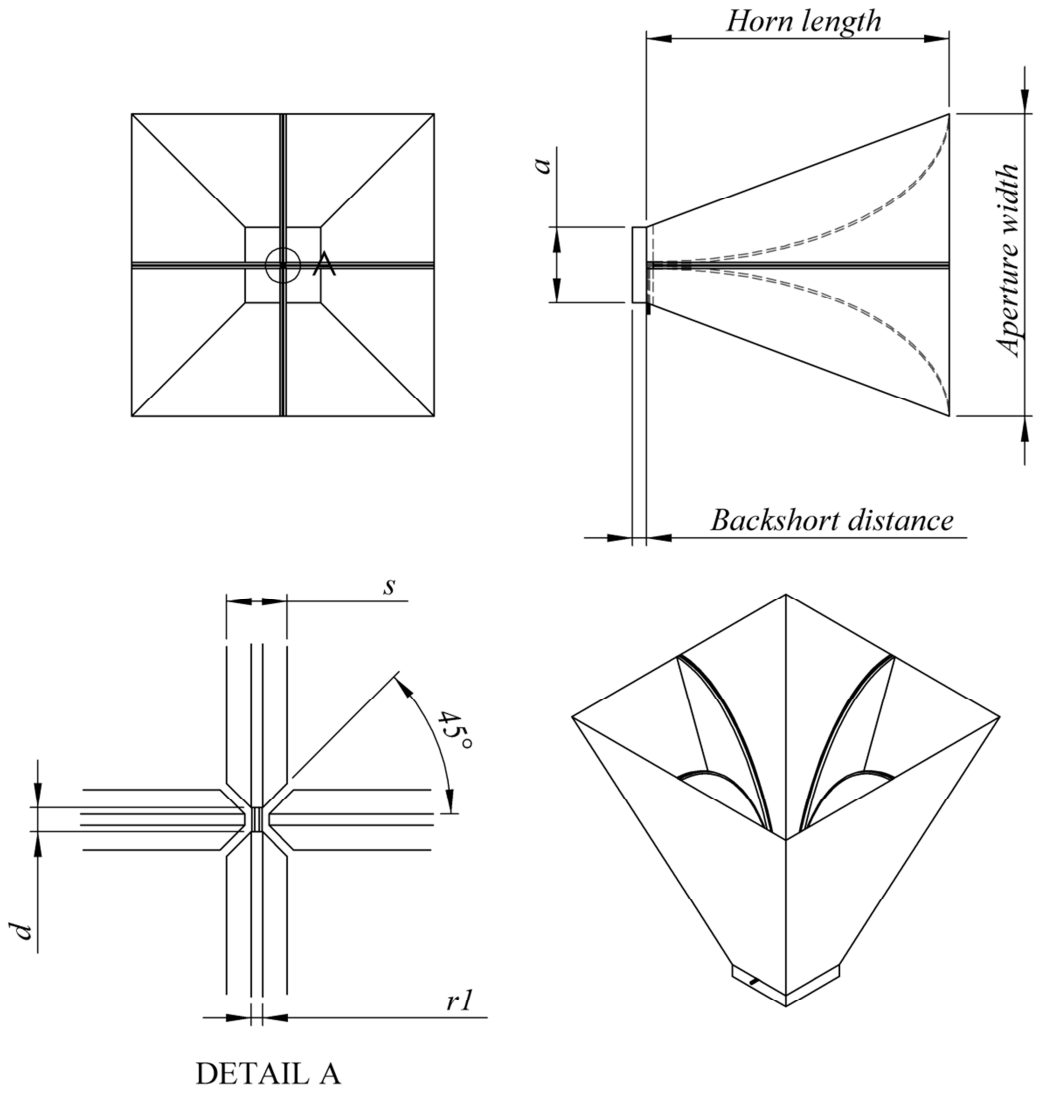

Figure 4.1. The basic model of the quad-ridge horn antenna used for the parametric study

As can be seen from Figure 4.1 the antenna model has partially chamfered ridges and used a simple backshort. The partially chamfered ridges were chosen as it provided a connection point for the centre conductor of the coaxial line (the flat section, *r1*, is as wide as the centre conductor). This chamfering also provided a good impedance match. The chamfering is gradually blended into the ridge. The ridge width and gap were chosen large enough to allow them to be manufactured relatively easily. The feed gap (*d*) was 3.2 mm

and the ridge width (*s*) was chosen to be 8 mm. This width was chosen as it provided a reasonably good impedance match and because standard aluminium plate is available in this thickness – this reduces the cost associated with manufacturing.

The ridge profile is elliptical – this provided a good match to the 50 Ω transmission line used to feed the antenna. The size of the coaxial transmission line was chosen to be close to that of SMA while still using sizes that are standard (standard drill size and pin diameter) to allow easy manufacturing. The antenna model used for the parametric study mostly had only one feed port. The second, orthogonal, port is located in a slightly different position in the waveguide. Despite the different position of the feed pins it is shown in the following section that the impedance and radiation characteristics of the two ports are similar. Using only a single port significantly simplifies the antenna model as a plane of symmetry can be introduced to the model, speeding up the calculation of the solution.

The antenna model neglected the conductive loss of the antenna and thus the directivity is calculated. However the conductive loss was regarded as small enough that the directivity and the gain could be regarded as essentially the same.

4.3 Orthogonal feed pin separation

The basic antenna model can be significantly simplified if the assumption is made that the impedance and radiation characteristics of the two orthogonal ports are similar. The second port can then be removed from the model, which allows a plane of symmetry to be included. The plane of symmetry reduces the computational time required to solve the problem. The assumption was tested by first simulating a model with two ports and comparing the impedance and radiation results that are obtained. This model is also used to investigate the effect of changing the distance between the orthogonal feed pins on the coupling between the ports ($|S_{21}|$). The orthogonal feed pins and the distance between them is indicated in Figure 4.2.

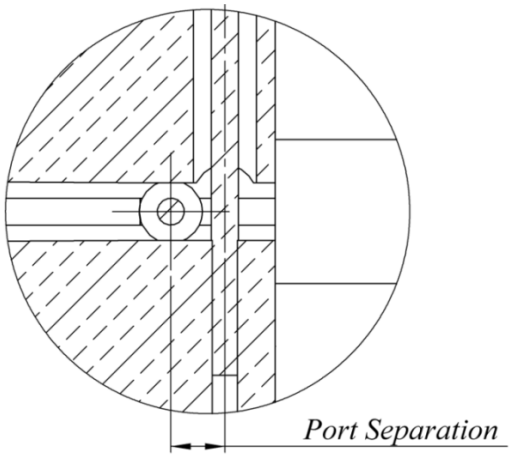

Figure 4.2. The port separation parameter, showing orthogonal feed pins.

The reflection coefficients obtained for the two ports are shown in Figure 4.3. The orthogonal feed pins are separated by 3 mm. The reflection coefficients correspond reasonably well across the band. $|S_{22}|$ is slightly worse than $|S_{11}|$ at low frequencies. The discrepancy is due to the different distances of the feed pin to the backshort. Smaller port separation parameters gave results that corresponded better. This has to be traded off against increased coupling between ports and increased mechanical complexity. Small port separations would be more difficult to implement. The increase in reflection coefficient seen in the region of 3 GHz is due to higher order mode propagation.

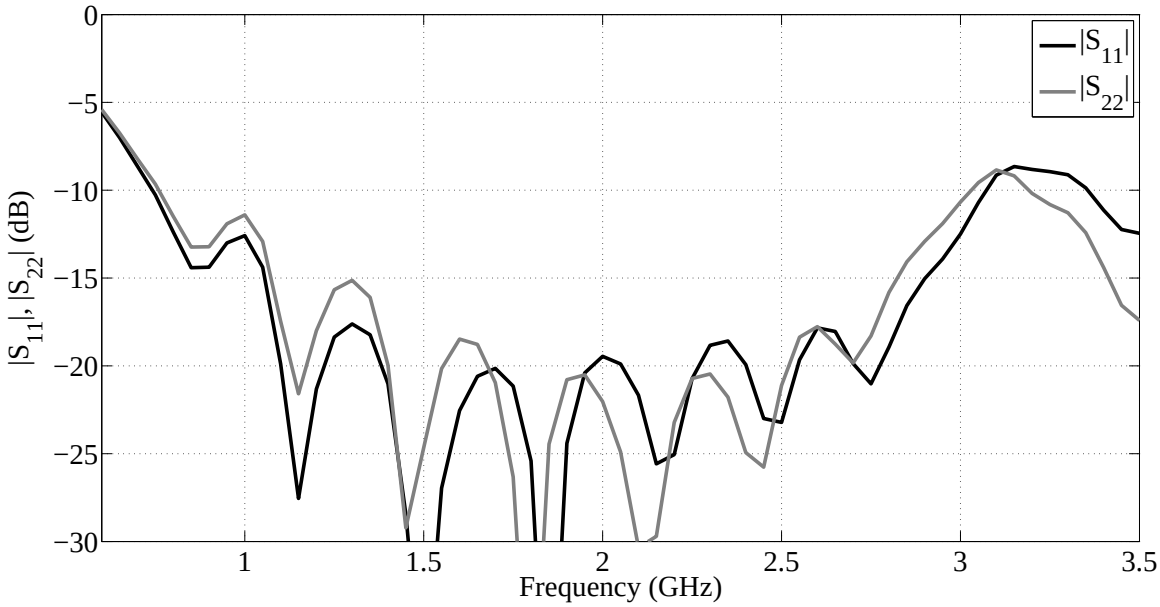

Figure 4.3. The difference between the port input reflection coefficients for a port separation of 3 mm.

The boresight gain for excitation at each of the two ports is shown in Figure 4.4. The difference in the boresight gain is limited to higher frequencies as the higher order mode excitation occur at slightly different frequencies due to the different distances to the backshort The radiation characteristics of the two ports correspond very well.

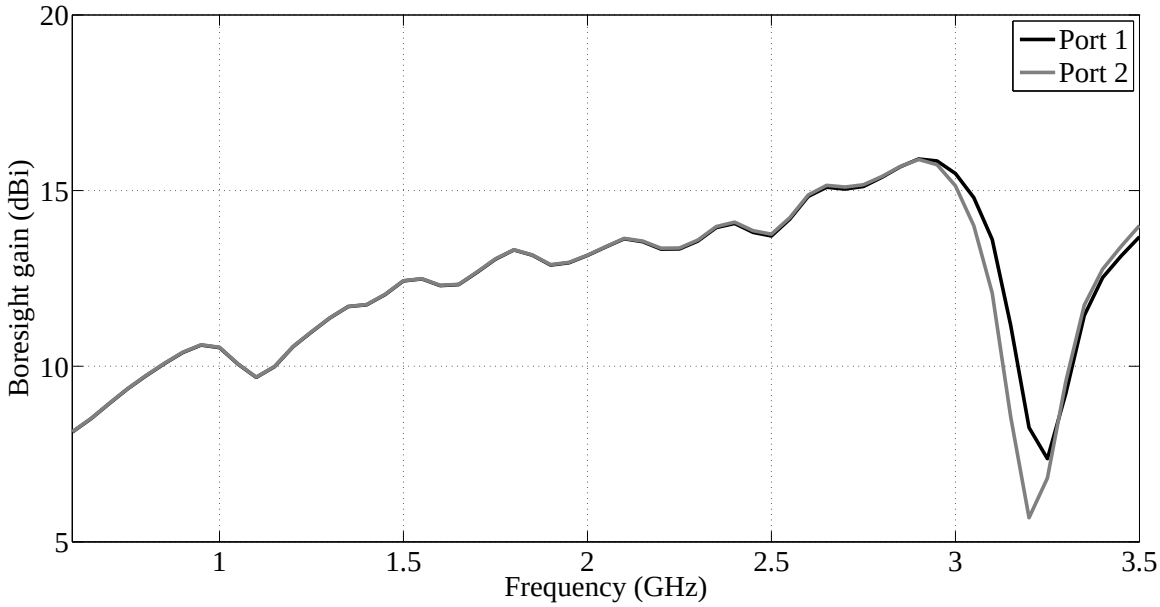

Figure 4.4. The difference in boresight gain for the two ports.

The coupling between ports for a number of different port separations are shown in Figure 4.5. The coupling is below -40 dB for the port separations that were considered.

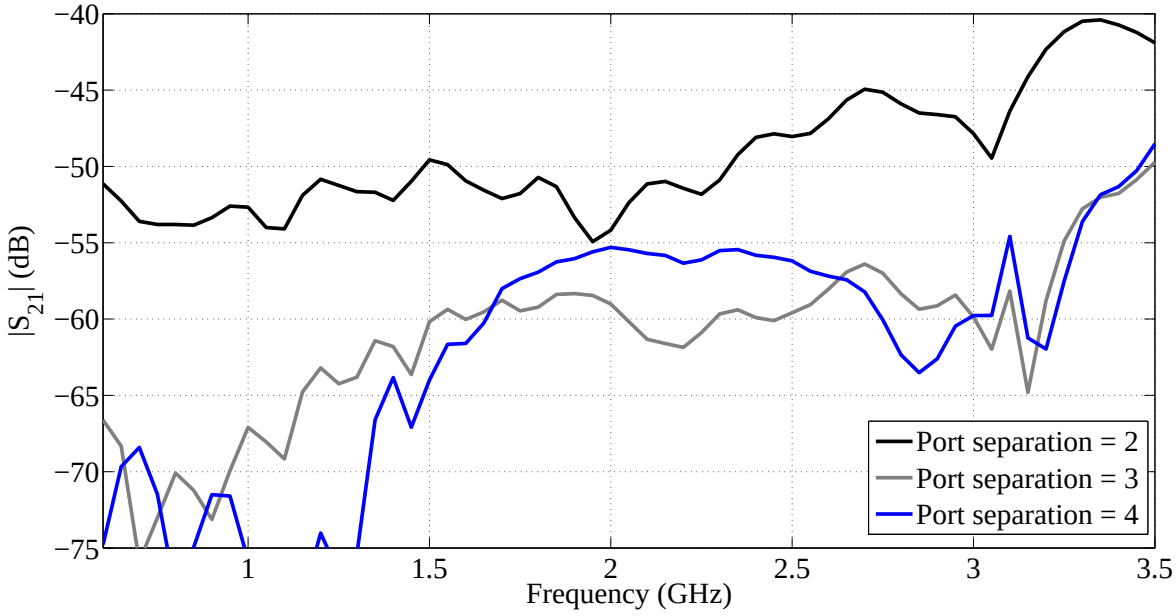

Figure 4.5. The port coupling ($|S_{21}|$) for different distances (mm) between the orthogonal feed pins.

Any asymmetry in the construction can significantly increase the coupling between the ports. A port separation of 3 mm gave good coupling results and the impedance and radiation characteristics corresponded well. With this port separation the outer conductors of the coaxial line did not overlap significantly.

The good agreement between the simulated impedance and radiation characteristics of the two ports of the antenna justifies the assumption that the performance of the two ports are similar and that the performance of only a single port needs to be considered in the parametric study. Simulating the antenna with a single port and a plane of symmetry significantly reduced the computational time required to complete the parametric study. The result obtained for the quad-ridge horn with a single port and a plane of symmetry was virtually identical to the results obtained for port 1 (the port with a corresponding position in the waveguide).

4.4 Waveguide

This section investigates the geometry features in the waveguide section. For this set of parameter changes very little change in the radiation pattern results are expected, except at the band edges where changes to the waveguide geometry can affect the cut-off frequency and suppress or allow higher order mode propagation. The value of the study lies in showing which changes can be used to affect the reflection coefficient of the antenna and whether these geometry features affect the impedance strongly and would require tight manufacturing tolerances. In addition the changes could also aid in obtaining wider impedance bandwidth by investigating how higher order mode propagation can be suppressed. Parameters that define the quad-ridge waveguide geometry are listed below.

- Ridge thickness. The width of the ridges. This width is a constant from the feed point to the aperture.
- Ridge gap. The gap between pairs of opposing ridges.
- Waveguide size. The size of the square waveguide that encloses the ridges.

4.4.1 Ridge thickness

The ridge thickness of the quad-ridge antenna was varied from 5 to 25 mm. The ridges had the same thickness throughout (from feed to aperture) and were chamfered as in Figure 4.6. All other parameters remained the same as that of the basic model.

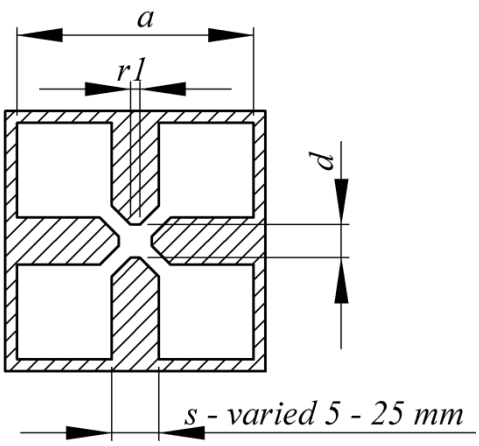

Figure 4.6. The geometry of the quad-ridge waveguide indicating changes to the ridge thickness parameter.

The simulated reflection coefficients of the antenna model with different ridge thicknesses are shown in Figure 4.7. The ridge thickness had a strong causal effect on the reflection coefficient of the antenna. For ridge thicknesses of 5 and 10 mm the antenna is reasonably well matched, while for larger ridges the reflection coefficient deteriorates (50 Ω system).

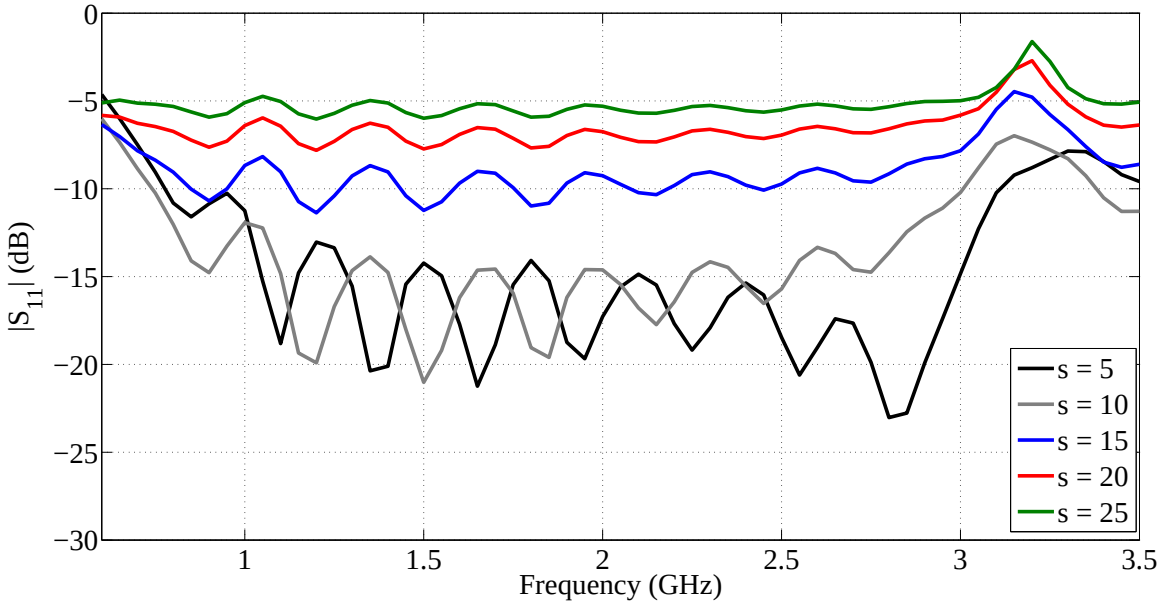

Figure 4.7. The reflection coefficients of quad-ridge horn antennas with different ridge thicknesses.

The boresight gain of the quad-ridge horn antenna for different ridge widths is shown in Figure 4.8. As expected the boresight gain varies little for different ridge thicknesses except for higher frequencies, where the cut-off frequency of higher order modes are affected by the waveguide dimensions. Slightly thicker ridges seem to offer a larger bandwidth in terms of the boresight gain, although with thicker ridges the impedance changes significantly and the impedance bandwidth becomes much smaller.

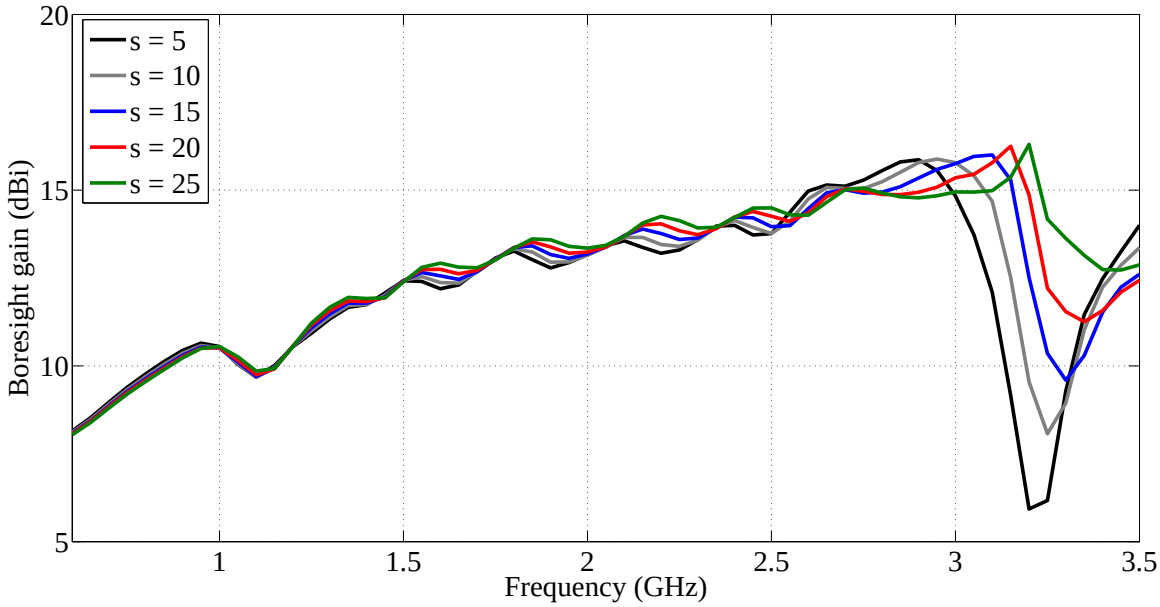

Figure 4.8. Boresight gains of quad-ridge horn antennas with different ridge thicknesses.

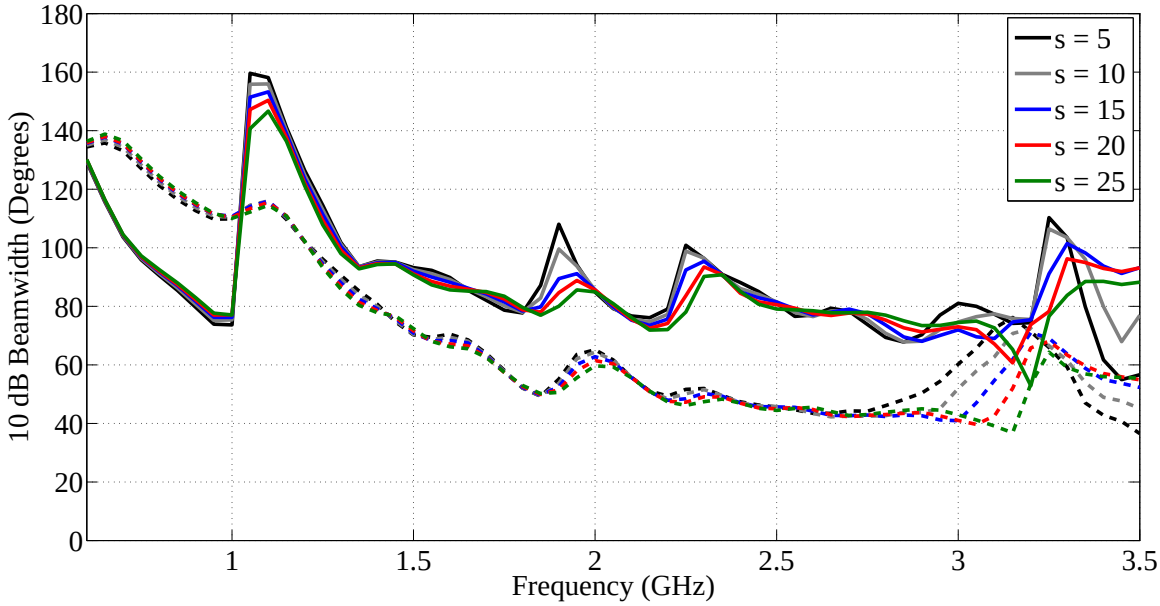

Figure 4.9. 10 dB beamwidths of quad-ridge horn antennas with different ridge thicknesses (E-plane: Solid, H-plane: Dashed).

The 10 dB beamwidth of the quad-ridge horn antenna for different ridge widths is shown in Figure 4.9. Little change is observed in the 10 dB beamwidth except at high frequencies, due to higher order mode propagation. The sudden changes in the beamwidth indicate the presence of side lobes in the radiation pattern close to the -10 dB level. This is undesirable as it leads to increased spill-over. It is also seen that the E- and H-plane beamwidth differ significantly and has large variations across the bandwidth (the beam narrows as frequency increases, as expected for an aperture type antenna).

4.4.2 Ridge gap

The ridge gap (d) is measured as in Figure 4.10 and was varied from 3 to 7 mm for s = 8 mm. Similar to the ridge thickness parameter changes, no or little change is expected in the radiation pattern except possibly for high frequencies.

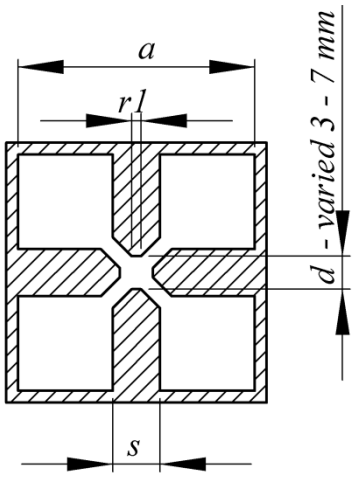

Figure 4.10. The geometry of the quad-ridge waveguide indicating changes to the ridge gap parameter.

The reflection coefficient, shown in Figure 4.11, is strongly affected the ridge gap and a smaller ridge gap tends to lead to improved reflection coefficients. Although this is not necessarily a monotonic improvement as can be seen when comparing models with d = 3 and d = 4 mm. Very small ridge gaps would be undesirable as it would make the antenna difficult to manufacture.

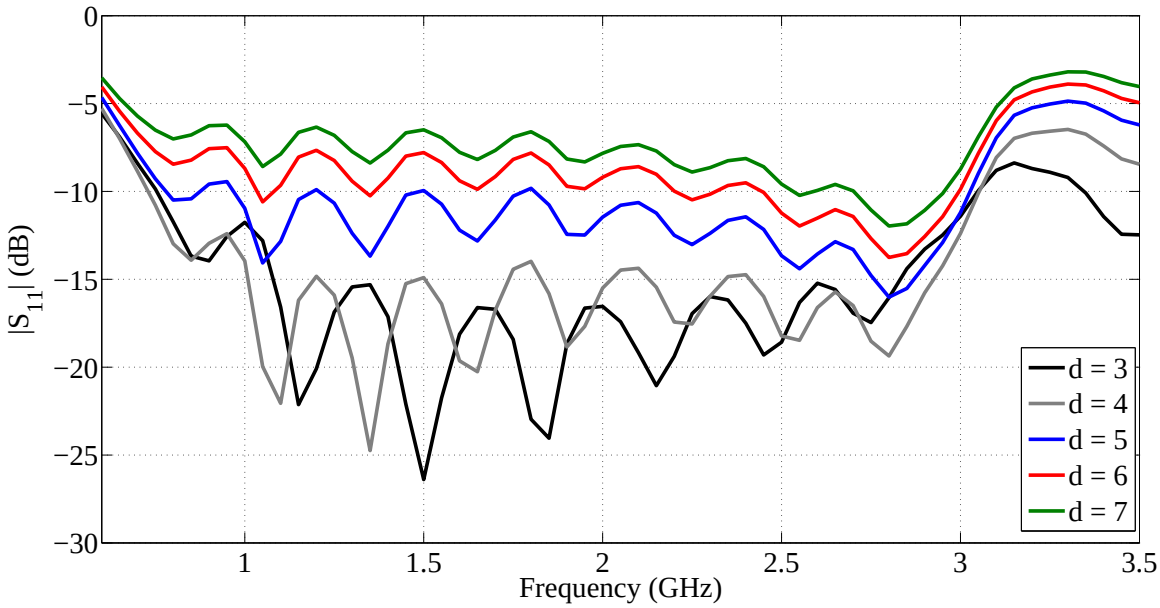

Figure 4.11. Reflection coefficients of the quad-ridge horn antennas with different ridge gaps.

The boresight gain in the Figure 4.12 shows that the ridge gap has very little influence on the radiation pattern.

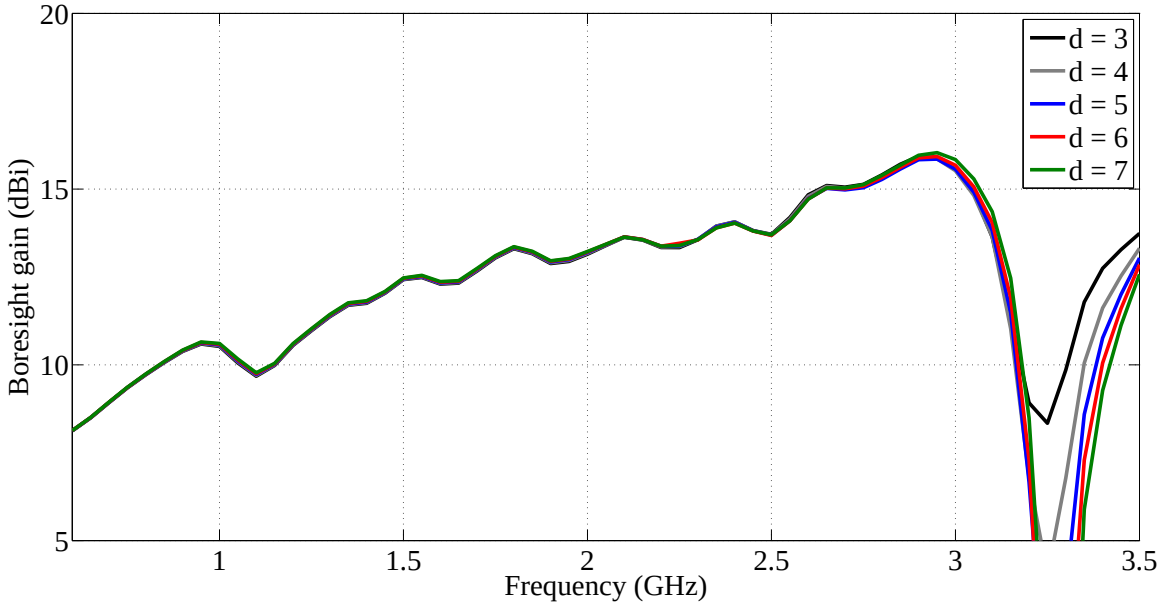

Figure 4.12. Boresight gains of quad-ridge horn antennas with different ridge gaps.

The 10 dB beamwidth, shown in Figure 4.13 confirms that this parameter has little effect on the radiation pattern. The only change in beamwidth is at the high frequency end due to higher order mode propagation – the frequency point at which higher order modes start to propagate remains reasonably constant. This indicates the ridge gap has little influence on the bandwidth of the waveguide.

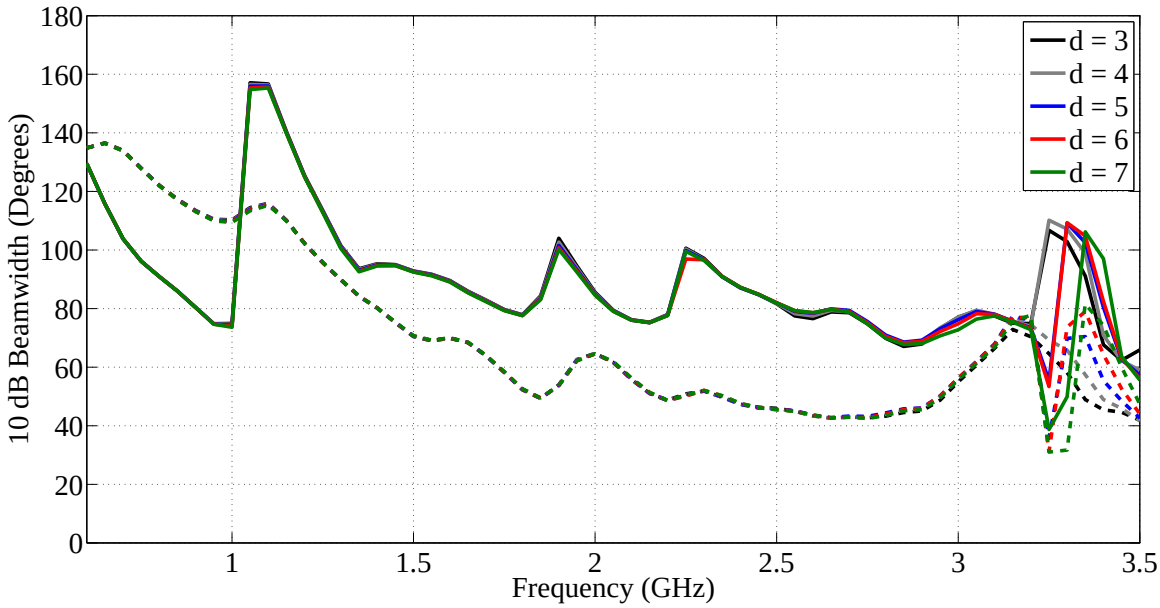

Figure 4.13. 10 dB beamwidths of quad-ridge horn antennas with different ridge gaps (E-plane: Solid, H-plane: Dashed).

4.4.3 Waveguide size

The waveguide size is varied while the ridge gap and width are held constant. This section demonstrates how the waveguide size primarily dictates the bandwidth of the antenna. As the waveguide size is increased the lower cut-off frequency decreases and the frequency at which higher order mode propagation occurs also decreases – shifting the bandwidth to lower frequencies. The waveguide size is expected to affect the radiation pattern strongly only for higher frequencies where higher order mode propagation occurs. The size was varied from 70 to 120 mm as shown in Figure 4.14.

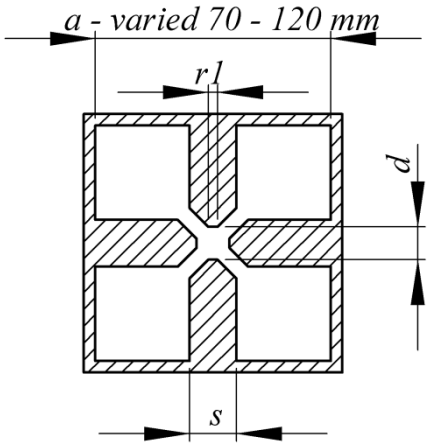

Figure 4.14. The geometry of the quad-ridge waveguide indicating changes to the waveguide size parameter.

The reflection coefficient, in Figure 4.15, clearly shows how the bandwidth of the antenna changes as the waveguide size is increased. Large waveguides leads to a shift towards lower frequencies.

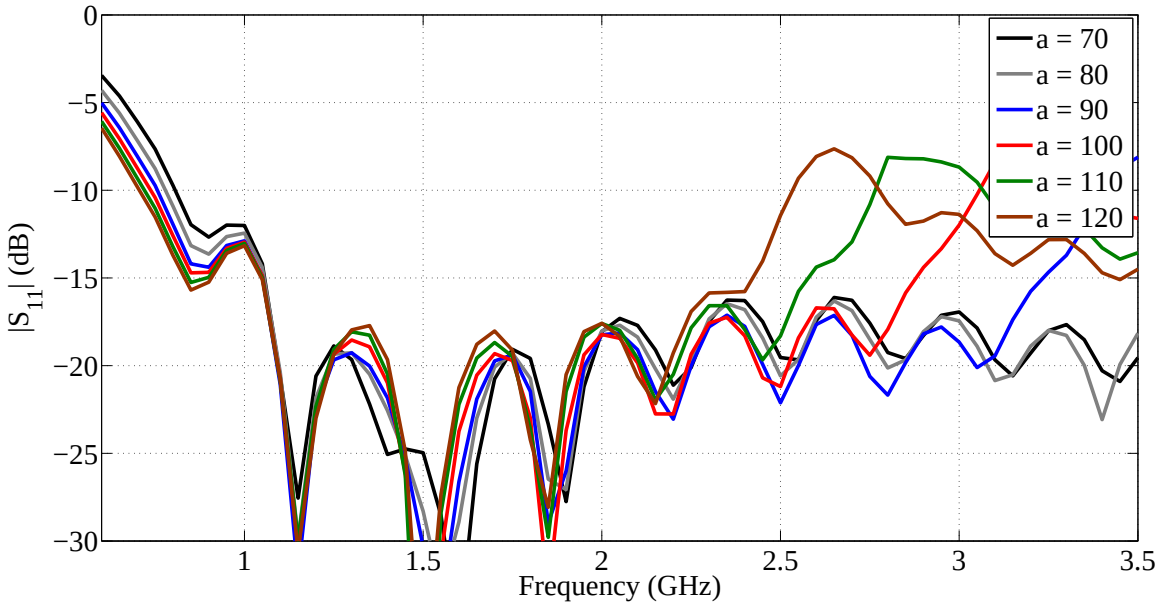

Figure 4.15. Reflection coefficients of quad-ridge horn antennas with different waveguide sizes.

The propagation of higher order modes for larger waveguides affects the radiation patterns at higher frequencies – causing a sharp decrease in boresight gain as a result of pattern break-up, the pattern split into four beams. Figure 4.16 shows the simulated boresight gain.

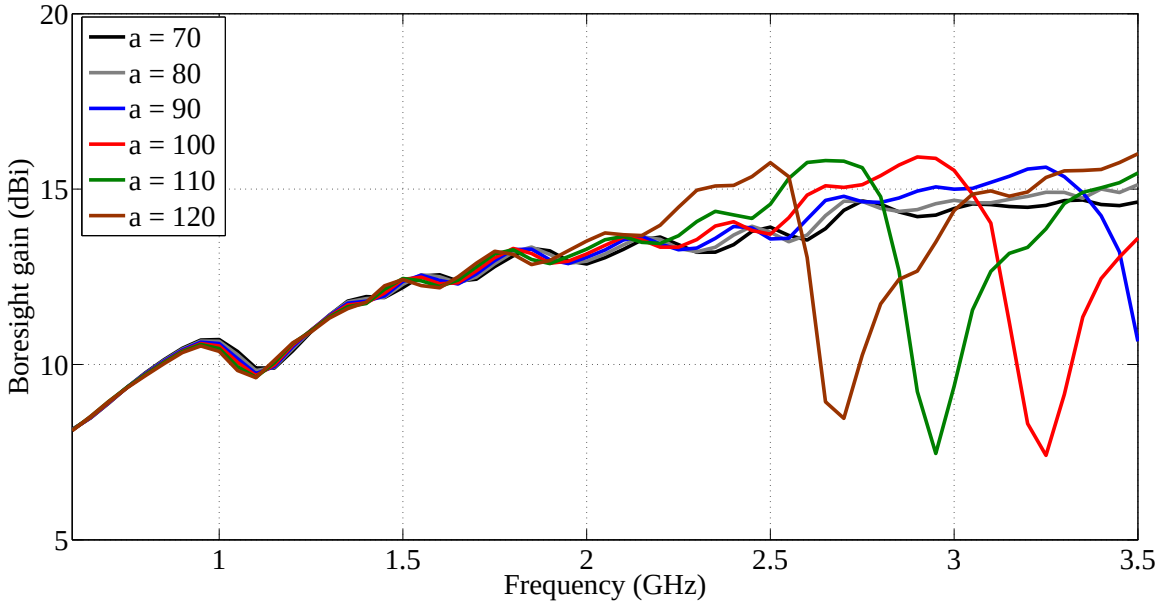

Figure 4.16. Boresight gains of quad-ridge horn antennas with different waveguide sizes.

The largest effect on the 10 dB beamwidth for this parameter change is at higher frequencies as with the boresight gain. The 10 dB beamwidth is shown in Figure 4.17.

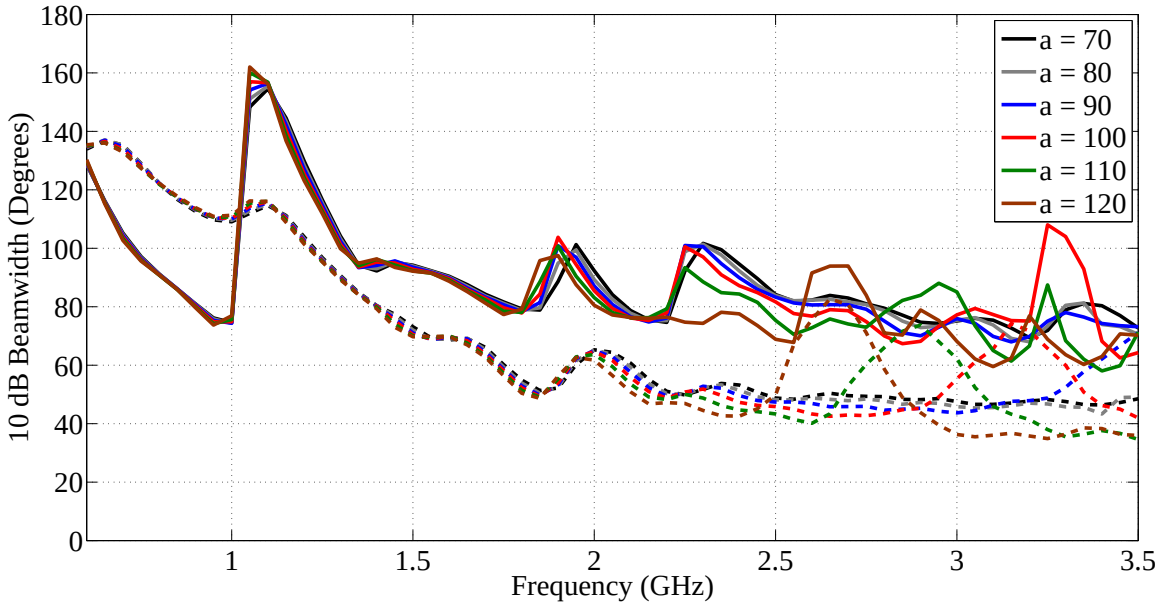

Figure 4.17. 10 dB beamwidths of quad-ridge horn antennas with different waveguide sizes (E-plane: Solid, H-plane: Dashed).

4.5 Backshort

The backshort is part of the transition from coaxial to quad-ridge waveguide. The backshort ensures radiation occurs towards boresight. Omitting the backshort leads to a design where the antenna radiates a large portion of the energy away from boresight, similar to a TEM horn antenna radiating in the dipole mode [80].

Improper design of the backshort can lead to increased reflection and the excitation of higher order modes. This section investigates the distance from the backshort to the ridges and the introduction of steps in the backshort to improve the bandwidth of the transition – and suppress higher order modes. The parameters investigated and their physical descriptions are listed below.

- Back plate distance. The distance from the end of the ridges to the back plate.
- Ridge step height. The height of a step in the ridge to transition into the backshort.

4.5.1 Back plate distance

The distance from the feed to the backshort has an effect on the reflection coefficient of the antenna. The backshort distance can affect the low frequency cut-off as well as reduce the effect of higher order mode propagation on the reflection coefficient. The geometry of the backshort is shown in Figure 4.18.

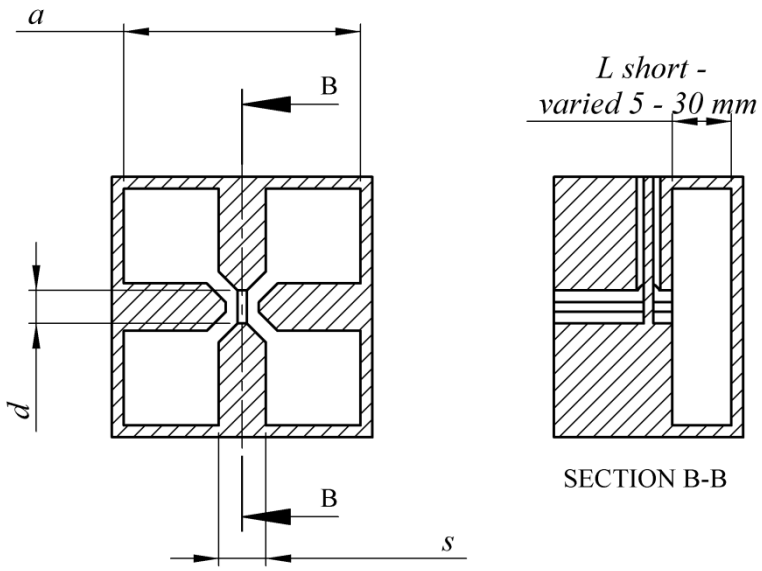

Figure 4.18. The geometry of the waveguide and backshort indicating changes to the back plate distance.

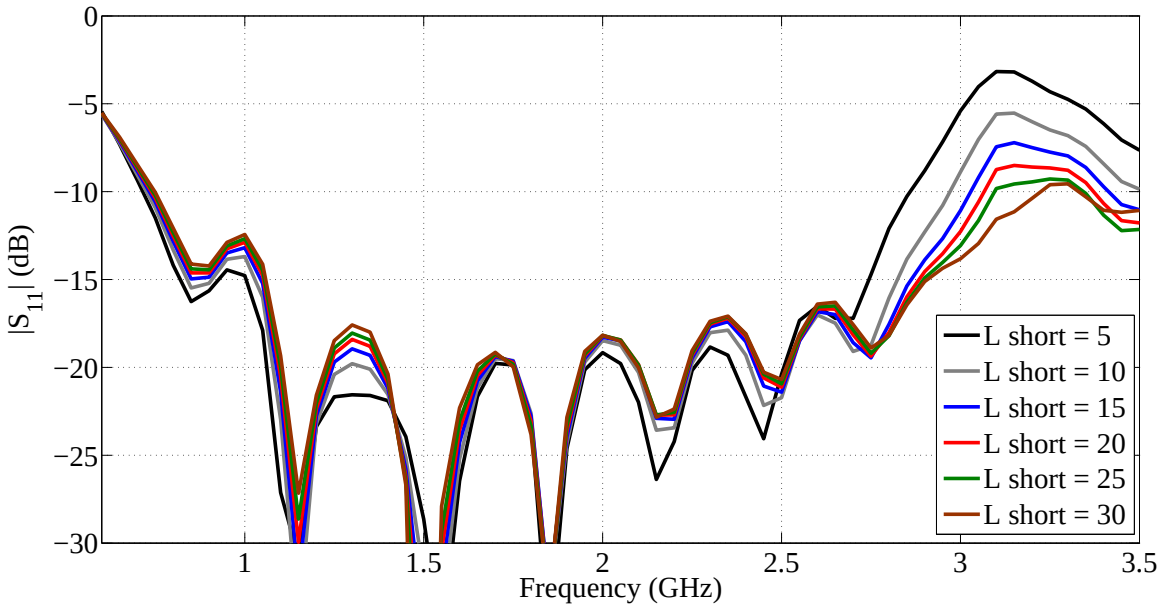

Figure 4.19. Reflection coefficients of quad-ridge horn antennas with different distances to the backshort

The simulated reflection coefficient, shown in Figure 4.19, indicates that the distance to the back plate affects the reflection coefficient at higher frequencies – and that by changing this parameter the impedance bandwidth of the antenna could be improved. A smaller effect is observed for low frequencies.

The boresight gain, shown in Figure 4.20, has a sharp drop in gain at the same frequency for different backshort distances and although $|S_{11}|$ might be less than -10 dB the radiation pattern is not suitable for a reflector antenna feed beyond this frequency. Over other portions of the bandwidth changing the backshort distance has little effect on the boresight gain as shown in Figure 4.20.

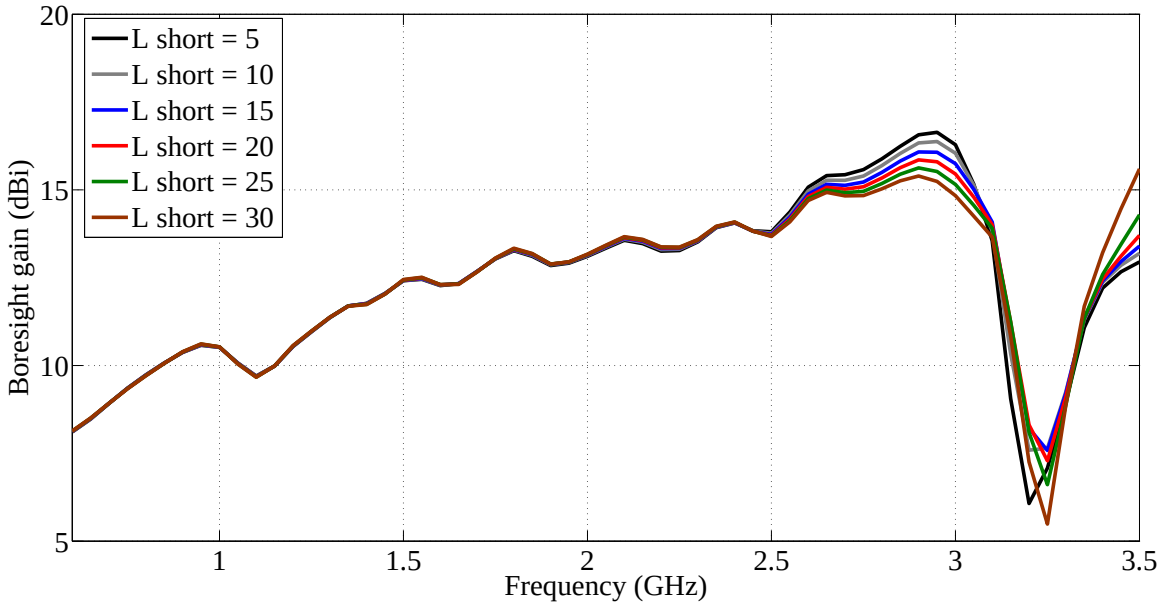

Figure 4.20. Boresight gains of quad-ridge horn antennas with different distances to the backshort.

The 10 dB beamwidth, shown in Figure 4.21, indicates that the backshort distance has little effect on the radiation patterns. It is evident that merely adjusting the distance to the backshort is not an effective method of controlling higher order mode propagation. The impedance bandwidth of the antenna might improve by optimizing this parameter but the radiation characteristics would remain largely the same and the bandwidth over which the antenna would be an effective reflector antenna feed would remain unchanged – limited by the onset of higher order modes affecting the radiation characteristics.

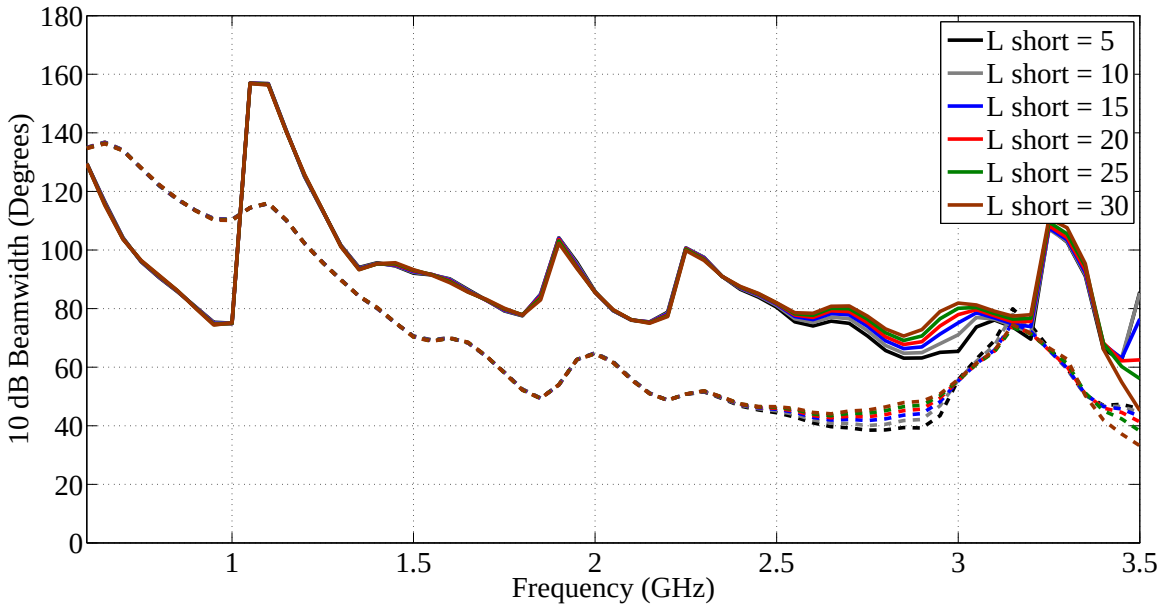

Figure 4.21. 10 dB beamwidths of quad-ridge horn antennas with different distances to the backshort (E-plane: Solid, H-plane: Dashed).

4.5.2 Ridge step height

Steps are introduced in the backshort to prevent the excitation of higher order modes in the coaxial to waveguide transition. This increases the overall usable bandwidth of the antenna. The height of the steps required to achieve a larger bandwidth is investigated. The steps are the same width as the ridges (instead of ending at the backshort the ridges are first stepped down). The geometry of the steps in the backshort is shown in Figure 4.22.

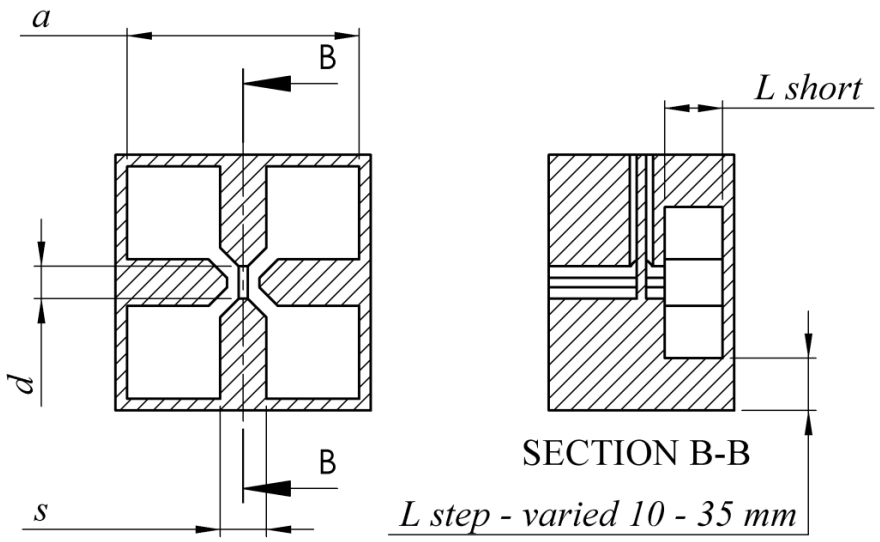

Figure 4.22. The geometry of the waveguide and backshort indicating the position and the changes to the height of the steps in the backshort.

The simulated reflection coefficient of the antennas is shown in Figure 4.23. As can be seen from the reflection coefficient the steps in the waveguide section are effective at preventing the excitation of higher order modes.

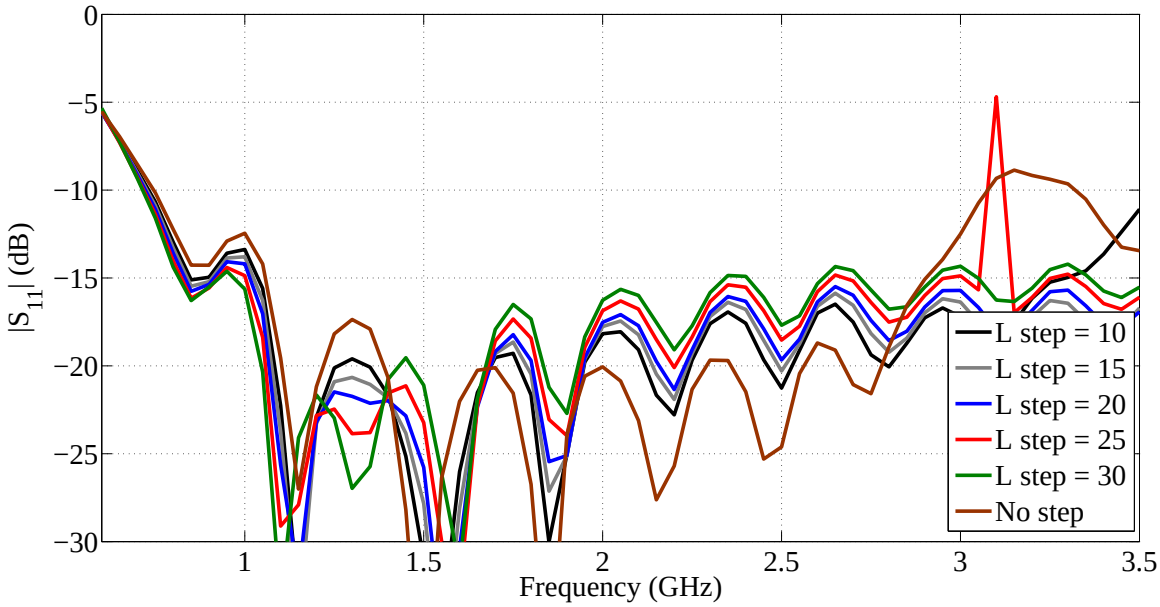

Figure 4.23. Reflection coefficients of quad-ridge horn antennas with different backshort step heights.

The steps increased the usable bandwidth of the antenna, although large step heights resulted in a slight increase in the reflection coefficient in the band. In addition for one of the step heights simulated (25 mm) the step caused a sharp resonance in the reflection coefficient. For this step height the waveguide section in the backshort has become a resonant cavity that trapped energy at a specific frequency. Narrow resonances such as these can be detected using FEKOs adaptive frequency sampling allowing the cavity to be redesigned to prevent these resonances. Resonances commonly occur in coaxial to quad-ridge waveguide transitions in OMTs, and often require special techniques to suppress [49].

The boresight gain in Figure 4.24 showed very little deviation for different step heights. The resonance observed in the reflection coefficient for L = 25 is also observed in the boresight gain. The model with the smallest step in the waveguide, L = 10, shows a reduction of boresight gain at the very edge of the band.

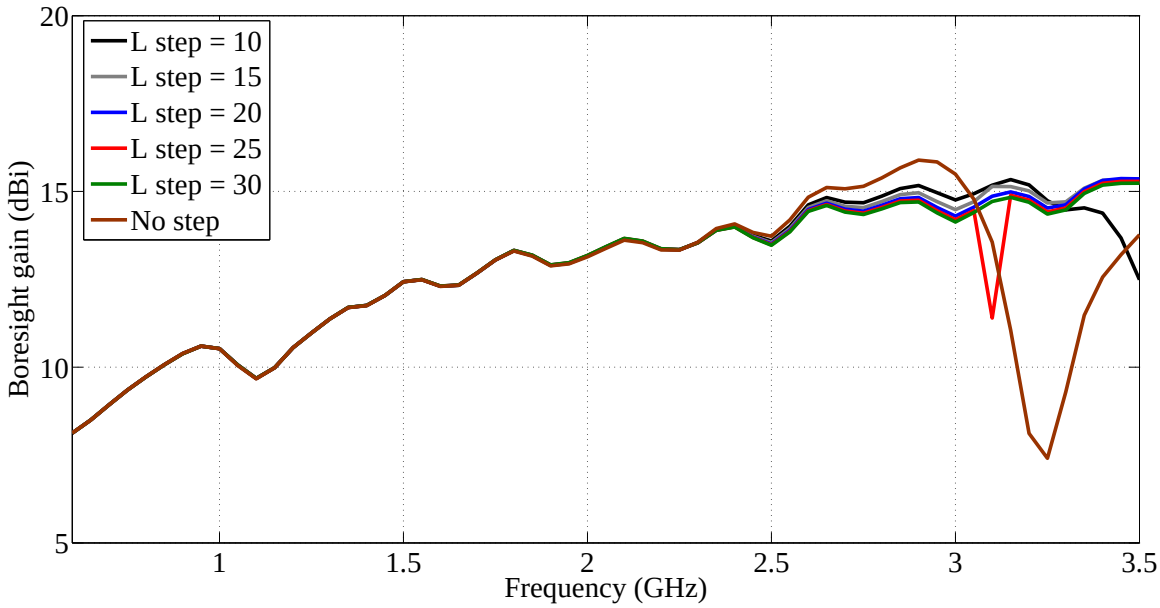

Figure 4.24. Boresight gains of quad-ridge horn antennas with different backshort step heights.

The 10 dB beamwidth shown in Figure 4.25 confirm that the radiation pattern shows very little change for different step heights. The radiation pattern has, however, been improved compared to an antenna without steps in the backshort, in that higher order mode excitation has been delayed to a much higher frequency extending the usable bandwidth.

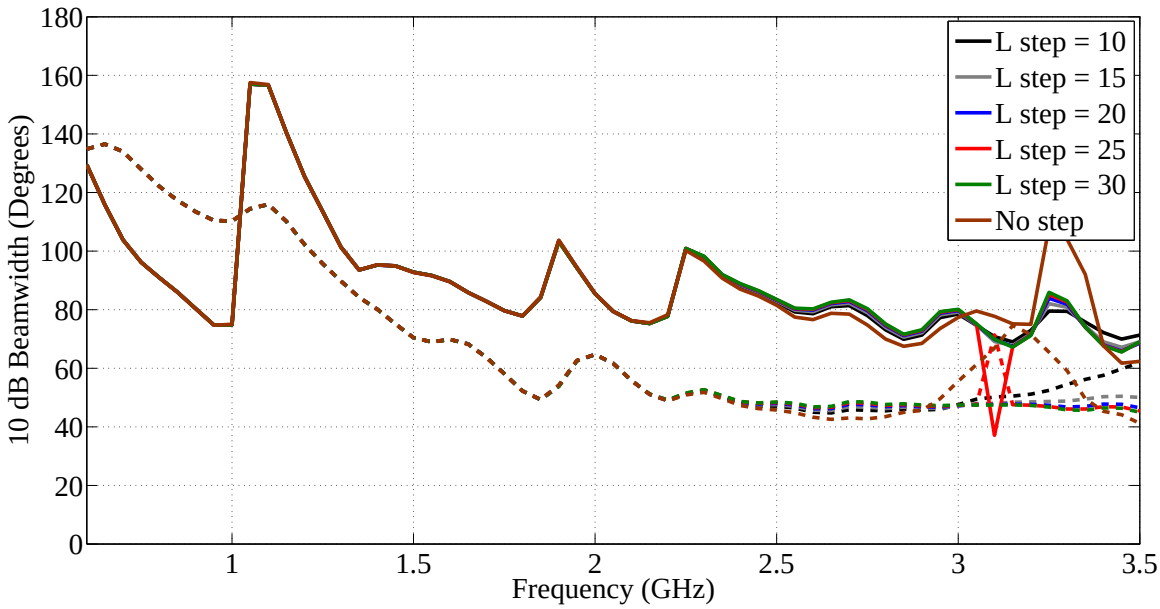

Figure 4.25. 10 dB beamwidths of quad-ridge horn antennas with different backshort step heights (E-plane: Solid, H-plane: Dashed).

Comparison of the 10 dB beamwidth to an antenna without the steps in the backshort shows that for frequencies higher than 3 GHz the boresight gain does not have a sharp

decrease, except for L = 10, the smallest step, where the gain just starts to decrease at the very edge of the band. The 10 dB beamwidth also does not have any sudden changes (indicating large side lobes) at these frequencies (3 – 3.5 GHz).

4.6 Ridge Profile

The ridges constitute the transition from guided wave to free-space. As such it has a direct effect on the impedance of the antenna by virtue of the fact that it is a transition from the impedance of the waveguide to free-space impedance. In addition the ridges have to be tapered in such a fashion as to prevent higher order modes from being exited in the transition while still allowing the low frequencies to propagate freely. The ridge profile also affects the radiation pattern in the pass band of the antenna.

The ridges that were investigated had exponential and elliptical profiles. The exponential profiled ridges are described by,

$$y = a(e^{Rx} - 1) \tag{4.1}$$

$$a = \frac{y_{end}}{(e^{Rx_{end}} - 1)} \tag{4.2}$$

where y_{end} and x_{end} are the desired end points of the ridge profile and R determines the growth rate of the exponential curve [81]. Examples of the ridges obtained for different values of R, is shown in Figure 4.26. A small value of R results in a nearly linear profile. Exponential ridges are also compared to an elliptical ridge profile.

The elliptical ridge profile is a quarter of an ellipse and can be described by,

$$y = y_{end} - y_{end}\sqrt{1 - \frac{x^2}{{x_{end}}^2}} \tag{4.3}$$

where y_{end} and x_{end} are the desired end points of the elliptic ridge profile (the ridge start point is at the origin).

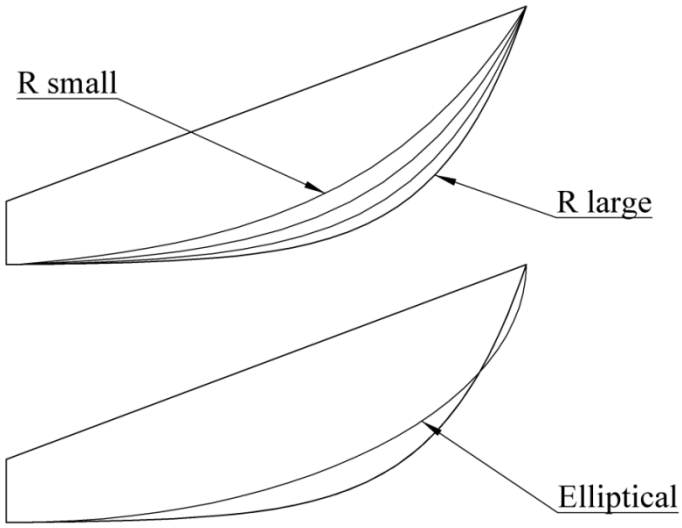

Figure 4.26. Comparison of some of the different ridge profiles that were investigated

The reflection coefficient obtained for a number of different ridges is shown in Figure 4.27. It can be seen that the ridge profile has a large effect on the impedance matching of the antenna. Smaller values of *R* (a more linear transition) resulted in deteriorated reflection coefficients.

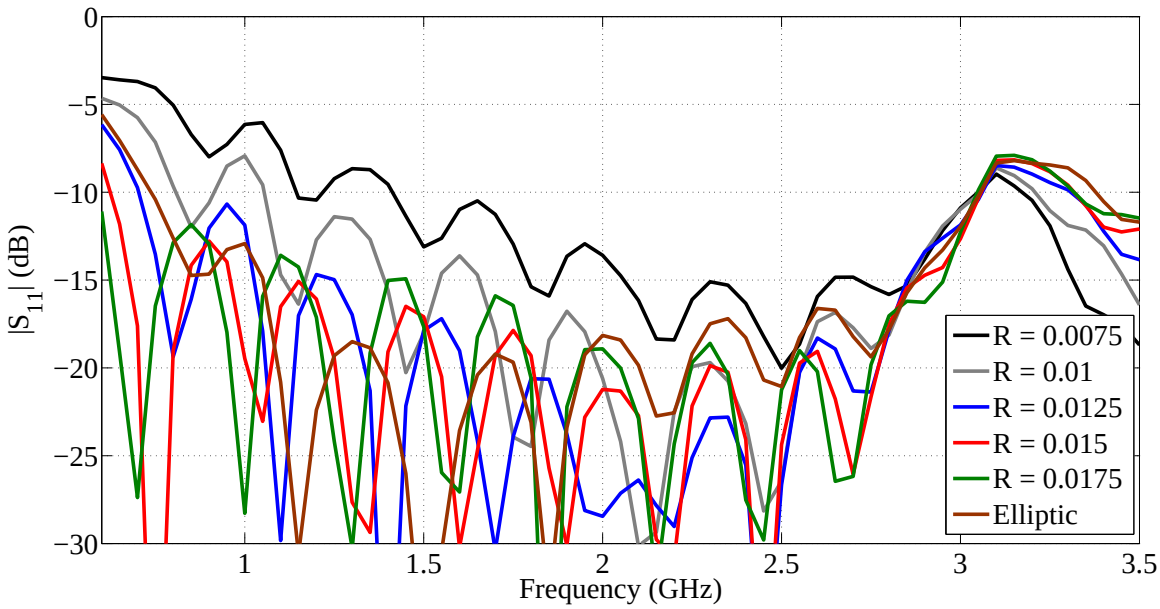

Figure 4.27. Reflection coefficients of quad-ridge horn antennas with different ridge profiles.

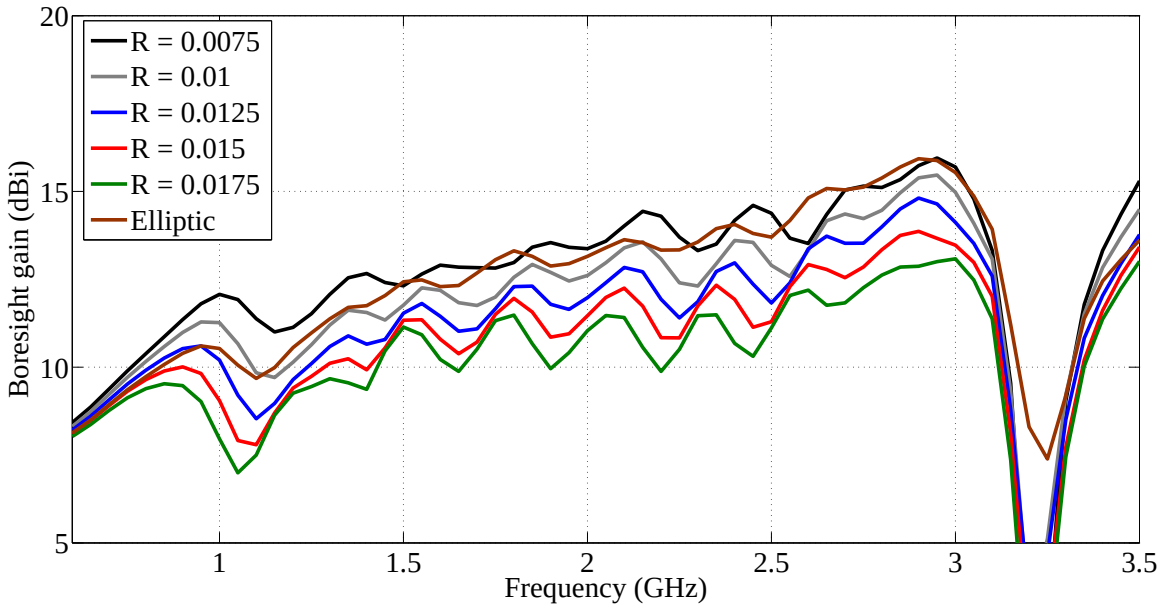

Figure 4.28. Boresight gain of quad-ridge horn antennas with different ridge profiles.

The boresight gain, shown in Figure 4.28, is affected by the ridge transition with large *R* values having a lower gain, wider beamwidths are thus expected. However, the 3 dB beamwidth in Figure 4.29 and 10 dB beamwidth in Figure 4.30 indicate that for large values of *R* the radiation patterns have significantly larger side lobes. This was confirmed by the radiation patterns.

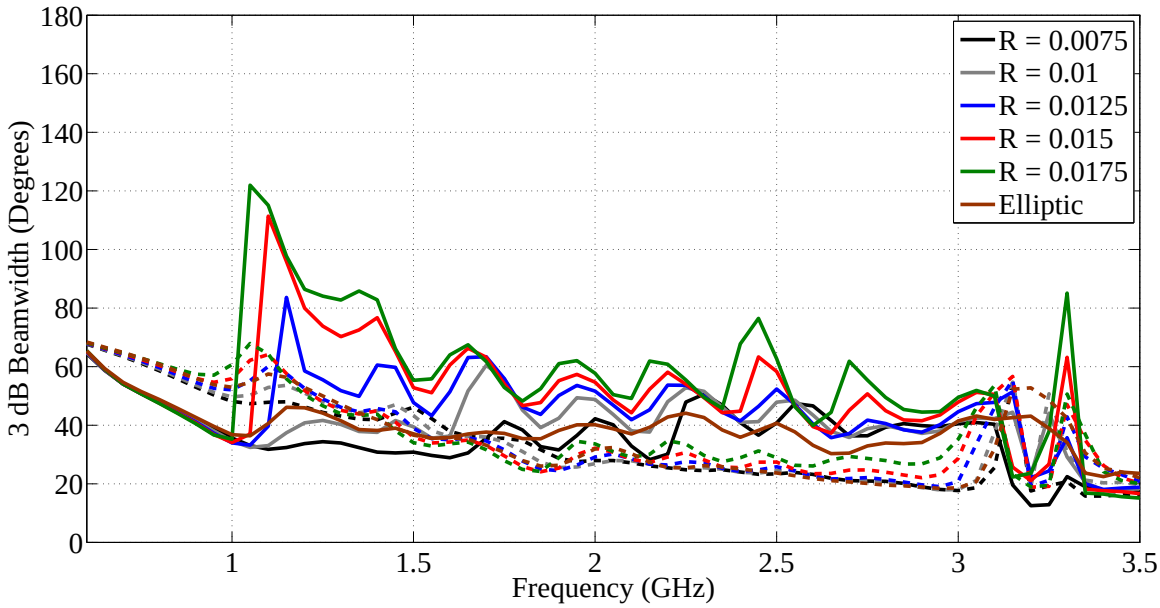

Figure 4.29. 3 dB beamwidths of quad-ridge horn antennas with different ridge profiles (E-plane: Solid, H-plane: Dashed).

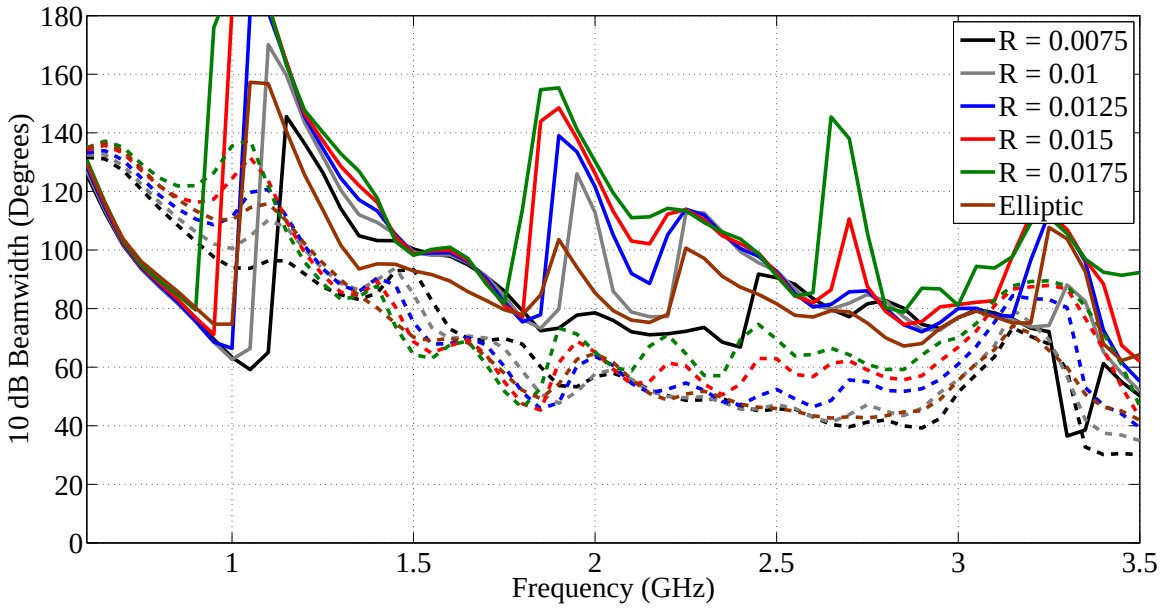

Figure 4.30. 10 dB beamwidths of quad-ridge horn antennas with different ridge profiles (E-plane: Solid, H-plane: Dashed).

These large side lobes are undesirable and in a reflector would cause significant spill-over. Increasing *R* had the effect of improving the reflection coefficient, lowering gain and widening the beamwidth – though at the cost of increased side lobes.

The elliptic ridge was seen as a good compromise between obtaining a good reflection coefficient and acceptable radiation patterns. The ridges were not seen as a very effective method of improving the radiation patterns of the quad-ridge horn. The patterns still have large variations in terms of beamwidth. The difference between the E- and H-planes was still significant – an increase in E-plane beamwidth was accompanied by an increase in the H-plane beamwidth.

Although the study indicates that adapting the ridge profile would not necessarily be a very effective method of obtaining improved radiation patterns it highlights that optimizing the ridge transition is essential to obtain acceptable reflection coefficients (as has been shown in previous studies) and radiation characteristics, especially with respect to side lobes.

4.7 Sidewalls

TEM and waveguide horn antennas with close to equal E- and H-plane patterns and reasonably constant beamwidths over a wide bandwidth have been demonstrated [24, 79].

In this section quad-ridge horn antennas with shaped sidewalls are compared to antennas with conventional (straight) sidewalls as well as open-boundary quad-ridge horns (quad-ridge horns without sidewalls) [18] to determine if the radiation patterns can be made more suitable for use as reflector antenna feeds. Shaped sidewall quad-ridge horn antennas have recently been demonstrated to have reasonably constant beamwidth [15, 26] and need to be investigated further.

Aspects related to the quad ridge horn antenna sidewalls that are investigated in this section are listed below.

- A comparison is made between antennas with shaped sidewalls, straight sidewalls and without sidewalls.
- The profile of shaped sidewall quad-ridge horn antennas is investigated.
- Quad-ridge horn antenna geometries are compared and the antenna geometry most suitable for a shaped sidewall quad-ridge horn antenna reflector feed is identified.
- Changes to the ratio between the aperture size and horn length for elliptically shaped quad-ridge horn antennas with various aperture sizes are investigated.

4.7.1 Comparison of shaped sidewall, straight sidewall and open-boundary antennas.

The method used to shape the antenna sidewall is demonstrated in Figure 4.31. In this case the sidewall is shaped elliptically (similar to the ridge profile that is used).

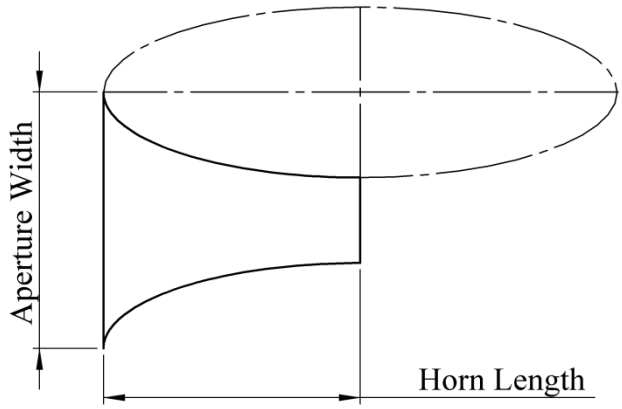

Figure 4.31. Demonstration of how the sidewall is shaped elliptically.

Model dimensions for the shaped antenna are the same as the straight sidewall model dimensions (the model used thus far for the parametric study). The open-boundary antenna is also identical, except the sidewalls have been removed beyond the coaxial to waveguide transition section. The three different FEKO antenna models are shown Figure 4.32 for comparison.

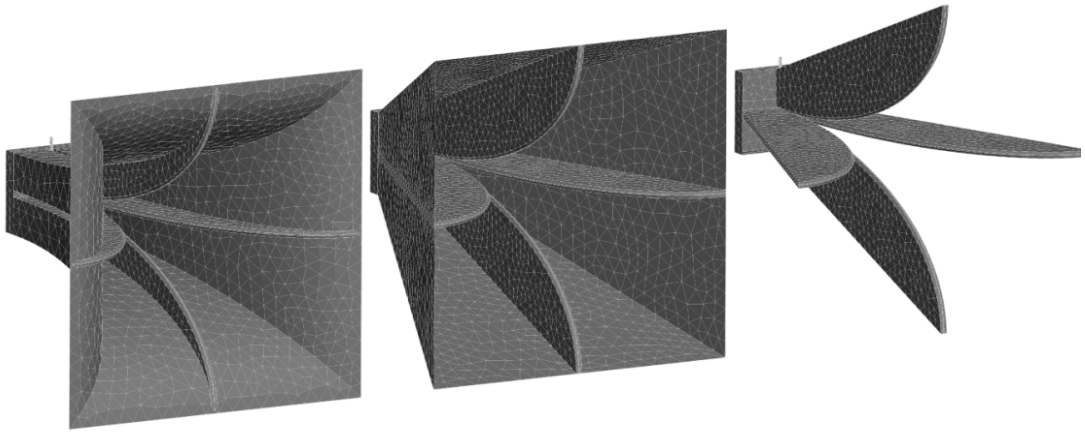

Figure 4.32. From left to right, the quad-ridge horn antenna with elliptically shaped sidewalls, with straight sidewalls and without sidewalls.

The simulated reflection coefficients of the three antennas are shown in Figure 4.33. The straight sidewall and open-boundary antennas are matched from a lower frequency than the shaped antenna and exhibit broader impedance bandwidths.

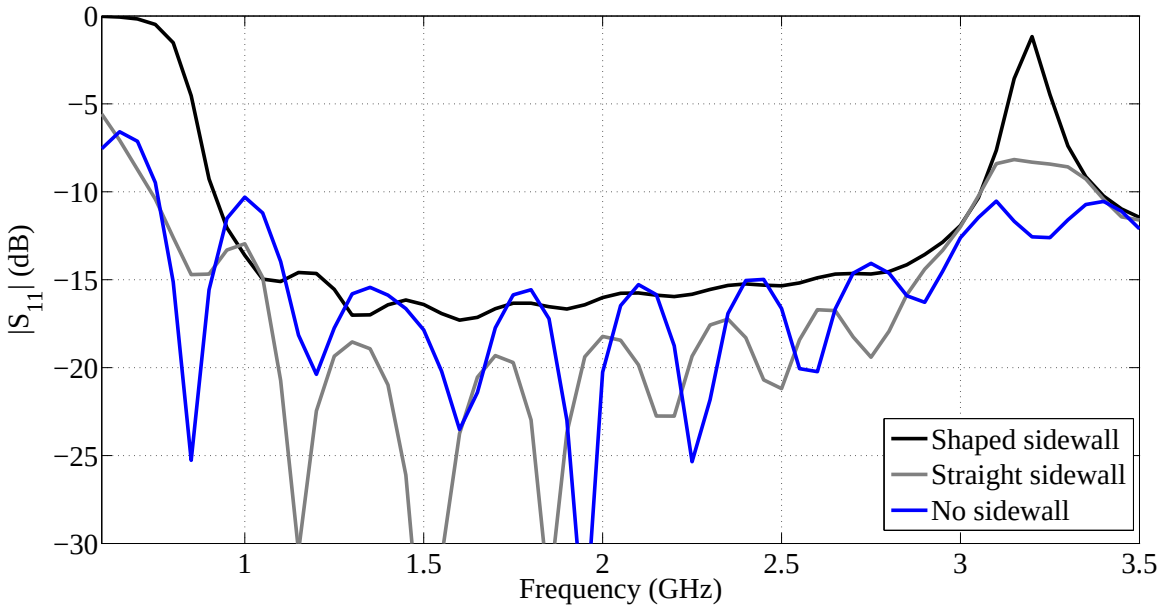

Figure 4.33. Reflection coefficients of quad-ridge horn antennas with different sidewall types.

The boresight gain of the three antennas is shown in Figure 4.34. The antenna without a sidewall has a lower gain, higher beamwidth levels and larger side lobes.

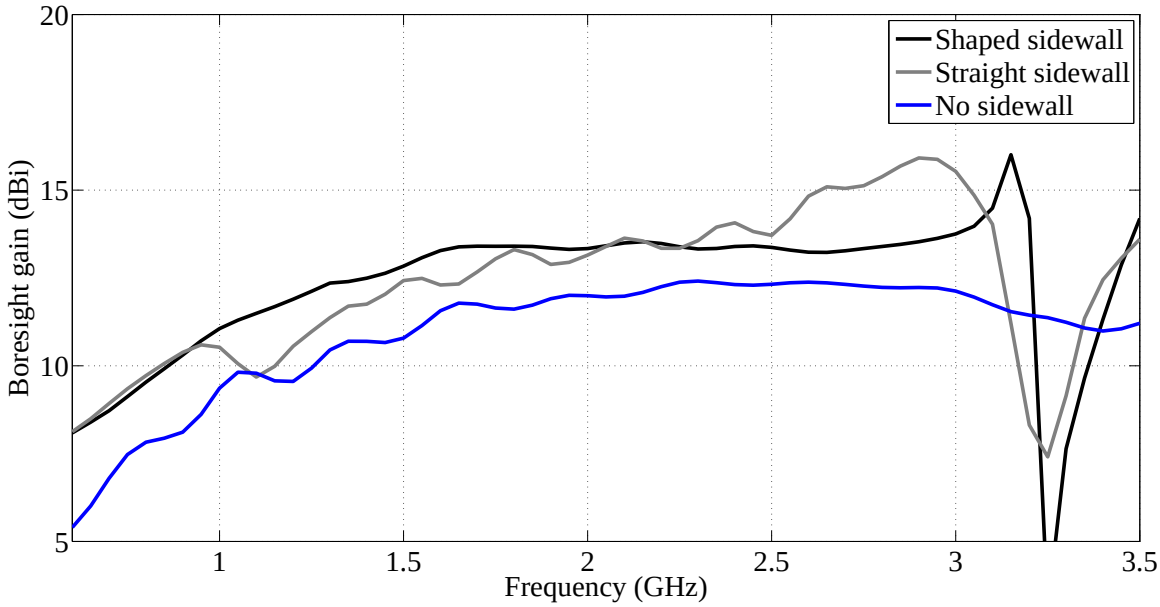

Figure 4.34. Boresight gains of quad-ridge horn antennas with different sidewall types.

The 3- and 10 dB beamwidths are shown in Figures 4.35 and 4.36 respectively. The beamwidths clearly indicate that although the open-boundary antenna has the broadest impedance bandwidth, it is the least suitable as a reflector feed.

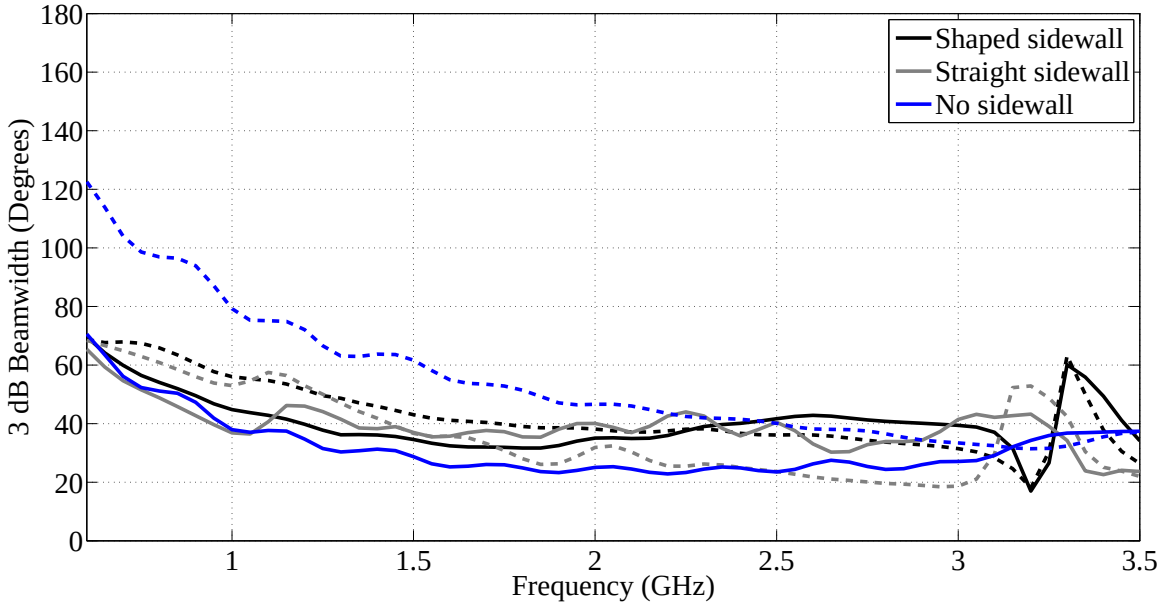

Figure 4.35. 3 dB beamwidths of quad-ridge horn antennas with different sidewall types (E-plane: Solid, H-plane: Dashed).

The E- and H-plane beamwidths are significantly different for this type of antenna and from the sudden changes in the 10 dB beamwidth and the radiation pattern it was seen that the open-boundary antenna has significant side lobes, especially in the E-plane.

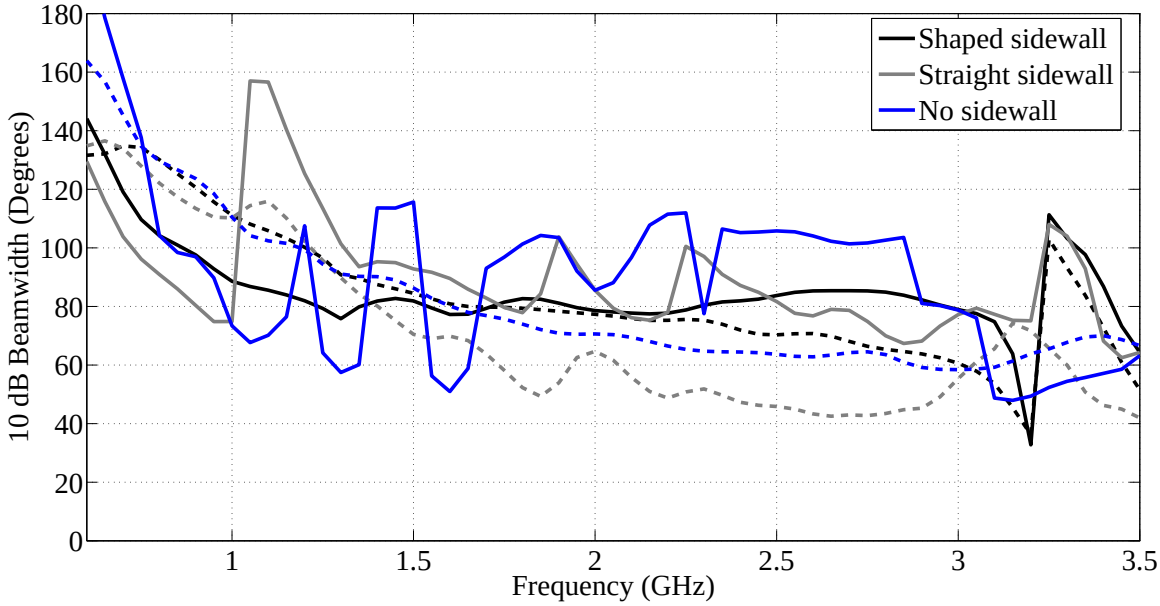

Figure 4.36. 10 dB beamwidths of quad-ridge horn antennas with different sidewall types (E-plane: Solid, H-plane: Dashed).

The straight sidewall antenna – the quad-ridge antenna on which the parametric study is based – has E- and H-plane patterns that are more rotationally symmetrical and have reduced side lobes compared to an open boundary antenna. The shaped sidewall quad-ridge horn has E- and H-plane beamwidths that indicate even greater rotational symmetry as well as no sudden changes in the beamwidth that could indicate side lobes.

The normalized radiation patterns are also shown in Figure 4.37 to clearly show the differences in the patterns. The patterns clearly show that the open-boundary antenna had very large side and back lobes and that the principal plane patterns are dissimilar. Although the parametric study was conducted on both open boundary and straight sidewall horn antennas only the straight sidewall results are presented as the open boundary antennas were found to have inferior radiation characteristics. The parametric study demonstrated that the shaped antenna has improved radiation patterns with respect to rotational symmetry and side lobes (this is especially evident for low frequencies).

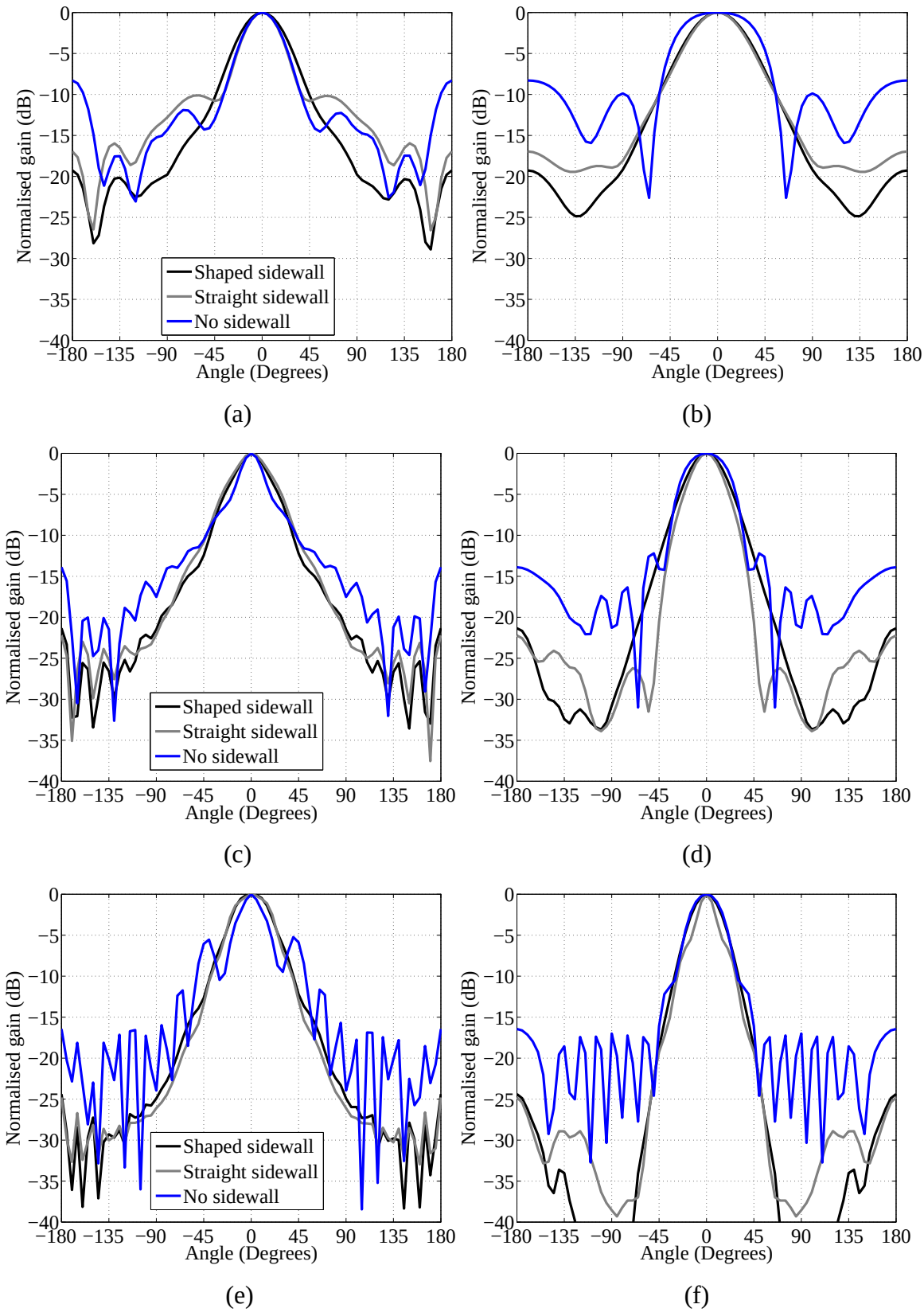

Figure 4.37. Comparison of radiation patterns of quad-ridge horn antennas with different type sidewalls, (a) E-plane at 1 GHz, (b) H-plane at 1 GHz, (c) E-plane at 2 GHz, (d) H-plane at 2 GHz, (e) E-plane at 3 GHz, (f) H-plane at 3 GHz

A disadvantage of the elliptically shaped sidewall is that it is not as well matched as the other antennas at low frequencies. This is due to the fact that the elliptic sidewall opens very slowly. This means there is effectively a section of waveguide before the antenna starts to taper open. Double ridge horn antennas with an exponential impedance taper presented similar problems that required a small linear offset to let the ridges taper open quickly close to the feed [73].

The profile of the ellipse was thus modified to improve the low frequency matching. This was done by shifting and re-scaling the ellipse. Instead of starting the elliptic sidewall as in Figure 4.31 where the centre is directly above the start of the flare the ellipse centre is moved backwards, while scaling the size of the ellipse to maintain the same horn length and aperture width. This results in improved low frequency impedance matching. Figure 4.38 illustrates how the ellipse is offset from the feed point. Only a small offset of the ellipse is required for this effect and it was found that between 1 and 5 mm can significantly improve the impedance matching.

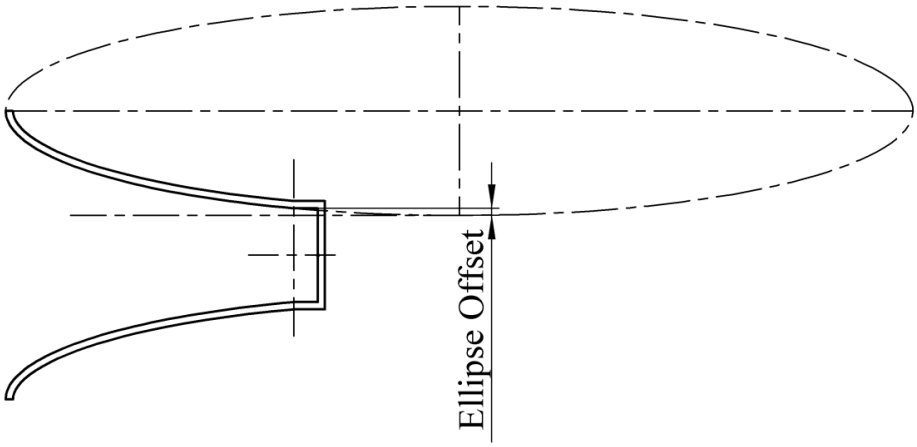

Figure 4.38. The modification made to the elliptic sidewall to improve low frequency impedance matching.

4.7.2 Shaped sidewall profiles

Quad-ridge horn antennas that have sidewalls shaped according to different profiles are compared in this section. Similar to the comparison of ridge profiles various exponential profiles and an elliptical profile are compared. The exponential curve is implemented as for the ridge profile in equations 4.1 and 4.2. The starting point is the edge of the waveguide

and the end point of the profile is at the aperture of the antenna. The antennas were identical in all respects save for the sidewall shape. The elliptically shaped sidewall did not incorporate the change proposed to improve the reflection coefficient for low frequencies (Figure 4.38) and was shaped according to equation 4.3.

The simulated reflection coefficient is shown in Figure 4.39. It can be seen that for exponential sidewalls that open slowly (larger values of *R*) the low frequency reflection coefficient deteriorates while for sidewalls that are closer to linear the low frequency reflection coefficient improves. All the antennas exhibit higher order modes at approximately the same frequency.

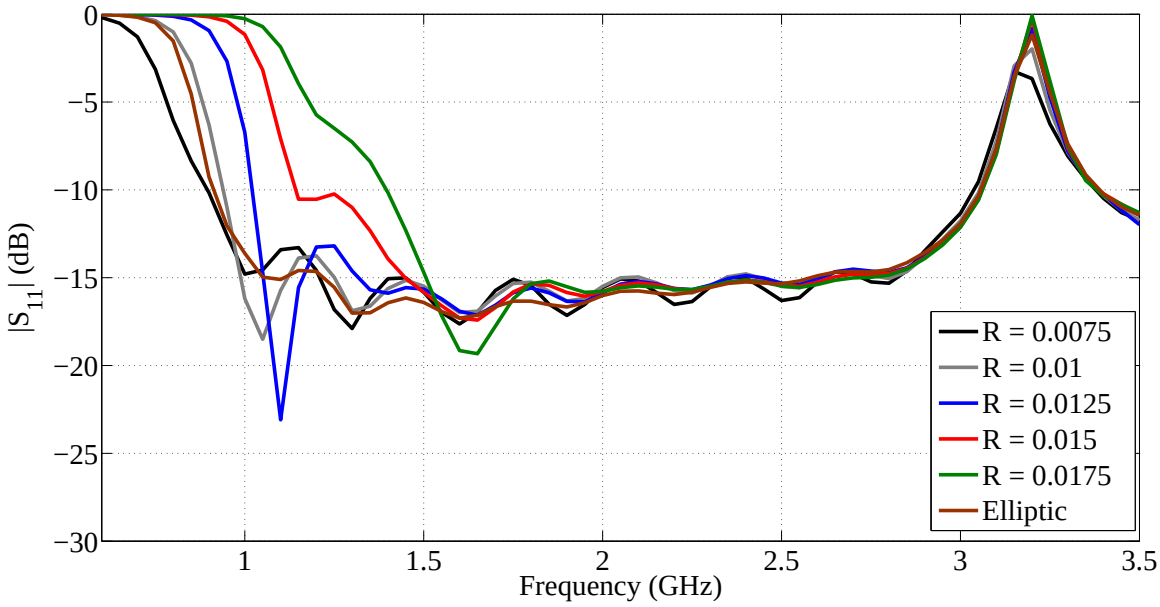

Figure 4.39. Reflection coefficients of quad-ridge horn antennas with different sidewall profiles.

The boresight gain is shown in Figure 4.40. The boresight gain does show some change due to the different sidewall profiles. Given the large changes to the sidewall profile these changes are relatively small – the maximum change in gain being not much more than 1 dB (excluding frequencies above 3 GHz).

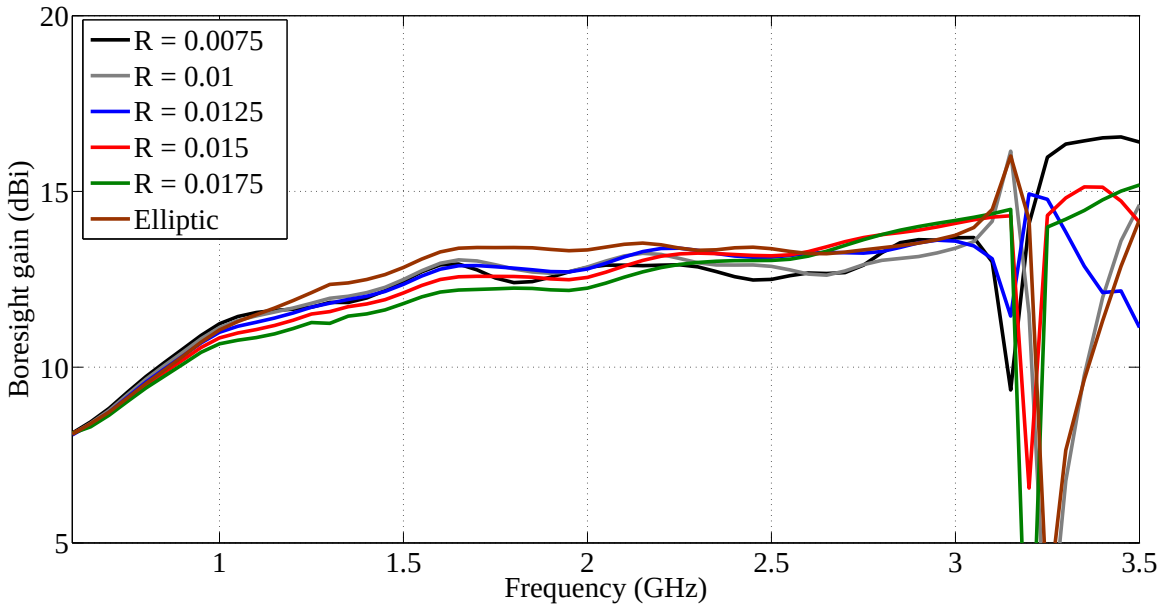

Figure 4.40. Boresight gains of quad-ridge horn antennas with different sidewall profiles.

The 3- and 10 dB beamwidths are shown in Figures 4.41 and 4.42, respectively. It can be seen from these figures that changing the profile shape resulted in relatively small beamwidth changes. Changing the specific profile of the shaped sidewall thus has a relatively large influence on the impedance matching while offering limited control over the beamwidth and hence the radiation pattern of the antenna.

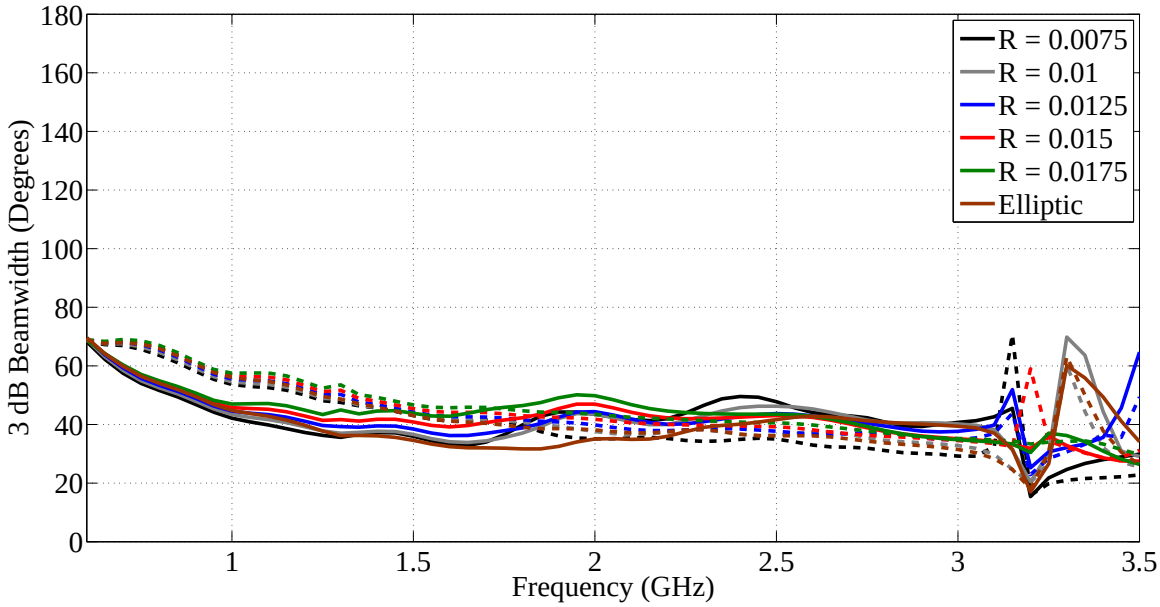

Figure 4.41. 3 dB beamwidths of quad-ridge horn antennas with different sidewall profiles (E-plane: Solid, H-plane: Dashed).

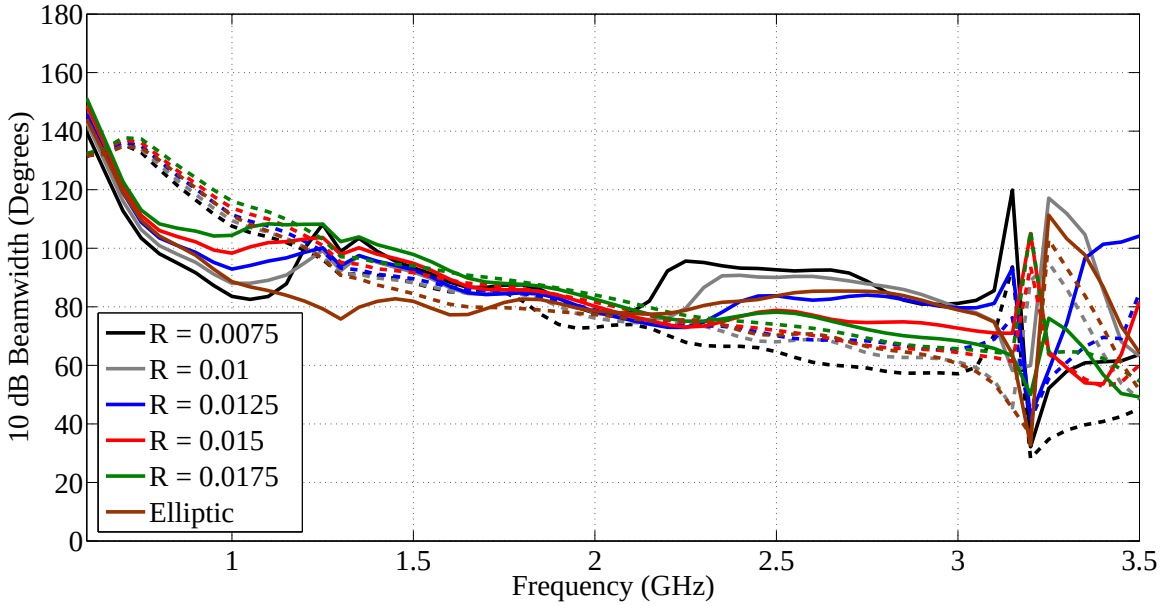

Figure 4.42. 10 dB beamwidths of quad-ridge horn antennas with different sidewall profiles (E-plane: Solid, H-plane: Dashed).

The elliptic profile is seen as a good compromise between obtaining a good reflection coefficient and constant beamwidth – especially when the modification to the elliptic profile start point is implemented to improve low frequency impedance matching. It is also simpler than the exponential ridge and offers similar performance while eliminating a variable that would have to be optimized for a final design.

4.7.3 Antenna Geometry

This section compares 6 different quad-ridge horn antenna geometries to determine which of these geometries would be the most suitable as a reflector feed. These geometries are quad-ridge horn antennas that have circular, square and diagonal layout both with shaped and straight sidewalls as shown in Figure 4.43 [26]. The conical straight and square straight geometries are well known configurations. Diagonal quad-ridge horns have been presented (albeit with a square cavity and dielectric sidewalls) [82]. The pyramidal quad-ridge horn are also investigated as diagonal waveguide horns exhibit equal E- and H-plane patterns and can be used as reflector antenna feeds [3].

The models all incorporated steps in the backshort to suppress higher order modes as in Figure 4.22 as it has been shown that these steps served to increase the bandwidth of qua-

ridge horn antennas. The elliptically shaped sidewall antennas also incorporated the offset elliptical profile, shown in Figure 4.38, to improve the low frequency reflection coefficient. The ridges are shaped elliptically and had a ridge width of 9 mm (compared to the width of the basic model of 8mm).

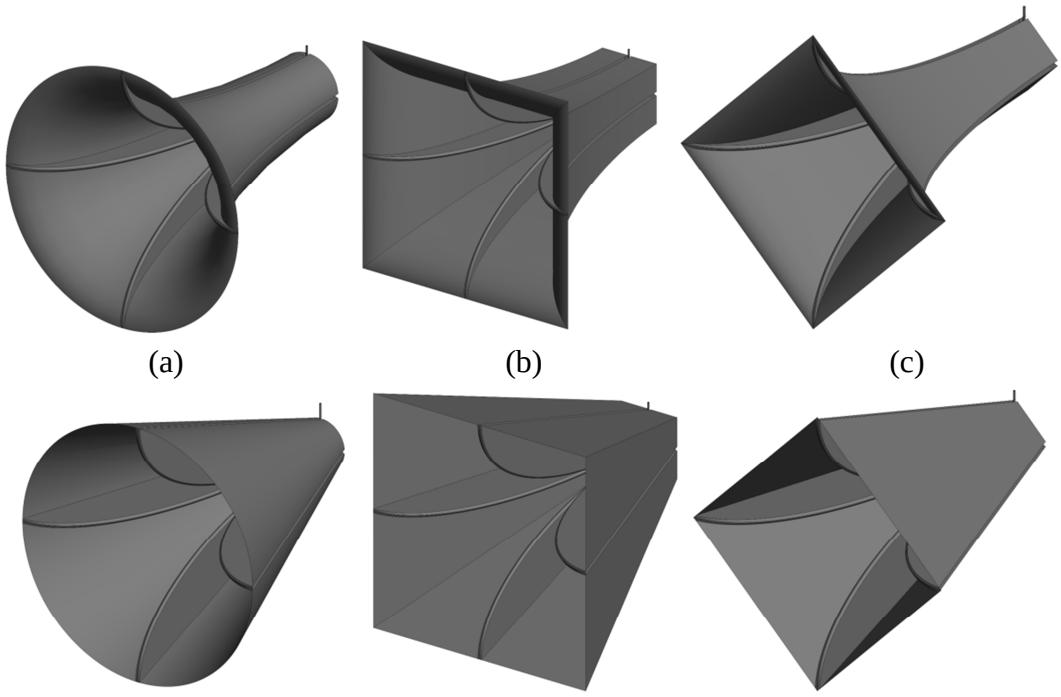

Figure 4.43. Quad-ridge horn antenna geometries, (a) Shaped sidewall conical. (b) Shaped sidewall pyramidal, (c) Shaped sidewall diagonal, (d) Straight sidewall conical, (e) Straight sidewall pyramidal (f) Straight sidewall diagonal.

Direct comparison of these antennas is somewhat difficult due to the different shapes. Such a comparison was made on the basis that the ridge profiles should be kept identical for all three antennas. It has been shown in previous sections that the ridge profiles strongly affect both the impedance matching as well as the radiation patterns. It would thus be difficult to draw conclusions from results obtained for antennas with different ridge profiles. The antenna geometries required to obtain identical ridges (both for the waveguide and aperture) are shown in Figure 4.44.

As can be seen from Figure 4.44 the aperture as well as the waveguide size of the antenna differs due to the requirement to have identical ridges between the antennas. The square aperture has the largest area, with the circular aperture having an area 78.5% and the diagonal horn 50% as large. This different waveguide and aperture sizes would result in

antennas that are matched from different frequencies and that have different beamwidths. The aspects of the antenna performance that are compared are the bandwidth – whether a 4:1 bandwidth is achievable, how constant the beamwidth is and the difference between the E- and H-planes of the beamwidths – as a measure of rotational symmetry.

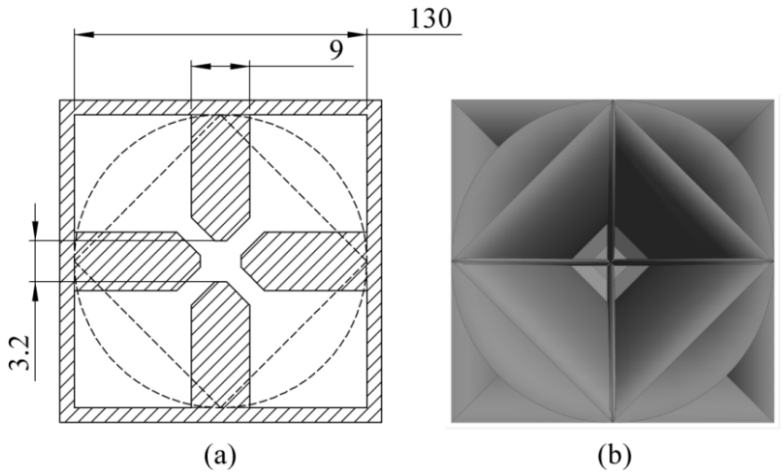

Figure 4.44. (a) The ridge waveguide dimensions and (b) comparison of the apertures of the three geometries that allows for identical ridges with horn outer dimension shown.

A comparison of the bandwidth was done by simulating frequency scaled versions of these antennas. All dimensions except the ridge gap and ridge width were scaled by the ratio between the current and desired lower operating frequency. The reflection coefficients and boresight gain of these antennas could then be directly compared to determine the bandwidth that could be achieved. The antennas were also simulated from 0.6 GHz to 4 GHz (a larger bandwidth than for previous simulations).

The reflection coefficient of the antennas with straight sidewalls and those with shaped sidewalls are shown in Figures 4.45 and 4.46 respectively. From these figures it can be seen the antennas are matched from different frequencies. The straight sidewall reflection coefficient varies a great deal more compared to the shaped sidewalls and are matched (or reasonably close to being matched) from an earlier frequency.

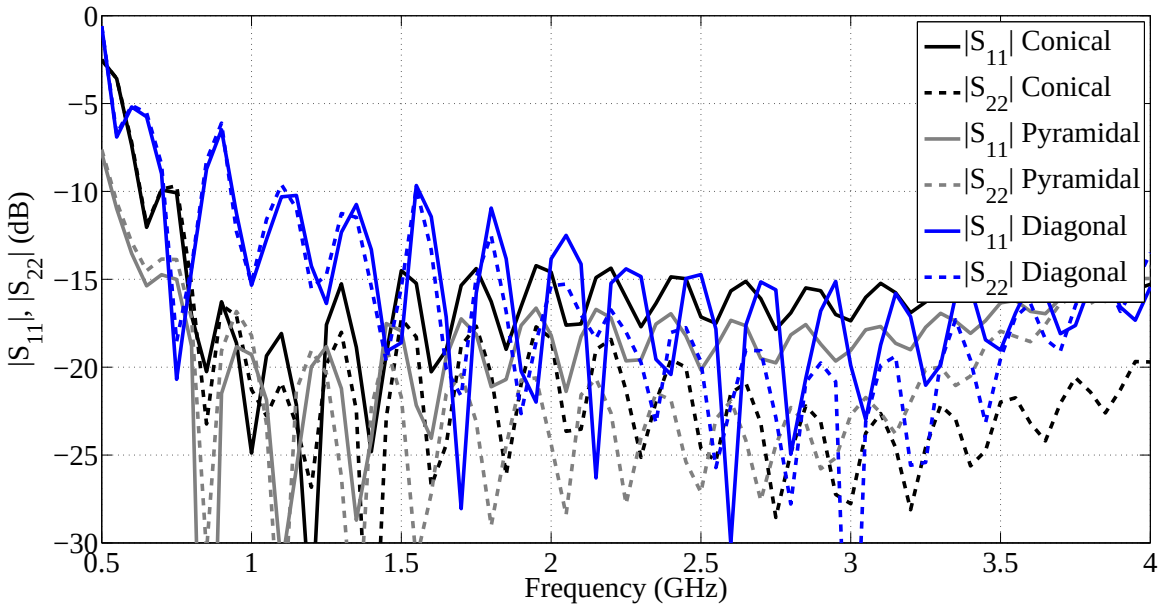

Figure 4.45. Reflection coefficients of quad-ridge horn antennas with straight sidewalls and different geometries.

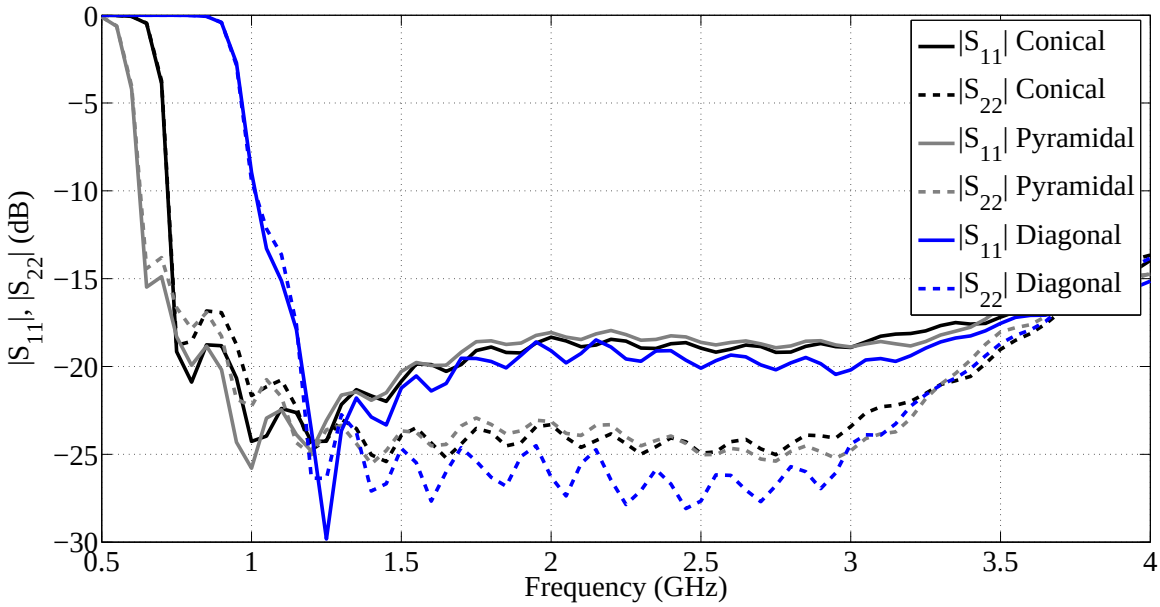

Figure 4.46. Reflection coefficients of quad-ridge horn antennas with shaped sidewalls and different geometries.

The 10 dB beamwidths of the antennas are shown in Figures 4.47, 4.48 and 4.49 for the conical, square and diagonal geometries respectively. For the conical and square antennas, shaping the antenna sidewalls resulted in radiation pattern improvements. The magnitude of the side lobes was reduced significantly – there are no sudden changes in the 10 dB beamwidth of the shaped sidewall antennas. The principal plane patterns also vary less and the patterns are closer to being rotationally symmetrical.

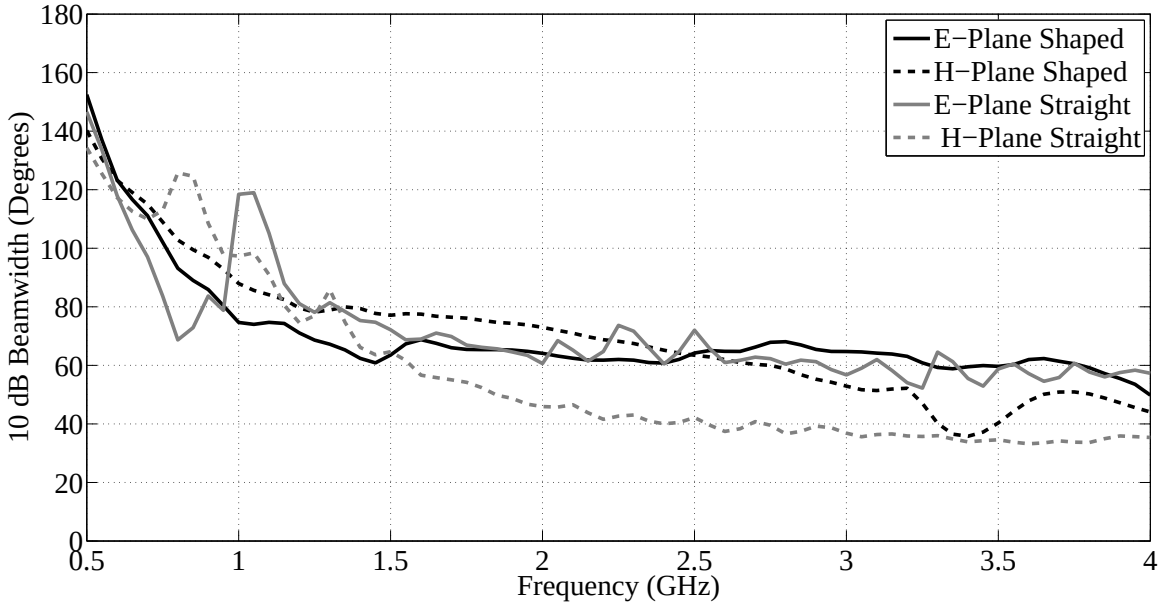

Figure 4.47. 10 dB Beamwidth of the conical geometry quad-ridge horn antenna.

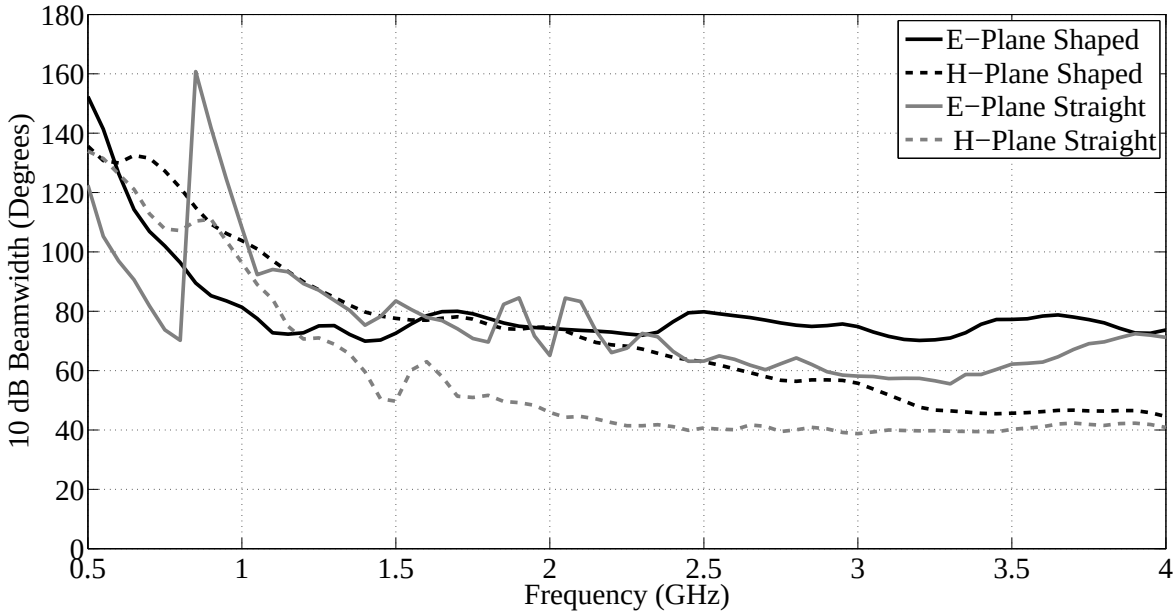

Figure 4.48. 10 dB Beamwidth of the pyramidal geometry quad-ridge horn antenna.

The diagonal quad-ridge horn already had principal plane patterns that were approximately equal over a large portion of the bandwidth. The sudden changes in the 10 dB beamwidth, however, show that the patterns have large side lobes. Shaping the antenna resulted in radiation patterns of which the E- and H-plane patterns differed significantly. The simulation of the frequency scaled diagonal shaped antenna indicated that the antenna could not attain a large bandwidth as there were large variations in the boresight gain at higher frequencies.

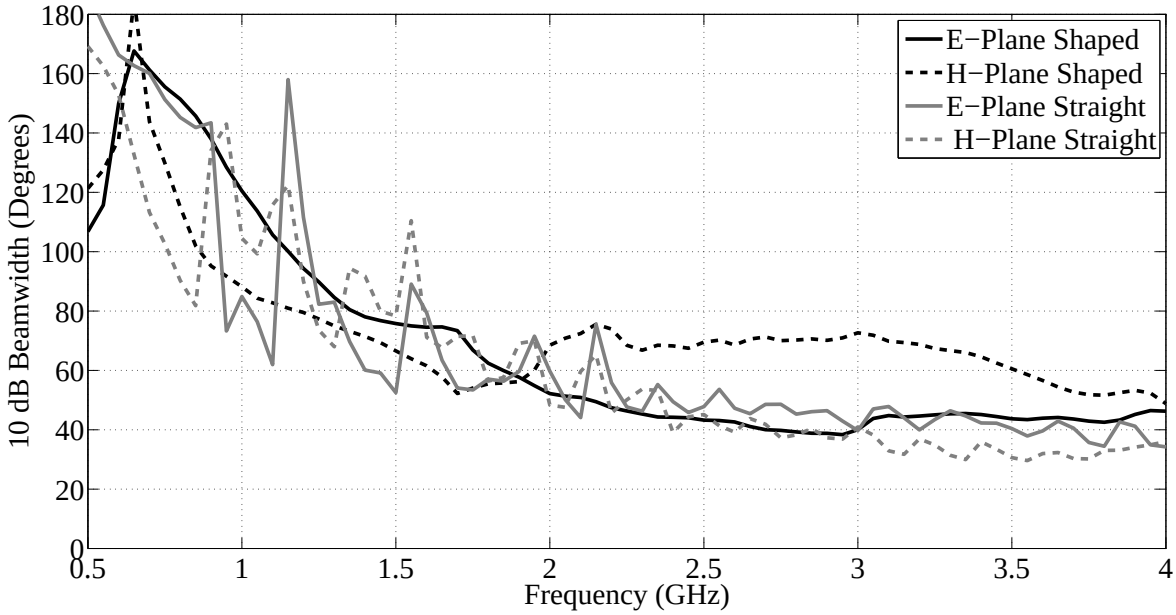

Figure 4.49. 10 dB Beamwidth of the diagonal geometry quad-ridge horn antenna.

A comparison of the mean and standard deviation of 10 dB beamwidth of the antennas in both planes is shown in Table 4.1.

Table 4.1 Comparison of mean and standard deviation of antenna 10 dB beamwidth (degrees)

From1 to 3 GHz

Model	E-plane mean	H-plane mean	E-plane standard deviation	H-plane standard deviation
Conical Straight	71.2	60.5	14.1	25.5
Conical Shaped	65.8	70.9	3.7	9.1
Pyramidal Straight	74.3	52.0	11.7	14.8
Pyramidal Shaped	74.8	66.8	2.7	12.7
Diagonal Straight	61.6	63.7	21.9	24.0
Diagonal Shaped	61.9	69.3	22.8	8.1

Of the quad-ridge horn antennas that were investigated as a possible candidate for a wideband reflector feed antenna the conical quad-ridge horn with elliptically shaped sidewalls shows the most promise.

The radiation patterns are close to being rotationally symmetric and the 10-dB beamwidth reasonably constant, over a wide frequency range. This is shown in the simulated 10 dB beamwidth as well as in Table 4.1 where the mean beamwidth of the E- and H-planes are reasonably close and the standard deviation of the 10 dB beamwidth for the antenna is relatively low.

4.7.4 Elliptical sidewall shaping ratio

The elliptically shaped sidewalls, for a conical type horn, were investigated further by examining the effect of changing the ratio between the horn length and the aperture diameter.

$$R = \frac{Horn\ Length}{Aperture\ diameter} \tag{4.4}$$

Figure 4.50 gives an indication of the effect of changing this ratio for an elliptically shaped sidewall with a constant aperture diameter.

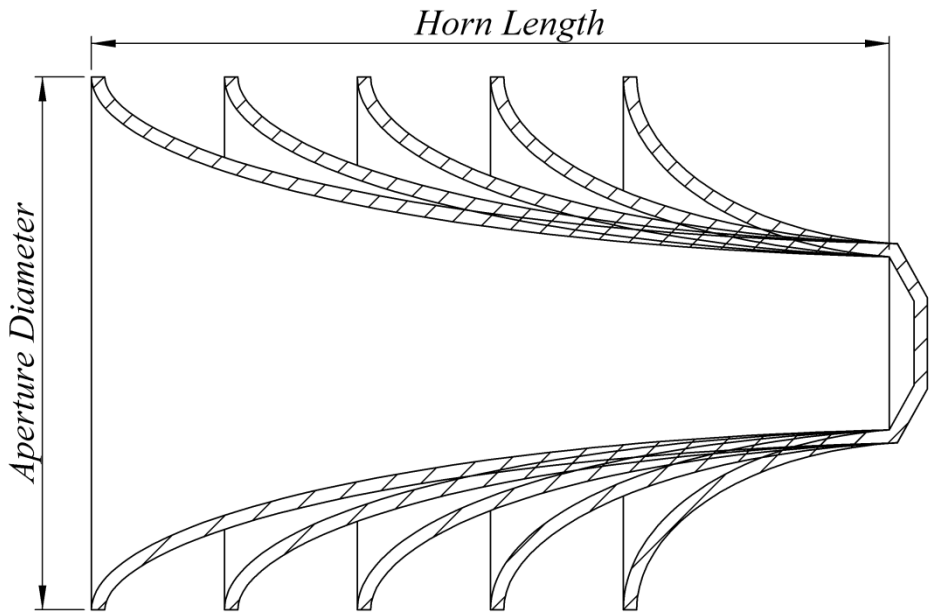

Figure 4.50. Elliptically shaped sidewalls for different ratios of horn length to aperture diameter with a fixed aperture width.

The ratio changes the elliptical profile of the sidewall as well as the profile of the ridge (also elliptical). This variable affects two geometry features – the aperture diameter as well as the length of the horn. Five different ratios (0.5, 0.75, 1, 1.25 and 1.5) were simulated for four different aperture sizes (350, 400, 450 and 500 mm) to ensure that the effect of changing the ratios could be observed (a total of 20 different antennas).

The models incorporated steps in the backshort as well as a conically shaped backshort. The elliptical sidewalls also had an ellipse offset of 1 mm to improve low frequency reflection coefficient. The conical backshort was used as it resulted in a slight improvement in the reflection coefficient. Shown in Figure 4.51 are five different antenna models with a fixed aperture size.

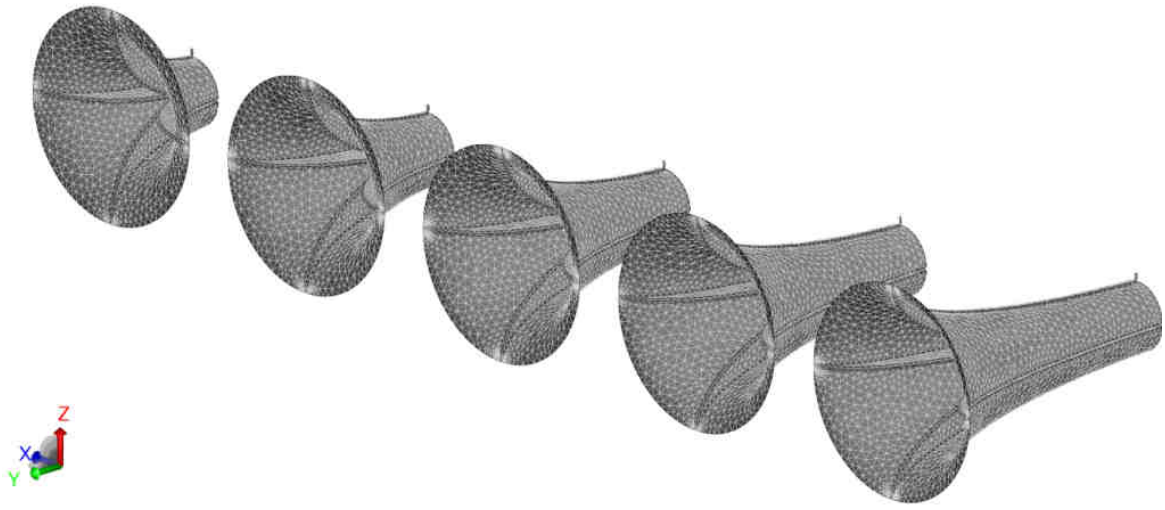

Figure 4.51. Models of the quad-ridge horn antenna with different horn lengths and fixed aperture.

The reflection coefficients of the antennas with different ratios for an aperture size (diameter) of 400 mm are shown in Figure 4.52. The reflection coefficient is shown only for this aperture size as the other aperture sizes follow a similar pattern. The abrupt transition for a ratio of 0.5 results in deteriorated reflection coefficient while more gradual transitions improve the reflection coefficient. For a ratio of R = 0.75 and smaller the antennas can be reasonably well matched from a low frequency.

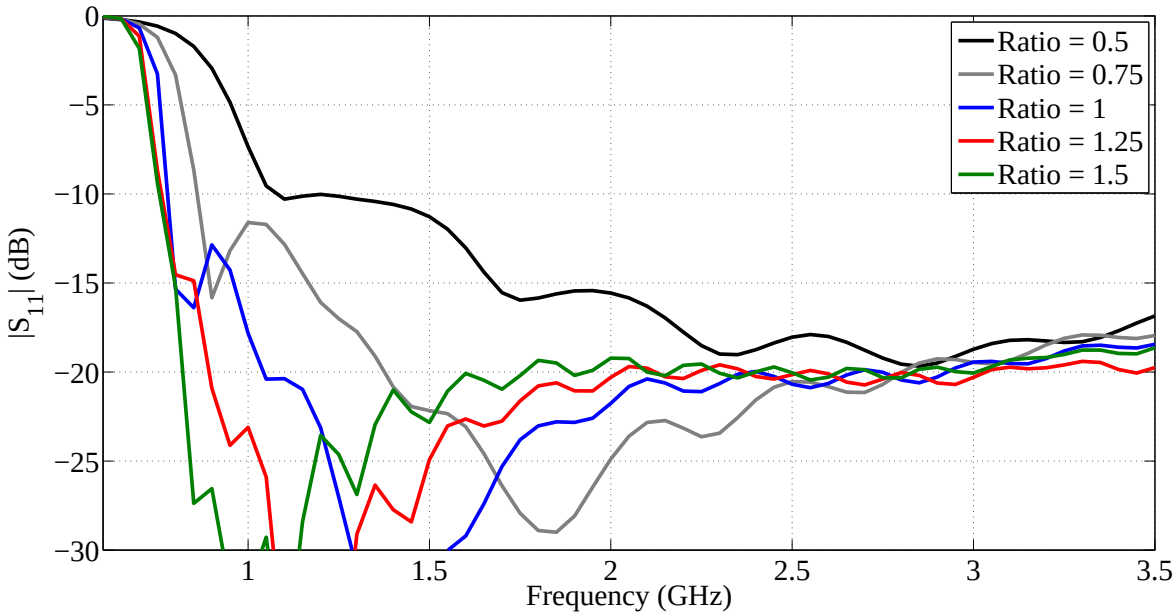

Figure 4.52. Reflection coefficients of quad-ridge horn antennas with fixed aperture width (400 mm) and different lengths.

The boresight gains of the antennas are shown in Figures 4.53 to 4.56. It can be seen that although the change in the size of the aperture affects the boresight gain, this effect occurs throughout the band as expected (increased gain for a larger aperture). The effect is also much smaller than the effect of changing the ratio between the aperture size and the horn length. A larger ratio (R) is thus seen to lead to a larger gain.

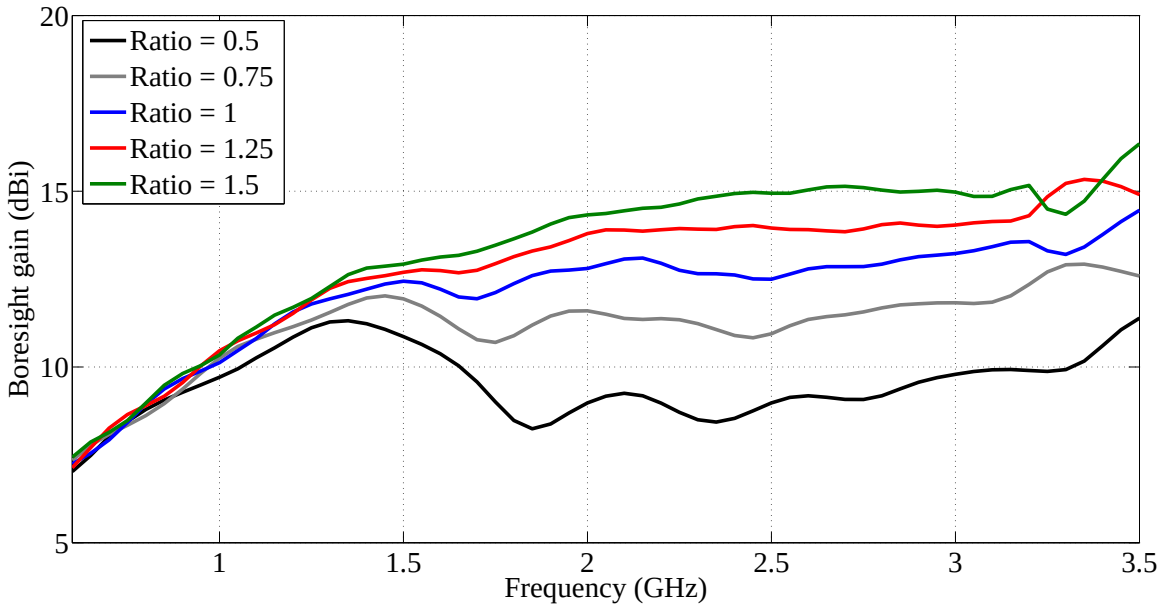

Figure 4.53. Boresight gains of quad-ridge horn antennas with fixed aperture width (350 mm) and different lengths.

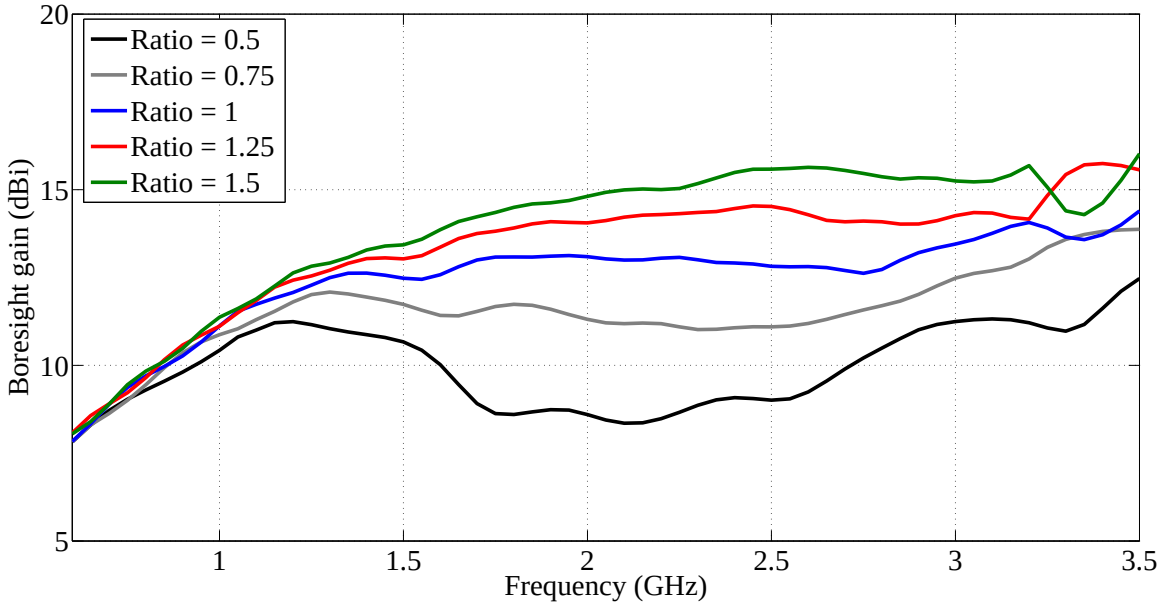

Figure 4.54. Boresight gains of quad-ridge horn antennas with fixed aperture width (400 mm) and different lengths.

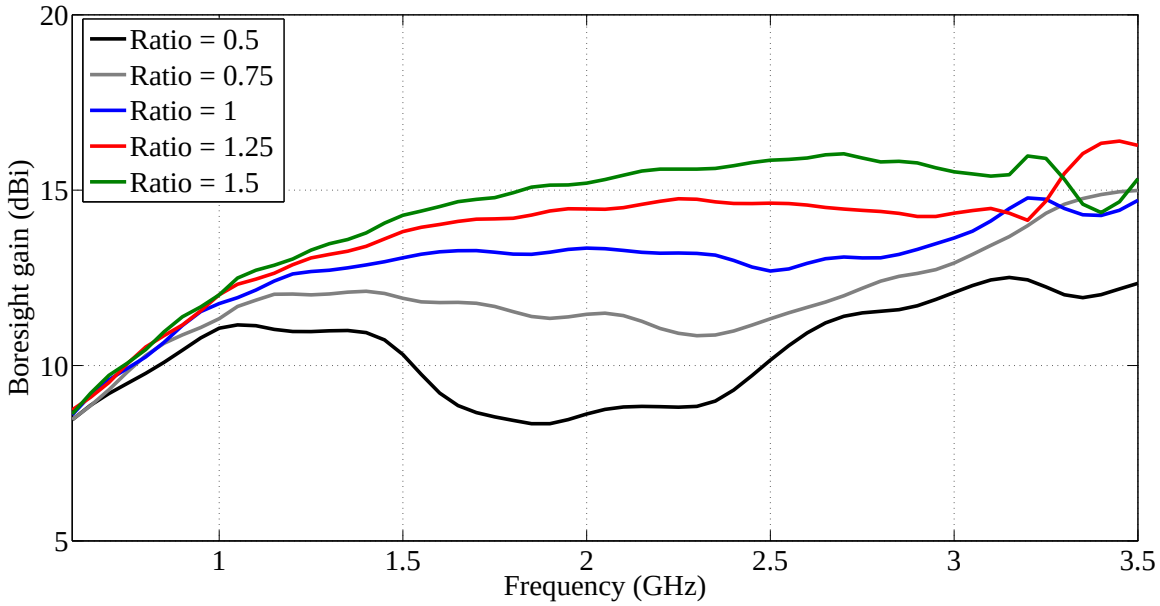

Figure 4.55. Boresight gains of quad-ridge horn antennas with fixed aperture width (450 mm) and different lengths.

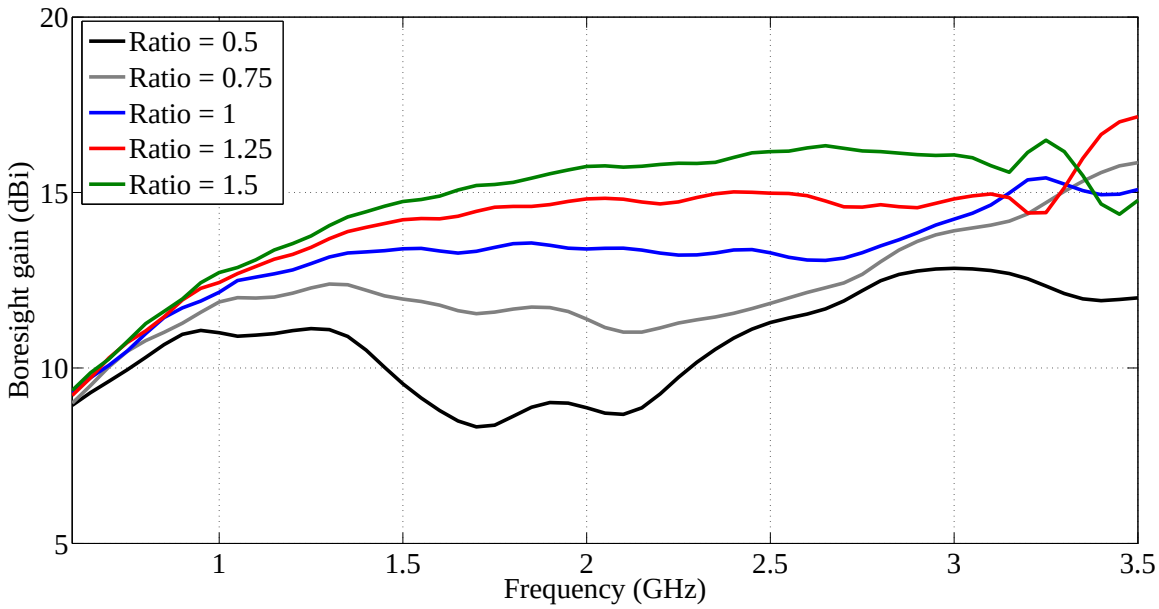

Figure 4.56. Boresight gains of quad-ridge horn antennas with fixed aperture width (500 mm) and different lengths.

Changing the ratio between the horn length and the aperture diameter allows the radiation pattern to be controlled much more effectively, and over a wider range, than the other geometry features that have been investigated. This is confirmed by examining the 10 dB beamwidths of the antennas as shown in Figures 4.57 to 4.60. The control over the beamwidth that can be achieved by changing the ratio is immediately apparent. It indicates that this type of antenna would be able to yield radiation patterns with a wide range of 10 dB beamwidths.

Although both the E- and H-plane beamwidths changes it can be seen from the figures that certain combinations of ratio and aperture size results in antennas that have E- and H-planes that are closer together and would thus yield patterns that are closer to being rotationally symmetric. A design process for a specific required beamwidth would thus consist of obtaining the ratio most suitable for attaining a specific beamwidth and then optimizing the aperture size to ensure a rotationally symmetric radiation pattern. Other elements (such as the ridge profile) that affect the beamwidth could then also be included.

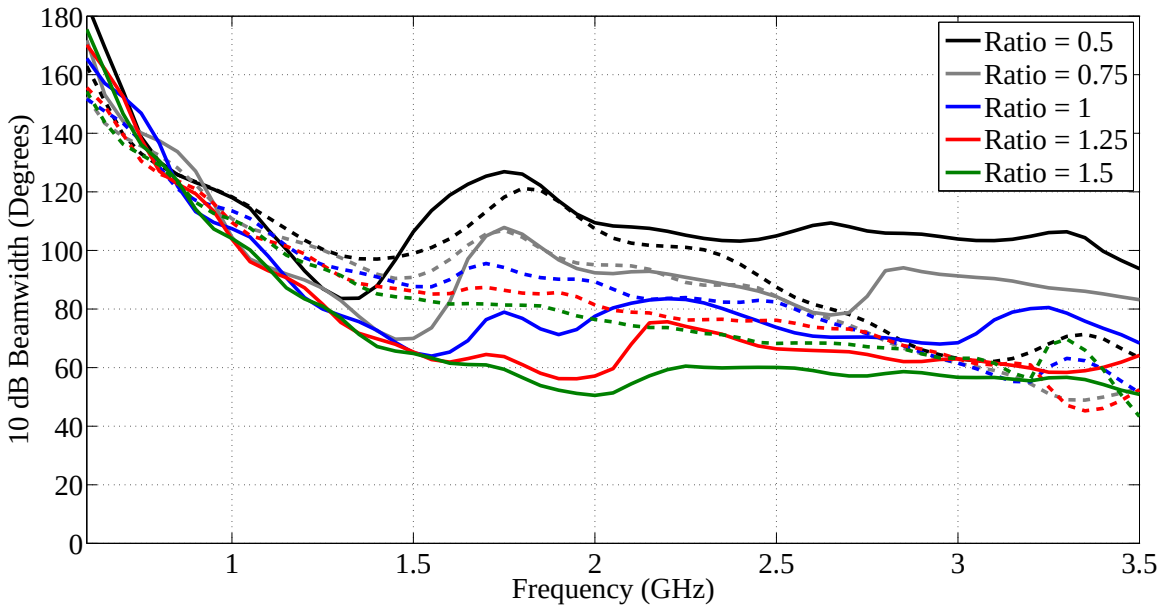

Figure 4.57. 10 dB beamwidths of quad-ridge horn antennas with fixed aperture width (350 mm) and different lengths (E-plane: Solid, H-plane: Dashed).

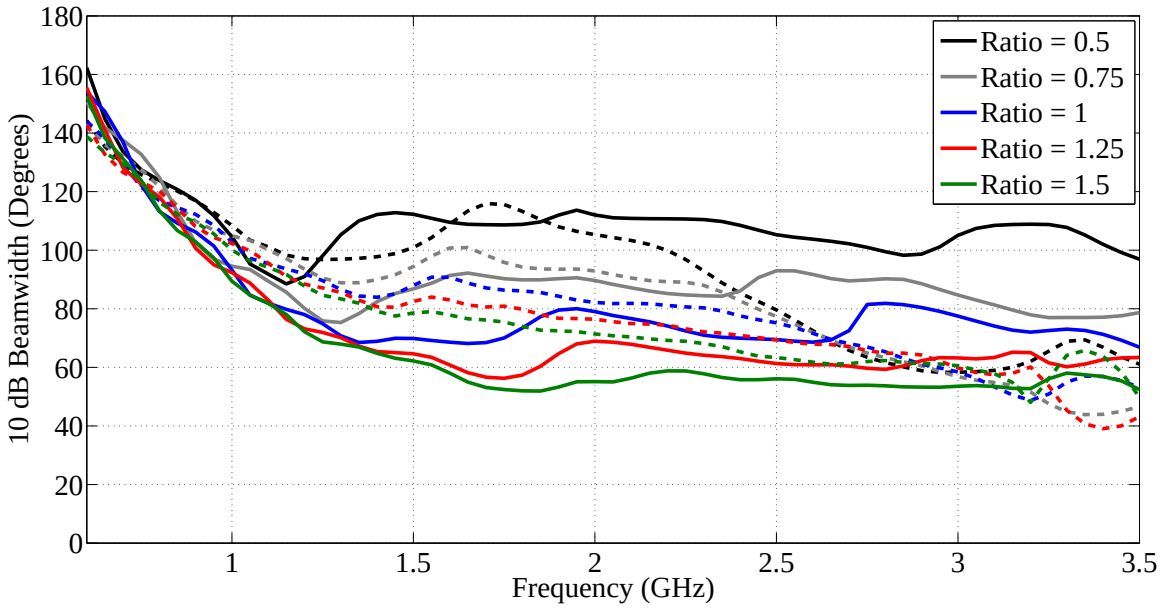

Figure 4.58. 10 dB beamwidths of quad-ridge horn antennas with fixed aperture width (400 mm) and different lengths (E-plane: Solid, H-plane: Dashed).

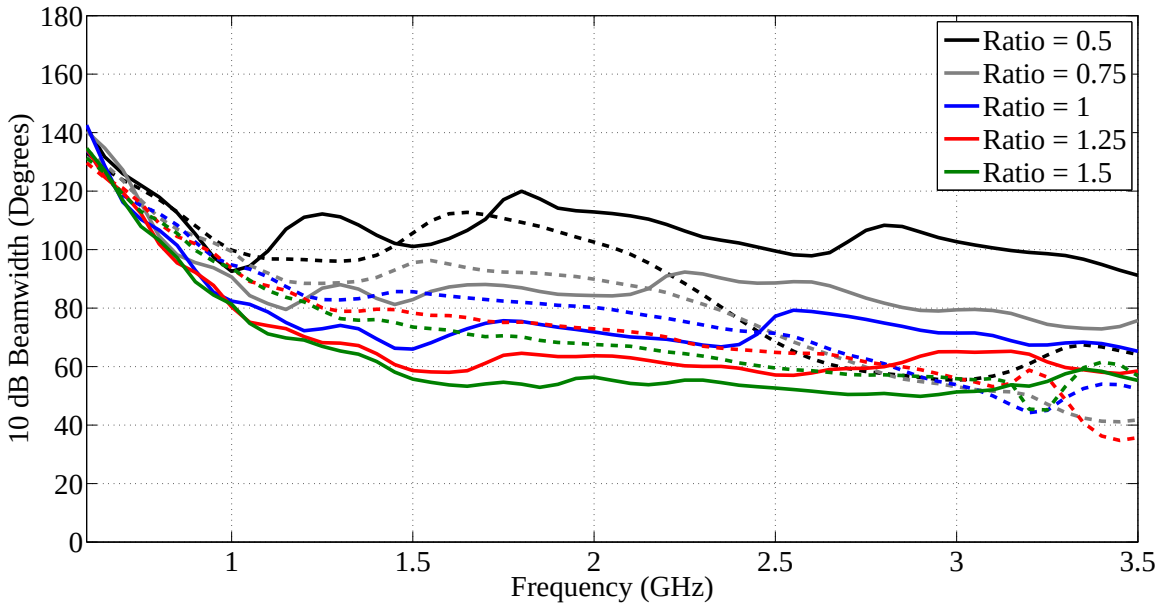

Figure 4.59. 10 dB beamwidths of quad-ridge horn antennas with fixed aperture width (450 mm) and different lengths (E-plane: Solid, H-plane: Dashed).

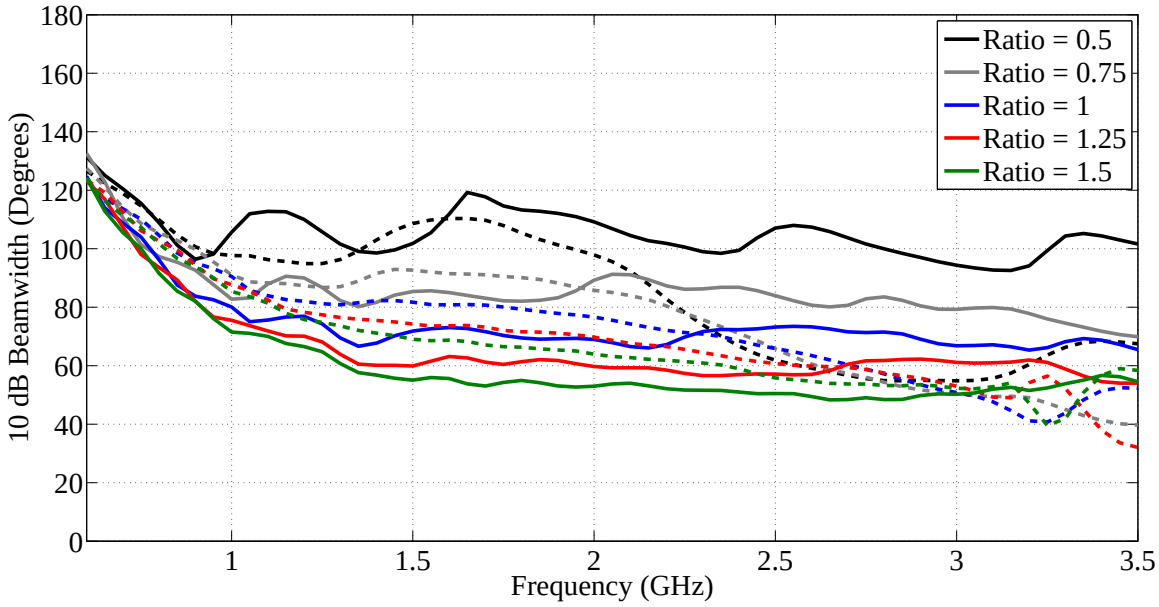

Figure 4.60. 10 dB beamwidths of quad-ridge horn antennas with fixed aperture width (500 mm) and different lengths (E-plane: Solid, H-plane: Dashed).

The mean and standard deviation of the 3 and 10 dB beamwidths are shown in Tables 4.2 to 4.5 (calculated between 1 and 3 GHz). Large ratios provide narrower beamwidths. Specific combinations of the ratio and aperture size yields beamwidths that are nearly equal. Larger aperture sizes tend to produce 10 dB beamwidths with smaller standard deviations indicating patterns that are more constant as a function of frequency.

Table 4.2. The mean 3 dB beamwidth (in degrees) from 1 to 3 GHz

Model	Plane	R = 0.5	R = 0.75	R = 1.0	R = 1.25	R = 1.5
AP = 350	E	56.84	45.85	38.21	33.22	30.94
	H	50.68	46.22	43.81	42.03	40.27
AP = 400	E	55.60	44.89	37.23	32.02	28.94
	H	48.76	44.18	41.31	39.15	37.34
AP = 450	E	56.47	44.07	36.56	31.10	27.65
	H	47.00	42.39	39.42	36.92	34.89
AP = 500	E	56.24	43.36	35.70	30.42	26.82
	H	45.31	40.79	37.71	35.15	32.95

Table 4.3. The standard deviation of the 3 dB beamwidth (in degrees) from 1 to 3 GHz

Model	Plane	R = 0.5	R = 0.75	R = 1.0	R = 1.25	R = 1.5
AP = 350	E	13.82	9.72	7.25	7.69	8.87
	H	8.97	6.38	5.80	5.99	6.59
AP = 400	E	11.87	8.25	5.85	6.01	6.97
	H	10.54	6.20	4.96	5.16	5.96
AP = 450	E	9.77	6.65	4.77	4.43	5.40
	H	11.86	6.57	4.59	4.46	5.18
AP = 500	E	8.49	5.48	3.57	3.40	4.30
	H	12.60	7.17	4.45	3.98	4.72

Table 4.4. The mean 10 dB beamwidth (in degrees) from 1 to 3 GHz

Model	Plane	R = 0.5	R = 0.75	R = 1.0	R = 1.25	R = 1.5
AP = 350	E	107.15	89.13	76.84	69.46	64.13
	H	97.20	90.27	86.15	82.37	78.81
AP = 400	E	105.77	87.69	74.69	65.66	59.88
	H	92.15	85.79	80.90	76.92	73.06
AP = 450	E	106.21	85.65	73.01	63.20	56.90
	H	88.16	81.59	76.68	72.24	68.32
AP = 500	E	105.43	84.47	71.19	61.71	54.89
	H	84.97	78.06	73.04	68.56	64.43

Table 4.5. The standard deviation of the 10 dB beamwidth (in degrees) from 1 to 3 GHz

Model	Plane	R = 0.5	R = 0.75	R = 1.0	R = 1.25	R = 1.5
AP = 350	E	10.30	9.32	9.60	10.90	12.80
	H	15.81	12.98	11.640	10.81	11.90
AP = 400	E	6.35	4.42	5.73	7.70	9.22
	H	17.79	13.33	10.40	9.76	10.42
AP = 450	E	6.15	3.55	4.03	5.23	7.35
	H	19.43	13.92	10.25	8.90	9.59
AP = 500	E	6.19	3.27	3.07	4.60	6.34
	H	20.33	14.40	10.23	8.57	8.84

The tables indicate that for this combination of ratios and aperture sizes 10 dB beamwidths of between 100 and 55 degrees could be obtained (3 dB beamwidth 55 to 30 degrees). Although for rotationally symmetric patterns and a good reflection coefficient 10 dB beamwidths of 90 to 60 degrees would be more realistic. Larger ratios and aperture size could possibly extend the range of beamwidths achievable, but would of course be less practical due to the size of the antenna. Further optimization of the radiation pattern could also include different ridge and sidewall profiles, although this would add significantly to the complexity of the optimization problem.

4.8 Antenna aperture phase error

Changing the sidewalls of the antenna would affect the phase error over the aperture of the horn antenna. The phase error of a shaped sidewall quad-ridge horn antenna was thus compared to a straight sidewall antenna to determine the change in aperture phase error. The comparison of the phase error in the electric near field at the aperture of the two antennas is shown as a function of frequency in Figure 4.61. This was calculated by subtracting the value of the phase at the edge of the aperture from the value at boresight. The phase was then converted to a distance (δ), using the frequency and normalized with the wavelength (λ).

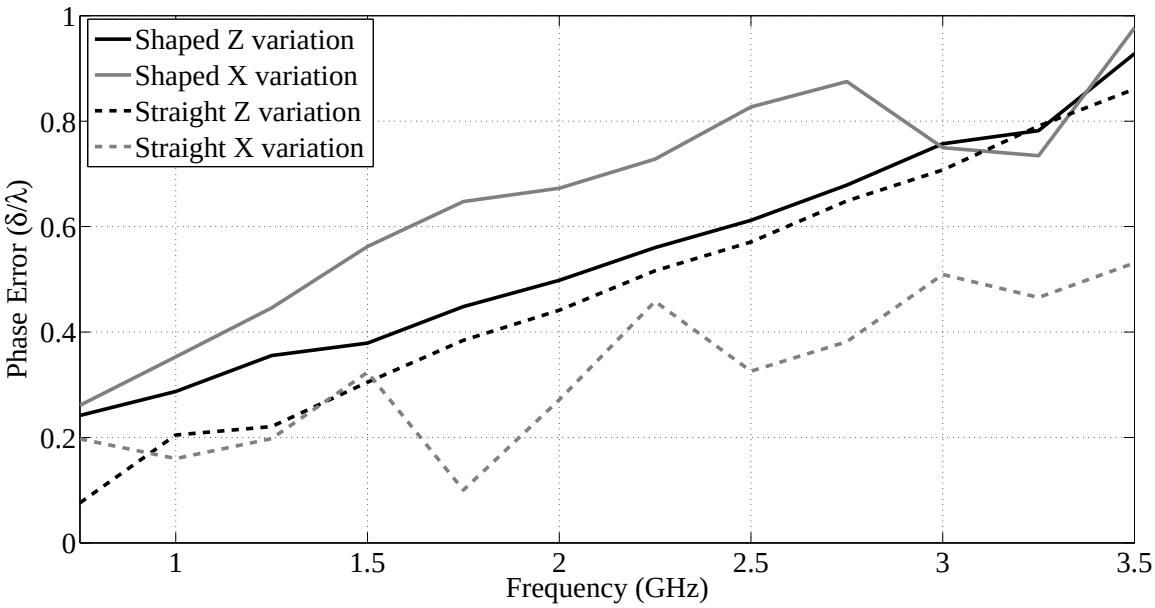

Figure 4.61. Comparison of the phase error for shaped and straight sidewall quad-ridge horn antennas.

From Figure 4.61 it can be seen that the phase error of the shaped antenna shows less variation in the *x*-direction (H-plane for the port that was excited) and is much higher compared to the phase error of the straight sidewall antenna. The additional phase error over the aperture of the shaped sidewall quad-ridge horn antenna reduces the gain at higher frequencies of the antenna leading to more constant beamwidths.

4.9 Summary

This chapter investigated various geometry features of the quad-ridge horn antenna with the goal of identifying the features that primarily affect the radiation pattern. The geometry features that were investigated and the results of the investigation are summarised in the list below.

- Orthogonal feed pin separation. The impedance and radiation characteristics of the two orthogonal feeds were found to be similar enough to allow one port to be neglected to simplify the model. Reducing the distance between the feed pins gave impedance and radiation results that corresponded better between ports, but increased the coupling.
- Waveguide parameters. The waveguide parameters had little effect on the radiation pattern of the antenna. The parameters did have a large effect on the impedance of

the antenna and the point at which higher order modes start to propagate. The parametric study indicated which combinations of variables can be used to match the antenna.

- Backshort parameters. The backshort parameters had little effect on the radiation patterns. The impedance characteristics were affected by these parameters and the bandwidth of the antenna could be significantly improved by modifying the backshort, although the parametric study indicated that the backshort would have to be designed with care to avoid resonant behaviour.
- Ridge profile. The ridge profile type affected both the radiation and impedance characteristics of the antenna. Changes to the profile resulted in large changes in impedance characteristics. The beamwidth could be changed using this parameter, but the change occurred over the entire bandwidth and for both planes. It was thus found that this parameter is not very effective at controlling the beamwidth. The elliptical ridge profile is seen to provide good performance characteristics.
- Sidewalls. Shaped sidewall quad-ridge horn antennas were shown to have more constant radiation patterns than straight sidewall horn antennas with patterns that are more rotationally symmetrical. The elliptical sidewall profile provided good impedance and radiation characteristics compared to exponential profiles, the impedance characteristics could be improved further by offsetting the elliptical profile. The conical quad-ridge horn antenna with elliptically shaped sidewalls was identified as a good candidate for a wideband feed and it was shown that by changing the ratio of the elliptical profile beamwidths of between 60 and 90 degrees could be obtained.
- Phase error. The phase error across the aperture of an elliptically shaped quad-ridge horn was compared to a quad-ridge horn with shaped sidewalls. The phase error of the shaped quad-ridge horn had less variation and was larger for higher frequencies.

In conclusion it was found that the elliptically shaped quad-ridge horn antenna was suitable for use as a wide band reflector feed antenna. A wide range of beamwidths can be achieved with this antenna. The antenna can be designed to obtain beamwidths that are close to constant and rotationally symmetric in the main beam. The parametric study also provided information that can be used to design such quad-ridge horn antennas for a set of specifications.

5. ANTENNA DESIGN

5.1 Introduction

This chapter details the design of an elliptically shaped sidewall, quad-ridge horn antenna prototype. The design is discussed from an electromagnetic standpoint – the design of the antenna using Computer ElectroMagnetic (CEM) simulation to achieve certain specifications. The antenna model used to design the prototype for the specifications is detailed and the process followed to complete the design is presented. The mechanical implementation of this design is also described.

5.2 Design specifications

The specifications that were regarded as most important for the design of the shaped sidewall quad-ridge horn antenna are detailed in Table 5.1.

Table 5.1. The design specifications for the prototype antenna.

Specification Type	Specification	Description
Bandwidth	At least 4:1	0.75 to 3 GHz
Reflection Coefficient	$\|S_{11}\|$, $\|S_{22}\|$ < -15 dB	Goal $\|S_{11}\|$, $\|S_{22}\|$ < -20 dB
Feed Taper	17 dB at 50 degrees	This is a typical requirement for an offset Gregorian configuration with a shaped sub-reflector.

Other aspects of the antenna performance that were considered was the rotational symmetry of the antenna, the isolation between ports ($|S_{21}|$), how constant the beamwidth is and ensuring low side- and back lobes.

The 10 dB beamwidths were used to gauge how constant the radiation patterns are and the principal plane pattern 10 dB beamwidths were compared to judge the rotational symmetry. The radiation patterns were also compared to ensure that the side lobes were low and to further ensure that the patterns remain reasonably constant across the 4:1 bandwidth.

5.3 Antenna model

The parametric study indicated that a conical quad-ridge horn antenna with elliptically shaped sidewalls could be used to design a prototype for the specifications in Table 5.1. A model of the antenna was created in FEKO. The antenna model was fully parametric allowing the design parameters to be easily modified to facilitate the design process. The model used elliptical sidewalls that were offset from the feed point to improve low frequency matching and incorporated steps in the backshort to increase the bandwidth of the antenna. The FEKO model of the antenna is shown in Figure 5.1 along with the simulation mesh of the model.

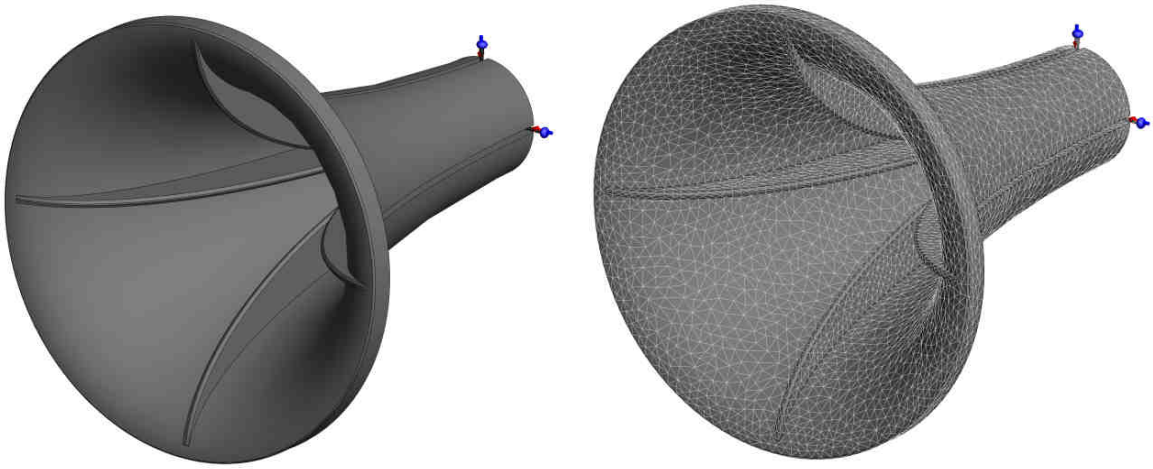

(a) (b)

Figure 5.1. (a) The geometry of the FEKO antenna model and (b) the mesh of the antenna model.

The model included both the orthogonal ports, the excitation ports can be seen in the FEKO model (the blue circles at the base of the antenna model). The model of the ports included the physical transition from SMA to air-line coaxial cable.

The SMA connector that was modelled was a Huber+Suhner 23 SMA 50-0-165/167 with 50 Ω impedance [83]. It is a flange mount connector with a receptacle for a centre conductor pin. The connector was modelled as a section of dielectrically filled coaxial waveguide that transitioned to an air-line of approximately 50 Ω. The model of the transition is shown in Figure 5.3. It was found that this transition did not significantly alter the impedance characteristics (the impedances are matched, but the mechanical mismatch

between the cable dimensions can cause some additional reflection). The green area is the dielectric of the connector that is modelled using the Surface Equivalence Principle (SEP).

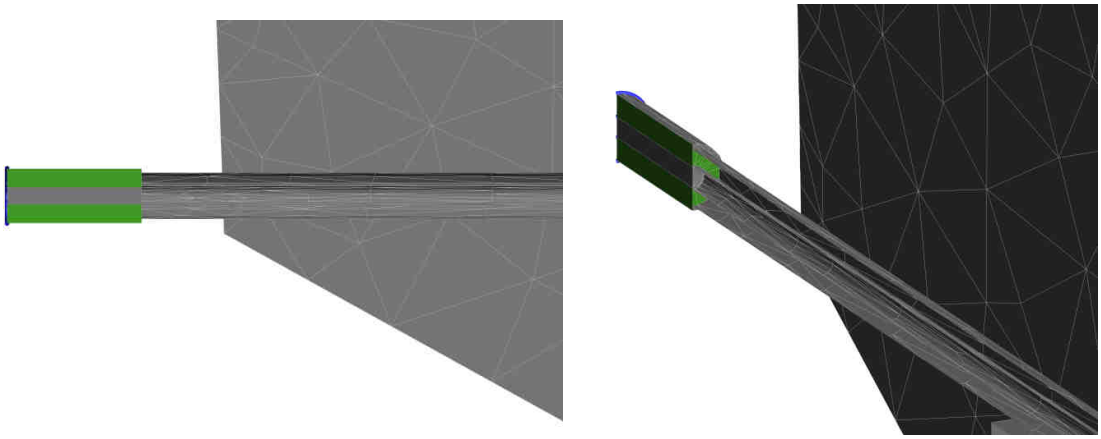

Figure 5.2. The modelling of the transition from the SMA connector to air-filled coaxial line.

The minimum width of the ridge was thus the width of the outer of the air filled coaxial transmission line. The low impedance of the coaxial line could only be achieved by chamfering the ridges at the feed point. The chamfering of the ridge was investigated for this antenna and it was found that a chamfer of 45° that gradually blended into the ridge was sufficient for obtaining a good reflection coefficient. The ridge had an elliptic profile. The cut-plane of the antenna at the feed point, in Figure 5.4, shows the chamfered ridges and the two orthogonal feeds.

Figure 5.3. A side, cut-plane view of the feed area of the quad-ridge horn antenna model, showing the backshort and the orthogonal feed pins.

The antenna model was initially simulated from 0.6 to 3.5 GHz and meshed at a sixth of a wavelength at the highest frequency. The feed point was meshed finer due to the 16-sided

coaxial line. The sidewall was meshed at a quarter of a wavelength. Models with finer meshes (up to 5 GHz) gave similar results to the coarsely meshed model.

5.4 Design procedure

The parametric study of the waveguide and backshort section in the previous chapter demonstrated that these sections did not significantly alter the radiation pattern of the antenna, provided higher order modes do not propagate. The size and shape of the horn section had an effect on the impedance characteristics. The horn section is thus designed first after which parameters in the waveguide section can be optimized to improve the reflection coefficient.

The horn section was designed by obtaining the ratio (between the horn length and aperture diameter) that gave the required beamwidth. Once the required beamwidth is obtained the aperture size parameter is fine tuned to obtain more constant beamwidth and equal E- and H-plane radiation patterns. The parameters in the waveguide section could then be optimized using the parametric study (the elliptical sidewall shaping ratio model) as a starting point. The value for this ratio that provided an average beamwidth close to the desired level was 0.91. The aperture size that gave a reasonably constant beamwidth was approximately 480 mm giving a horn length of 530 mm.

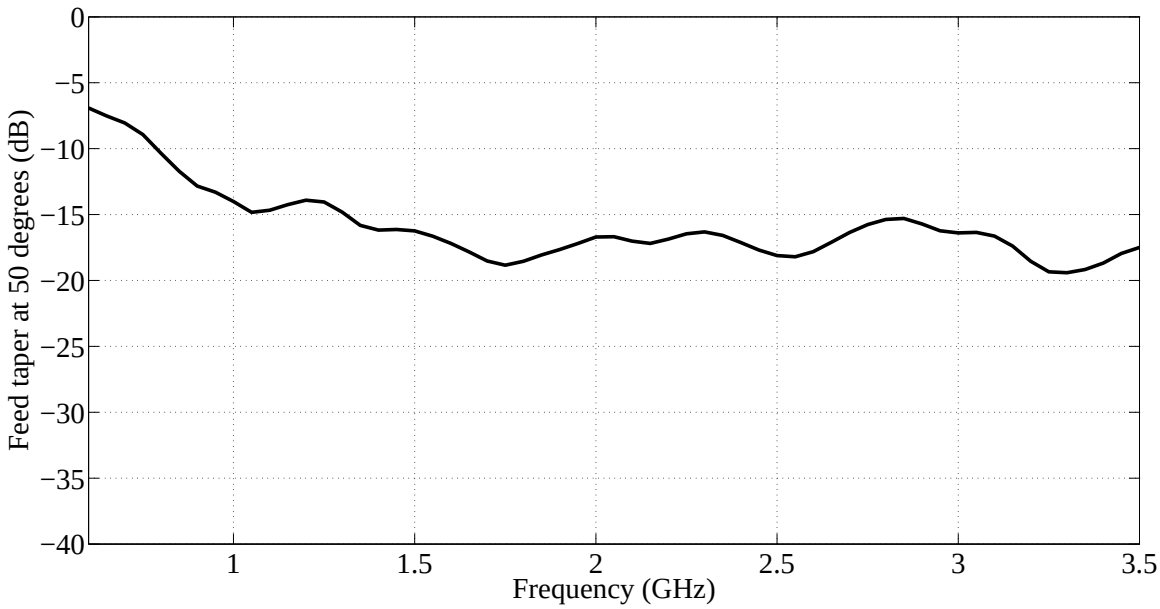

Figure 5.4. The E-plane feed taper of the antenna design at an angle of 50 degrees from boresight.

The feed taper in the E-plane at 50° from boresight as a function of frequency is shown in Figure 5.4. From Figure 5.4 it can be seen that the feed level at 50 degrees is somewhat high for low frequencies, but remains reasonably constant over a large portion of the band and varies around -17 dB as desired. The E-plane was used for the design as the H-plane beamwidth narrows somewhat at high frequencies at this beamwidth level.

The waveguide and backshort sections were optimised with this combination of aperture diameter and horn length although the ridge width was fixed at 8 mm as aluminium plate of this thickness was available and gave good reflection coefficient results. The simulations indicated that a reflection coefficient of -15 dB would be achievable across the band. The full simulated results are provided in the next chapter where they are compared to measured results.

5.5 Mechanical implementation

The electromagnetic design also had to take into account certain mechanical implementation considerations. The mechanical implementation of the FEKO model is described in this section. Mechanical and electromagnetic design of an antenna model can to some extent be seen as an iterative process where what is mechanically possible needs to be explored to determine if the electromagnetic model can be implemented in a cost effective manner. Modifications can often be made to the electromagnetic model that have little effect on the performance of the antenna but makes the manufacturing significantly easier and more cost effective.

The antenna design was again split into a number of parts, namely the backshort, ridges, feed pin and sidewall. These parts were manufactured separately and assembled to obtain as close a representation of the FEKO model as possible. As Computer Numerically Controlled (CNC) machines (mills and lathes) were used the tolerances of the parts were accurate enough for the frequencies the antenna is expected to operate over.

5.5.1 Backshort

The backshort contained recesses for the ridges to slot into, to ensure symmetry at the feed point and prevent the ridges from moving out of position during assembly. The sidewalls and backshort bolt onto the backshort. Figure 5.5 shows the conical backshort and how a ridge slots into the recesses to ensure symmetry. The backshort was machined out of aluminium.

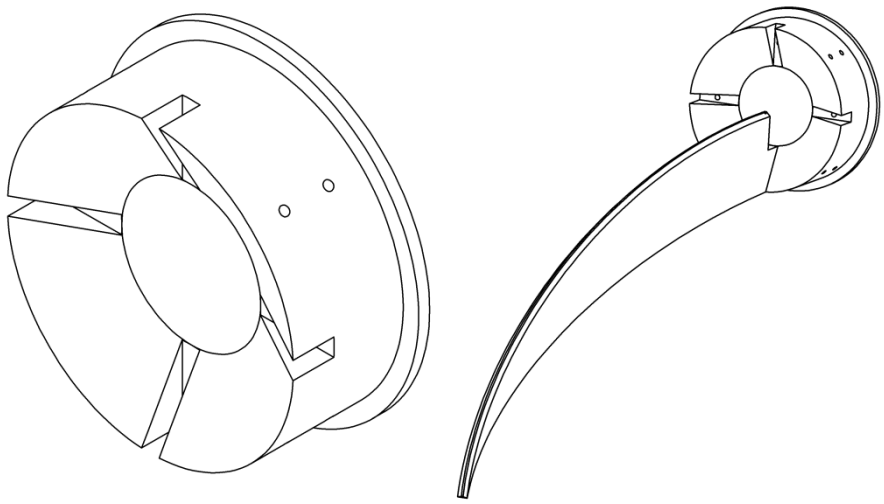

(a) (b)

Figure 5.5. (a) Isometric view of the backshort block and (b) the backshort block with a ridge indicating how the ridges slot into and are held in position by the backshort.

5.5.2 Ridges

The ridges did not extend the full length of the antenna, but stopped a few millimetres short of the antenna aperture. This prevents the ridges from becoming too thin close to the aperture as these thin sections are difficult to manufacture and could easily shear off during manufacture. The ridges had an edge chamfered at 45° close to the feed that gradually blended into the ridge. The blending of the chamfer was done by gradually moving the cutting head of the mill away from the ridge as the chamfer is cut along the edge. The reduced chamfer at the end of the ridge also served to improve manufacturability as the ridge is thinnest at the end. The ridges were machined from aluminium using a 3-axis CNC mill. The tip of the ridge (close to the aperture) was rounded.

5.5.3 Feed pin

The feed pin was manufactured from a 1.5 mm diameter brass pin. The pin was cut down to 0.98 mm for 2.5 mm of its length. This allowed a snug fit into the connector receptacle (which has a collet to ensure good contact). Attaching the feed pin to the ridge was done by cutting a 1.4 mm threaded hole into the ridge and 1.4 mm threads onto the pin. The pin was large enough to be manufactured using a CNC lathe. The feed pin could be screwed into the ridge, though the hole cut into the ridge to serve as the coaxial outer, by gripping the necked down section (that plugs into the coaxial connector) using a pin vice. The feed pin plugs into the coaxial connector. Alignment of the connector and the coaxial line is ensured due to a recess cut to the dimensions of the coaxial connector into the sidewall.

5.5.4 Sidewall

A spinning process was explored to determine if the sidewall could be manufactured as a single part. This manufacturing method deforms a flat metal plate or sheet onto a spinning mandrill using levered tools (usually called spoons). Due to the size of the antenna this mandrill would have been very expensive to manufacture and extremely heavy. For spinning the final thickness of the antenna is difficult to control and would have tapered down from the edge. The size and length of the antenna also calls for very large deformation of the work piece which could have led to cracks. Due to the cost of the tooling, uncertainty in the process and the risk associated with this process the antenna was rather machined in sections.

Machining the part out of aluminium shifted the cost driver of the prototype from tooling to material. By carefully choosing the length of each section the aluminium billet could be used with less waste as some subsequent sidewall sections could be cut from the same piece of material.

The sidewall sections were cut so as to allow them to fit closely together and to be held in place by means of the ridges as well as small overlapping lips as in Figure 5.6. This ensured the sidewalls were positioned concentrically and helped to support the weight of the antenna. Lateral support of the antenna (pulling the sidewalls sections together) is by means of the ridges (the curvature of the antenna and ridges causes lateral force on the

sidewall sections) as well as M6 threaded rods that could be bolted into the largest section and fastened to the mounting behind the backshort of the antenna (a polycarbonate back plate was manufactured to bolt the threaded rods to).

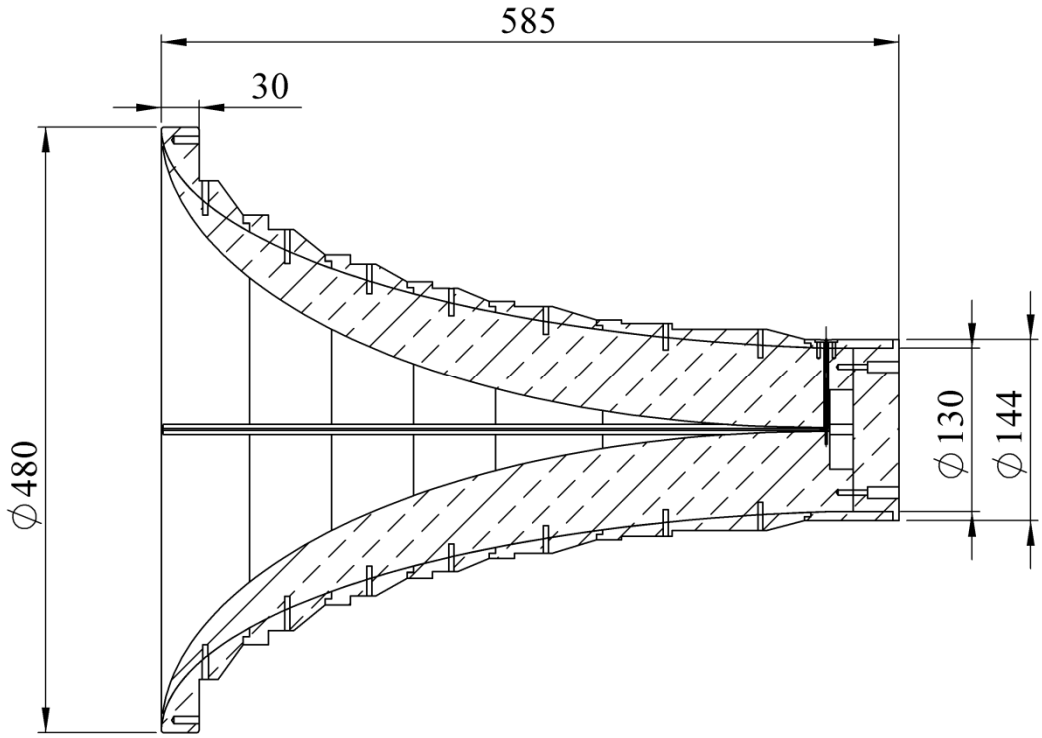

Figure 5.6. A cut plane drawing of the antenna assembly, indicating outer dimensions (in mm).

In Figure 5.6 it can be seen that the antenna model outer profile is not smooth. The section directly behind the aperture had a constant diameter that improved the back lobe as it reduced diffraction. The section also served as an attachment point for CNC lathe/mill gripping tools reducing material waste as a section to grip the work piece and a section to allow a parting tool to enter was no longer required. Beyond this section the outer profile had very little effect on the antenna performance and could be designed to improve manufacturability. The outer profile thus has flat sections (constant diameter) in areas where holes had to be drilled. This allowed the holes to be drilled without having to first use a milling tool to cut a flat face. Each section also has at least a 20 mm section with constant diameter to allow the work piece to be gripped by the machine tools. This outer profile resulted in an increase in the weight of the antenna, but improved manufacturability and reduced cost.

A simulation was conducted in FEKO to ensure that constructing the sidewall using this process would have little effect on the performance of the antenna. Gaps in the sidewall of

up to 0.5 mm were simulated. It was found to have limited effects on the simulated results. The electric field at the sidewall is much smaller than closer to the ridges and the change was very small in terms of waveglength. It was, however, observed that contact between the sidewalls and ridges are important. A front view of the antenna is shown in Figure 5.7.

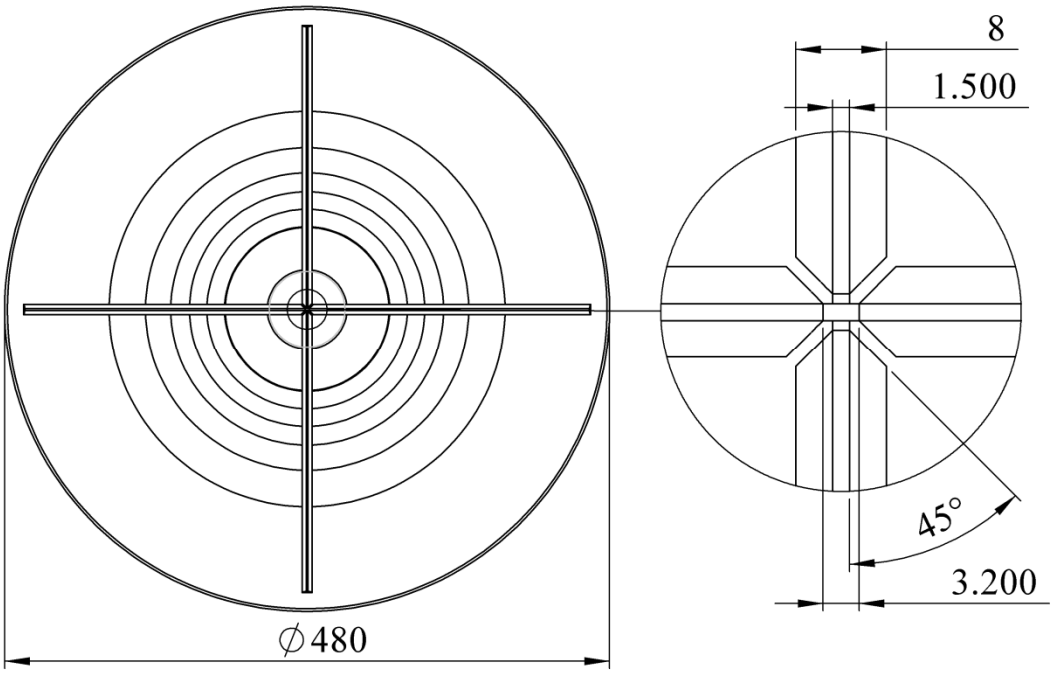

(a) (b)

Figure 5.7. (a) The front of the antenna along with, (b) a detail view indicating the dimensions of the ridge waveguide section.

5.5.5 Antenna assembly

The antenna is assembled by stacking all the sidewall sections on the backshort block. The ridges are set into position inside the recesses cut into the backshort and bolted to the backshort. The sidewall sections are then rotated until the holes in the ridges align with the holes in the sidewalls. The ridges are bolted to the sidewall (using M4 high tensile hex bolts) from the bottom up to ensure that any misalignment of the sidewall sections do not twist the ridges at the feed point. When the ridges are bolted to the sidewall the antenna is very rigid, the curvature of the ridges and tolerances the parts were manufactured to pin the sidewall sections tightly into position.

The feed pins are screwed into position by gripping the 2.5 mm section that plugs into the receptacle of the connector using a drill bit vice and aligning the feed pin to the hole in the ridges by feel through the feed gap. The connector is then placed in the recess cut into the sidewall to accommodate it, with the feed pin plugging into the connector receptacle. It was verified that the feed pins did not make contact (short out) by placing a small LED lamp inside the antenna and observing that two distinct shadows formed.

A mounting cradle was made for the antenna for use during radiation pattern measurements. The model of the antenna made for manufacturing purposes is shown in Figure 5.8 (the mechanical layout was designed using Solid Works). Also shown in Figure 5.8 is an exploded view of the antenna indicating how the antenna is assembled. Photographs of the antenna are shown in Figure 5.9, along with a 150 mm vernier for scale.

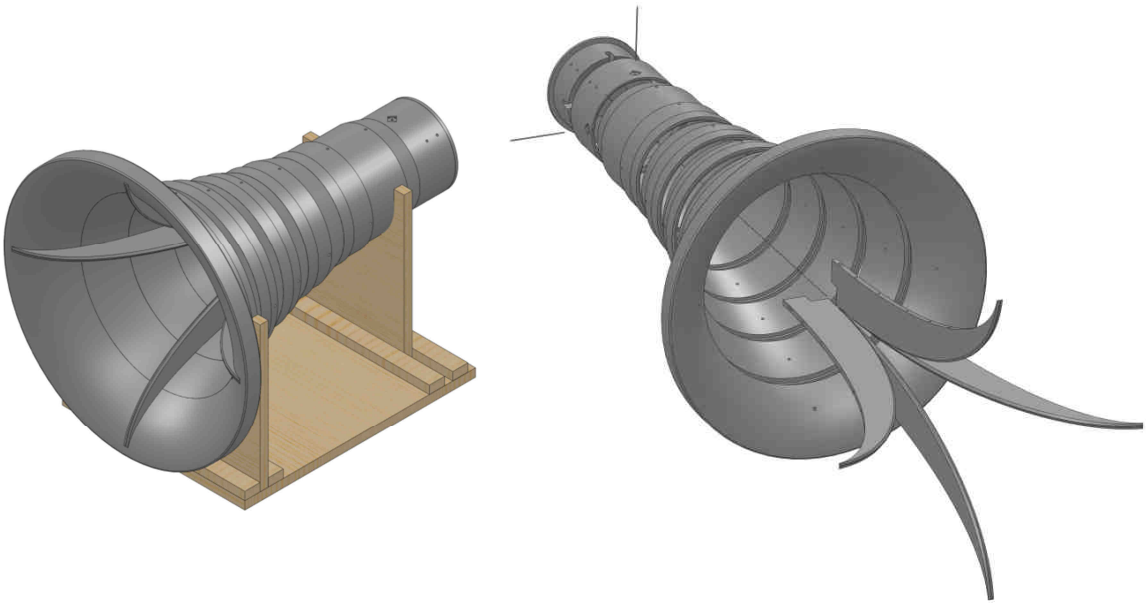

(a) (b)

Figure 5.8. The antenna assembly (a) complete assembly with mounting cradle for pattern measurements and (b) exploded view of the antenna assembly indicating the constituent parts.

5.6 Summary

The electromagnetic and mechanical design of a prototype elliptically shaped sidewall quad-ridge antenna has been presented. The antenna is designed to obtain a specific beamwidth specification for a shaped sub-reflector antenna system. The antenna was

manufactured out of aluminium. Details of the required antenna specifications, antenna model, design process and the manufacturing have been provided.

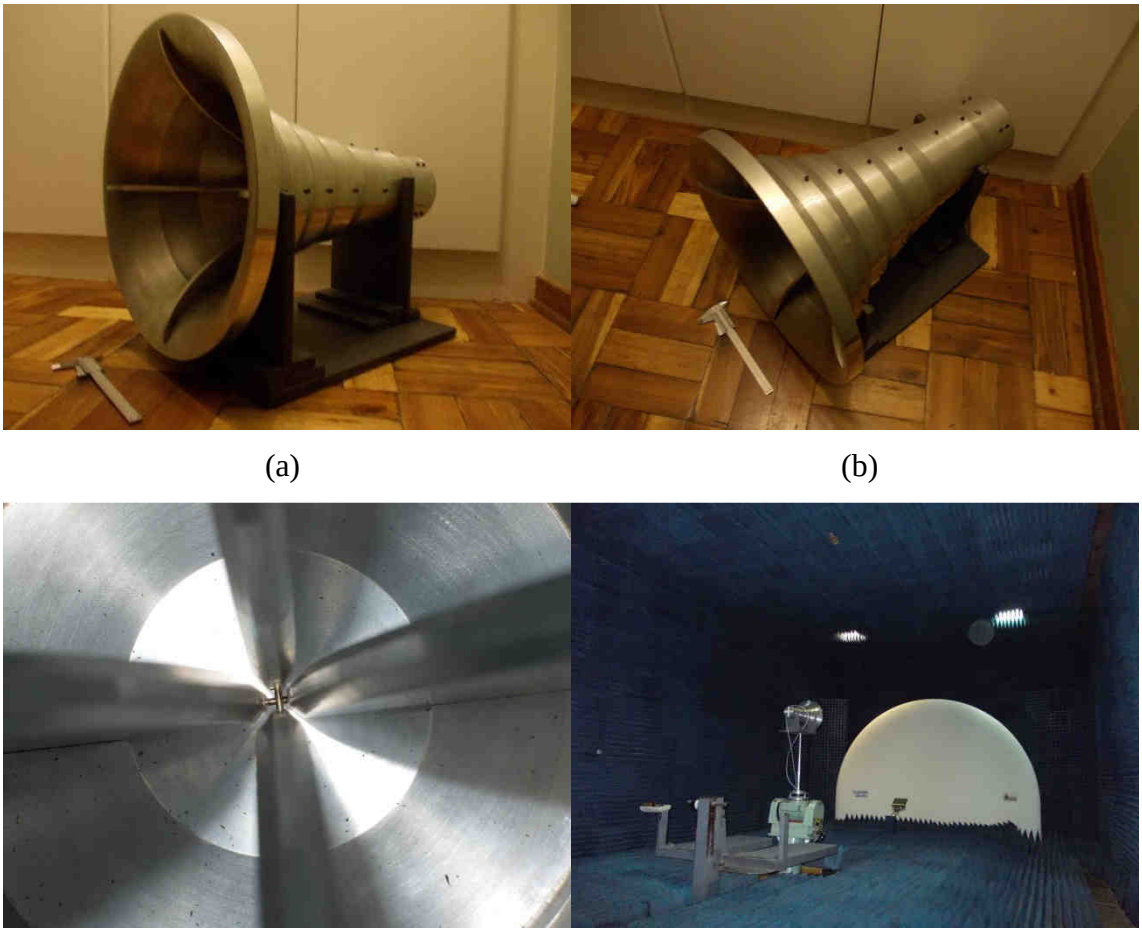

(a) (b)

(c) (d)

Figure 5.9. (a) and (b) Photographs of the antenna in manufactured form with a vernier (150 mm) for scale, (c) the feed pins of the antenna and (d) the antenna in the compact range.

6. ANTENNA PERFORMANCE EVALUATION

6.1 Introduction

This chapter evaluates the performance of the antenna prototype. Measured results are compared with simulated results to validate the antenna models and the accuracy of the antenna assembly. Other aspects of antenna performance are also evaluated such as conductive loss and the efficiency of the antenna when used as a reflector feed.

6.2 Impedance characteristics

The impedance characteristics of the antenna were determined by measuring full 2-port S-parameters of the antenna using an HP 8510 vector network analyser. The antenna was measured in a room partially covered with radar absorbent material with the antenna pointing towards an angled sheet of absorber to prevent reflections from outside sources.

6.2.1 Reflection coefficient

The measured and simulated reflection S-parameters are compared in Figure 6.1.

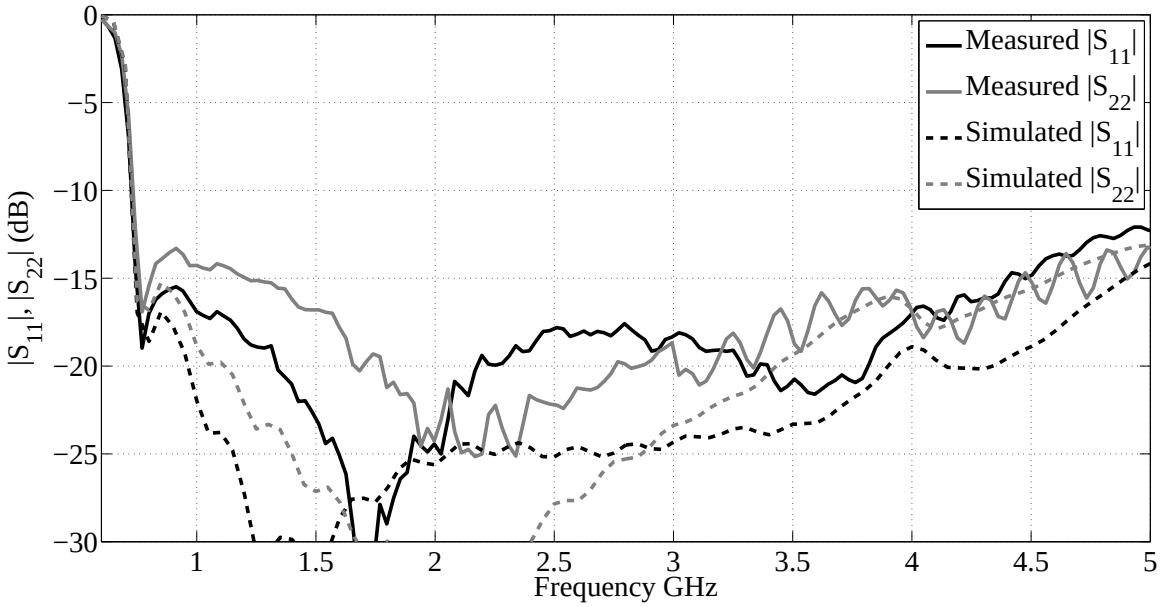

Figure 6.1. A comparison of the measured and simulated reflection S-parameters.

The measured and simulated results agree reasonably well. The measured results did not quite achieve the low predicted reflection coefficient, but followed the same trend as the simulated results. The reflection coefficient of port 1 was better than -15 dB for the 4:1 band while port 2 had a maximum value of -13.3 dB in this band with values significantly below -15 dB for the largest portion of the band. The antenna is also well matched beyond the original 4:1 band (0.75 to 3GHz).

The reflection coefficient measurements showed that the feed region of the antenna – the transition from SMA to air-line dielectric, and the connection of the feed pin to the connector strongly influenced the measurements. Obtaining good positive contact between the feed pin and the connector receptacle was essential to achieving good return loss across the band. Good contact between the sidewall and the connector outer was also required to ensure good return loss. The antenna feed section thus has to be assembled with great care.

The VSWR of the measured and simulated results are compared in Figure 6.2. The agreement between measured and simulated results can be seen clearly from the VSWR. The VSWR is better than 1.5:1 for both ports over most of the band.

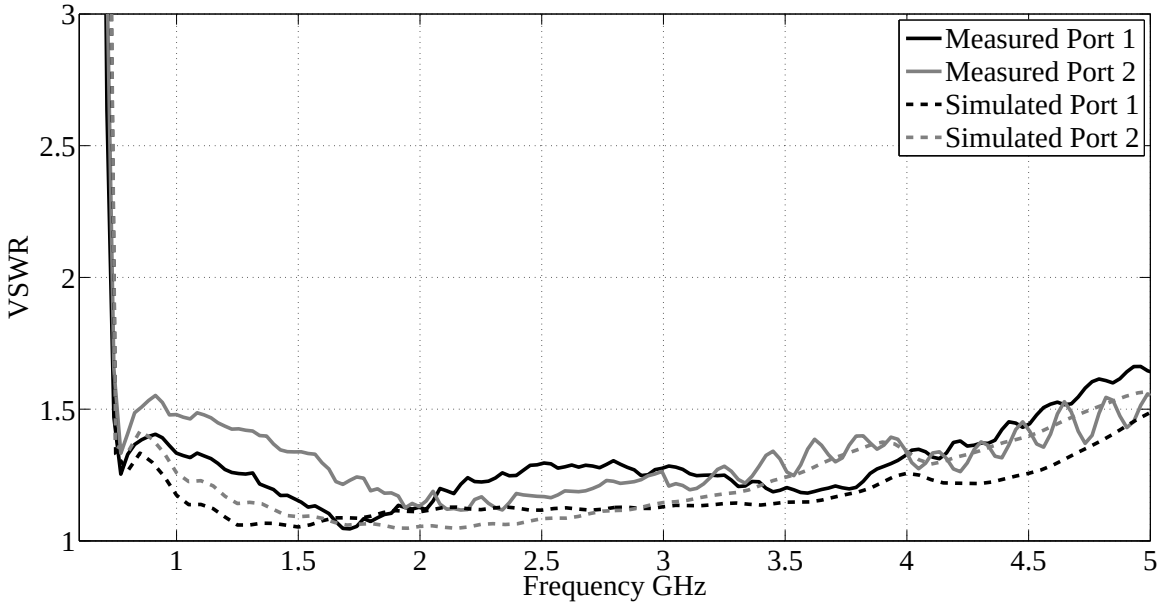

Figure 6.2. A comparison of the measured and simulated VSWR.

6.2.2 Port Isolation

The measured and simulated coupling between the ports is shown in Figure 6.3. The measured isolation between the two ports is better than 30 dB throughout the band. Simulated coupling was significantly less than the measured results. The simulated results assumed a perfectly symmetric antenna. Any asymmetry in the antenna assembly significantly increases the coupling between the two ports.

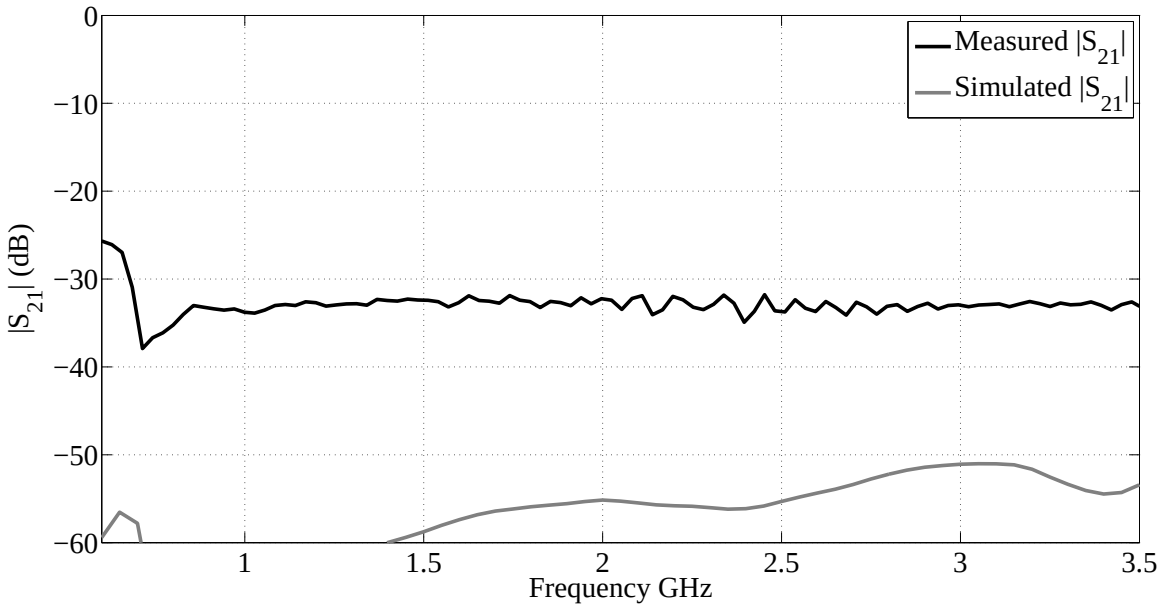

Figure 6.3. The measured coupling between the orthogonal ports.

6.3 Radiation characteristics

The radiation characteristics were measured at two facilities. Low frequency (0.6 to 3 GHz) patterns, boresight gain and cross-polarization were measured in a tapered chamber at Saab Electronics Defence Systems (EDS) while higher frequencies (0.8 to 5.5 GHz) were measured in a compact range at the Centre for Electromagnetism, University of Pretoria.

6.3.1 Gain

The measured boresight gain of the antenna is compared to the simulated gain in Figure 6.4. The measured values were obtained at the compact range and are thus only shown from 0.8 GHz. The measured and simulated gain show good agreement. As the conductive

loss was regarded as small enough to neglect, the simulated directivity is also referred to as the gain of the antenna. Beyond 5 GHz the boresight gain shows a large dip and large variations appear as the radiation patterns deteriorates due to higher order mode propagation. Only a single port is shown for the simulated results as the radiation pattern results of the two ports closely matched each other.

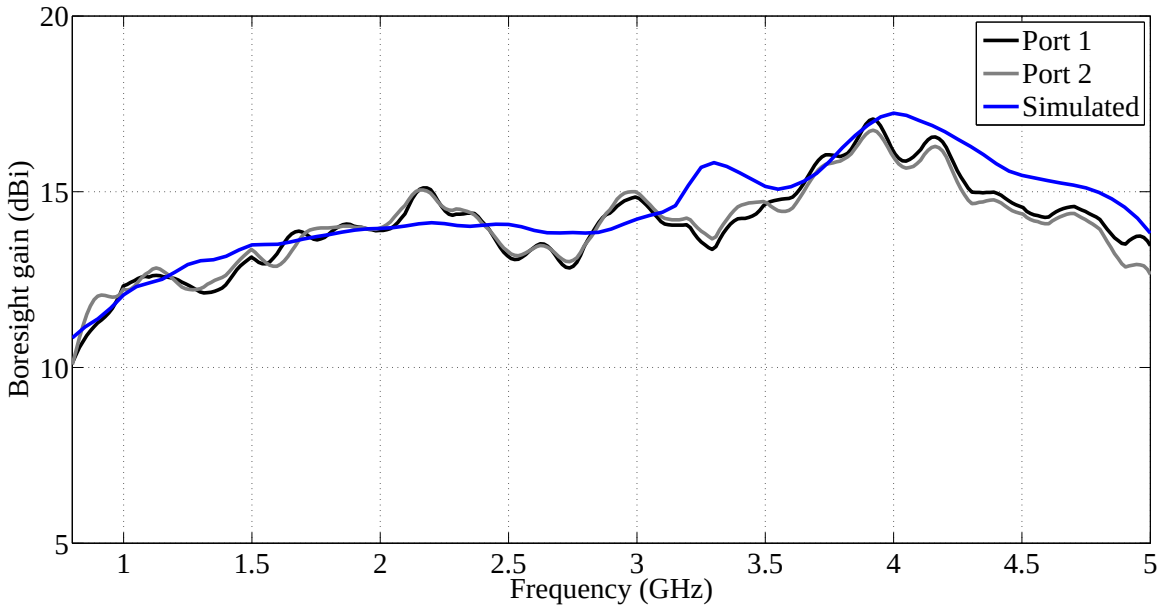

Figure 6.4. A comparison of the measured and simulated boresight gain.

The boresight gain is compared to the cross-polarization in Figure 6.5 from 0.6 GHz to 3 GHz.

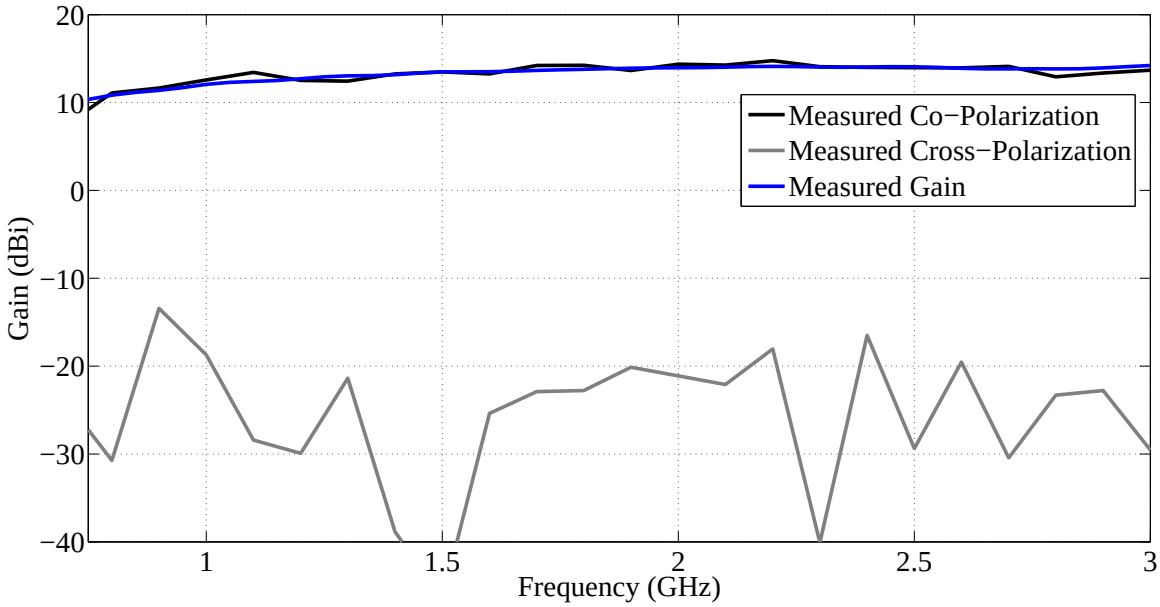

Figure 6.5. Measured boresight gain and cross-polarization.

The measurements indicated a boresight cross-polarization that was typically more than 30 dB down from the boresight gain. The FEKO simulated results obtain lower cross-polarization under the assumption of perfect symmetry. Any asymmetry in the antenna construction can increase the boresight cross-polarization. Cross-polarization levels lower than 30 dB are difficult to measure accurately.

The front-to-back ratio measurements were also done at the tapered range. The front-to-back ratio compares well against the predicted results from the FEKO simulations as shown in Figure 6.6. The front to back ratio is less than -15 dB across the band.

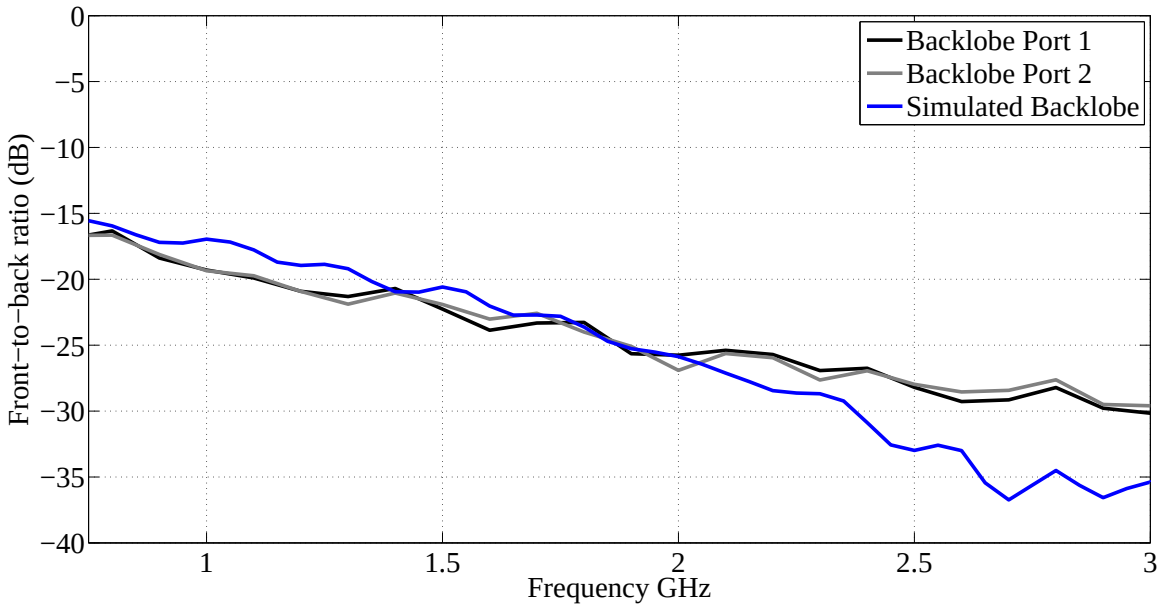

Figure 6.6. A comparison of the measured and simulated front-to-back ratio.

6.3.2 Radiation patterns

The radiation patterns of the antenna are shown for a number of frequencies on the following three pages. As the radiation patterns of the two ports closely matched each other the results are shown only for port 1. The measured principal plane patterns are compared to simulated results. The 45° plane pattern and cross-polarization is also compared to simulated results (the cross-polarization tends to be a maximum in the 45° plane). The measured and simulated radiation patterns of the antenna are shown in Figure 6.7 up to 1.5 GHz.

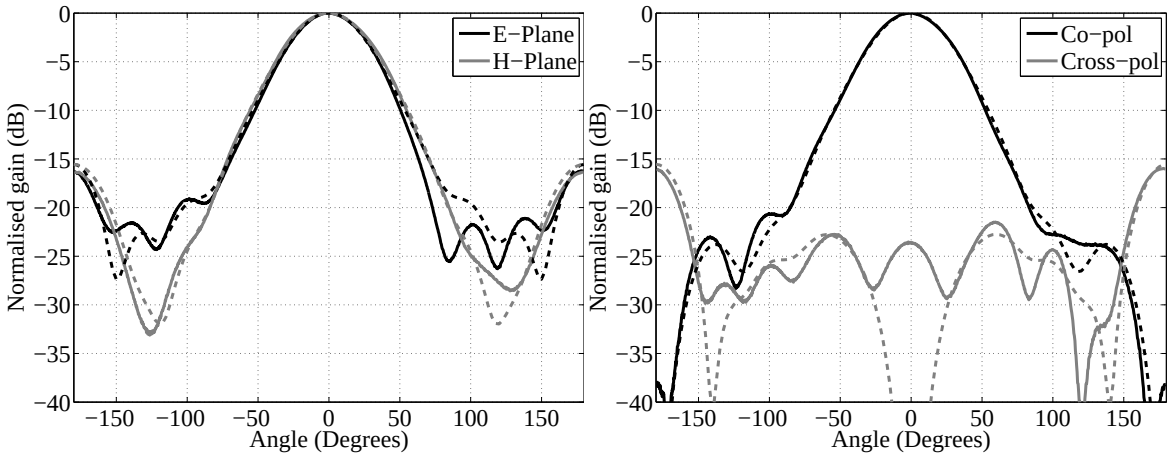

0.75 GHz Elevation and Azimuth 45° Plane Co- and Cross-polarization

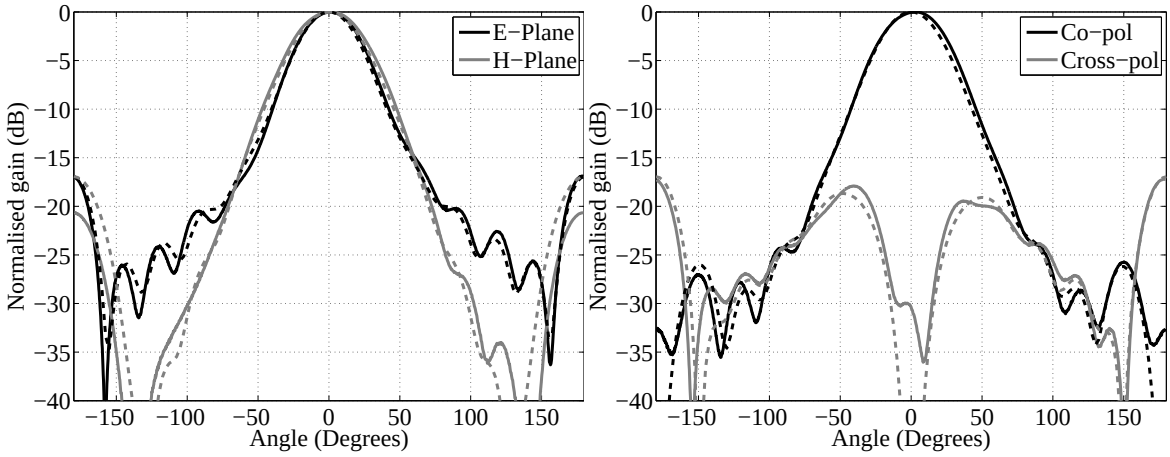

1 GHz Elevation and Azimuth 45° Plane Co- and Cross-polarization

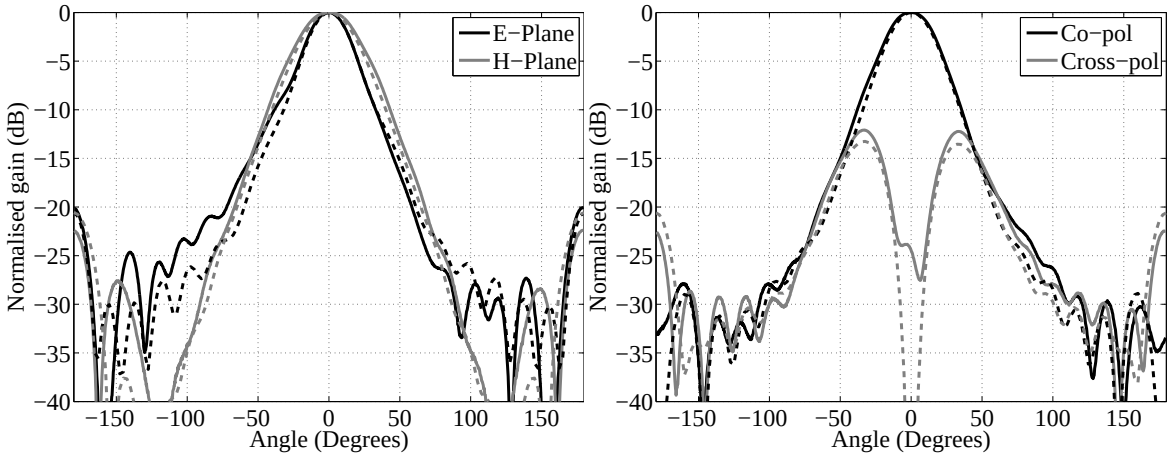

1.5 GHz Elevation and Azimuth 45° Plane Co- and Cross-polarization

Figure 6.7. Radiation patterns of the quad-ridge horn antenna up to 1.5 GHz (Measured: Solid and simulated: Dashed).

The measured and simulated radiation patterns of the antenna up to 3 GHz are shown in Figure 6.8.

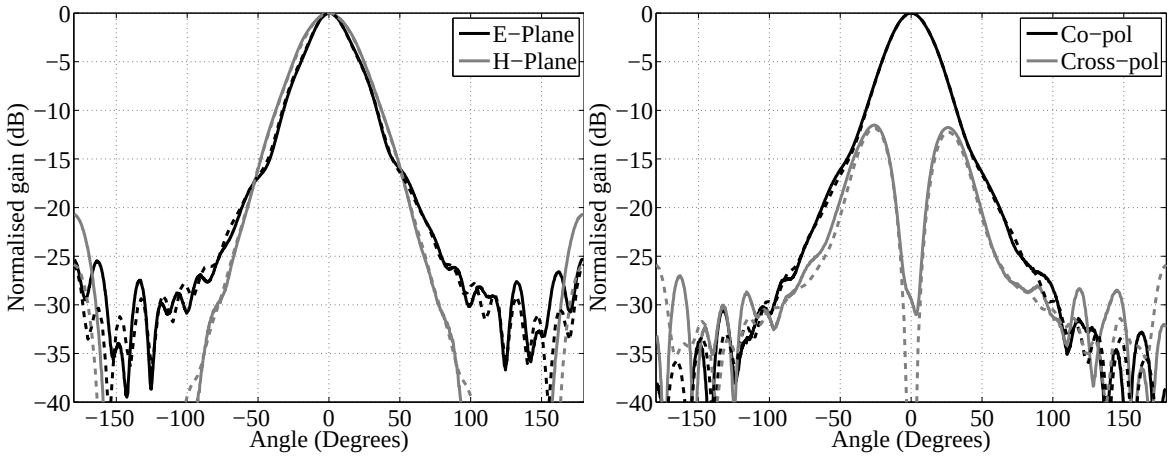

2 GHz Elevation and Azimuth 45° Plane Co- and Cross-polarization

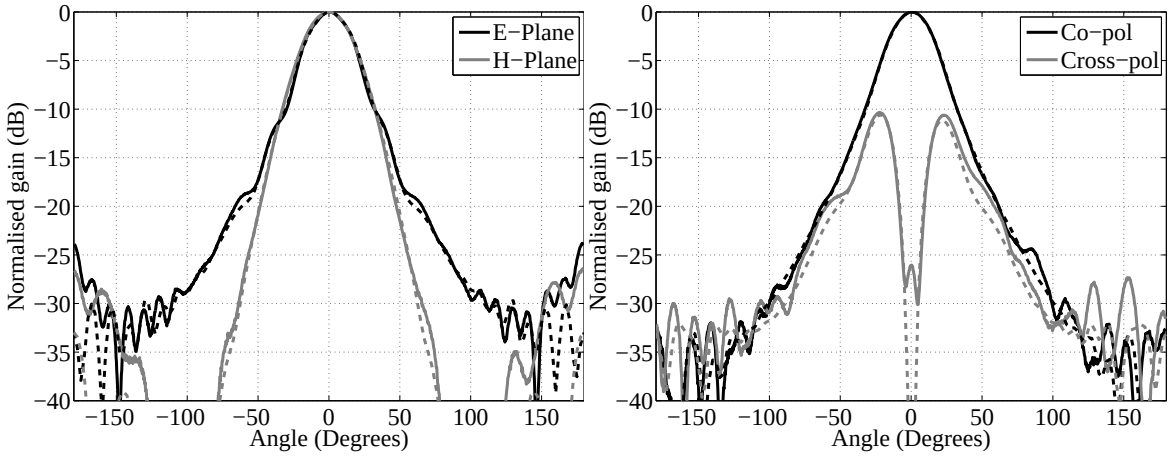

2.5 GHz Elevation and Azimuth 45° Plane Co- and Cross-polarization

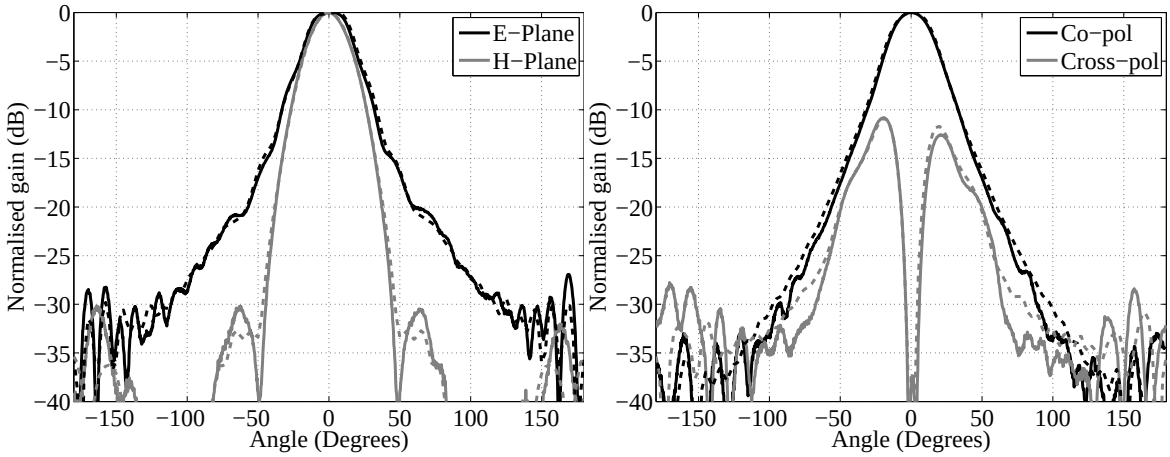

3 GHz Elevation and Azimuth 45° Plane Co- and Cross-polarization

Figure 6.8. Radiation patterns of the quad-ridge horn antenna up to 3 GHz (Measured: Solid and simulated: Dashed).

The measured and simulated radiation patterns of the antenna up to 4.5 GHz are shown in Figure 6.9.

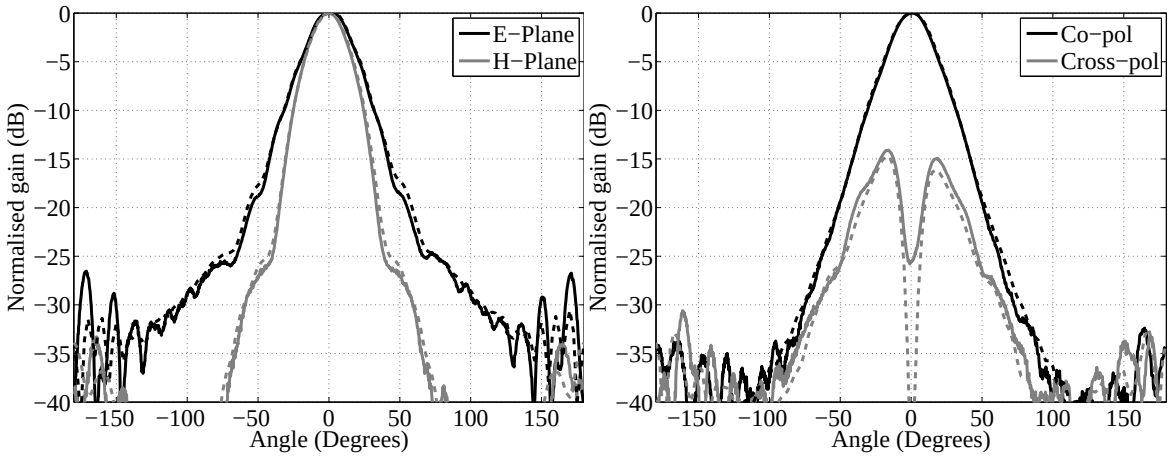

3.5 GHz Elevation and Azimuth 45° Plane Co- and Cross-polarization

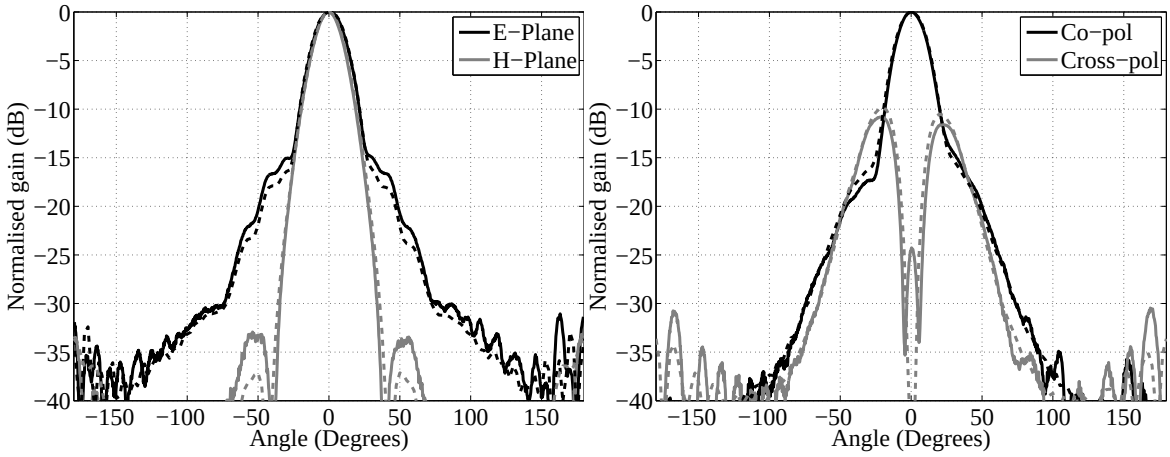

4 GHz Elevation and Azimuth 45° Plane Co- and Cross-polarization

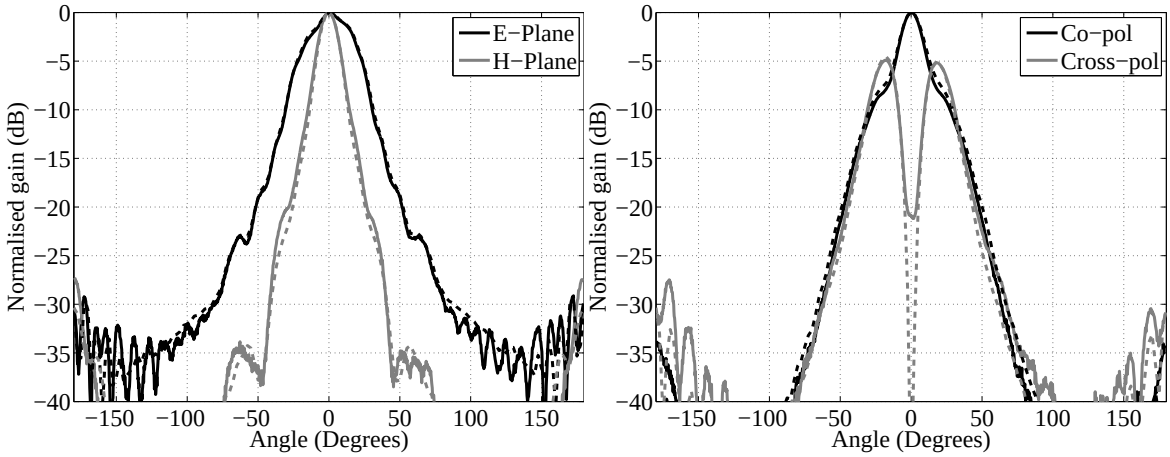

4.5 GHz Elevation and Azimuth 45° Plane Co- and Cross-polarization

Figure 6.9. Radiation patterns of the quad-ridge horn antenna up to 4.5 GHz (Measured: Solid and simulated: Dashed).

It can be seen from these patterns that the measured and simulated results show very good agreement throughout the bandwidth and that the patterns are reasonably constant until it begins to deteriorate at higher frequencies. The patterns are close to being rotationally

symmetrical (the azimuth, elevation and 45° planes patterns match reasonably well). The cross-polarization increases for higher frequencies. The 3 dB beamwidth calculated from these patterns is shown in Figure 6.10. The measured and simulated results compare favourably and are reasonably constant over a wide bandwidth.

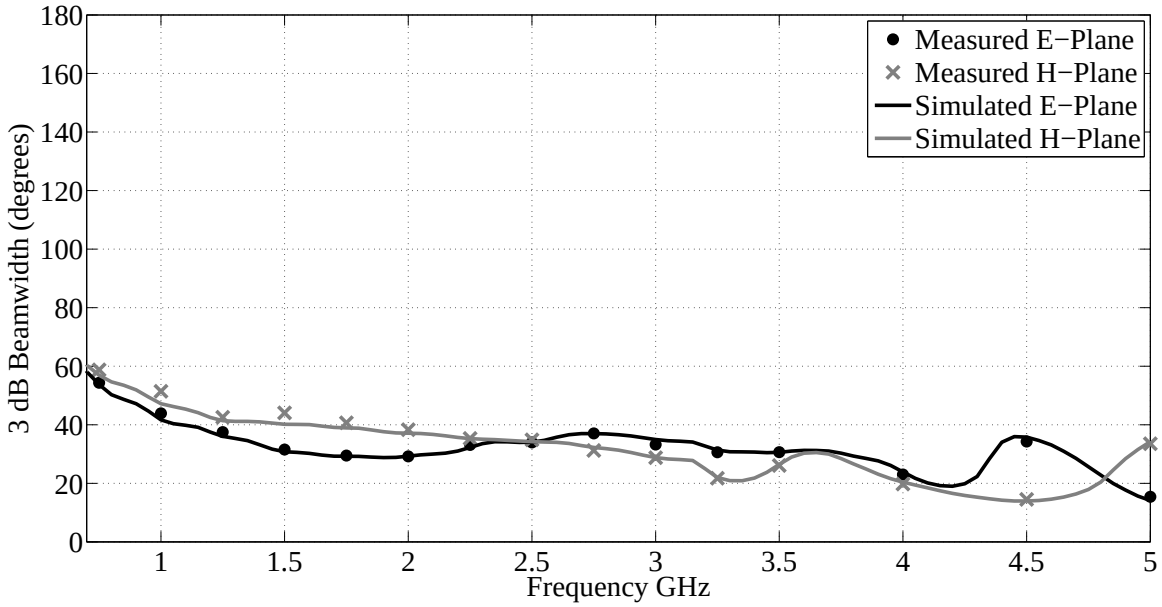

Figure 6.10. A comparison of the measured and simulated 3 dB beamwidth.

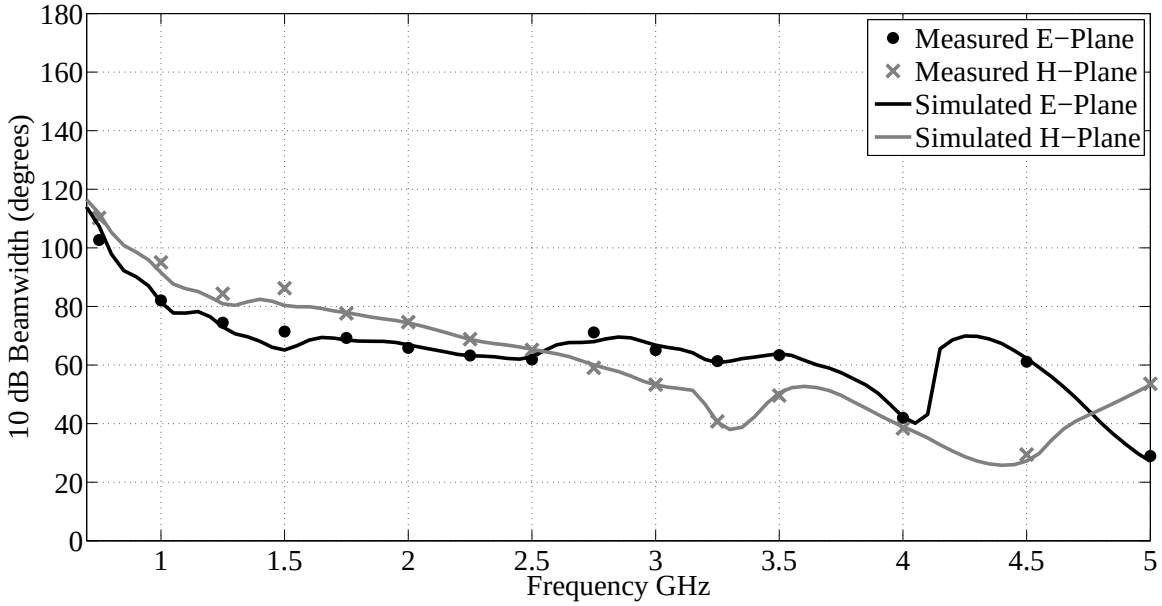

Figure 6.11. A comparison of the measured and simulated 10 dB beamwidth.

This is also true of the 10 dB beamwidth, which is shown in Figure 6.11. The largest beamwidth variation occurs at higher frequencies. The elevation pattern is close to constant

while the azimuth 10 dB beamwidth decreases slightly as a function of frequency. The 45° plane beamwidth falls approximately between the principal plane beamwidths.

The beamwidth and radiation patterns of the antenna limit the bandwidth of the antenna. Even though the antenna is matched over a very wide bandwidth the radiation characteristics limit the practical use of the antenna to approximately 4 GHz, this is a bandwidth of more than 5:1, exceeding the goal of a 4:1 bandwidth.

As a further measure of the rotational symmetry of the antenna the simulated normalized 3D radiation patterns are shown in Figure 6.12. The patterns are aligned such that the E-plane corresponds to the elevation plane of port 1. The patterns are reasonably symmetrical in the main beam, with the H-plane pattern narrowing somewhat at higher frequencies.

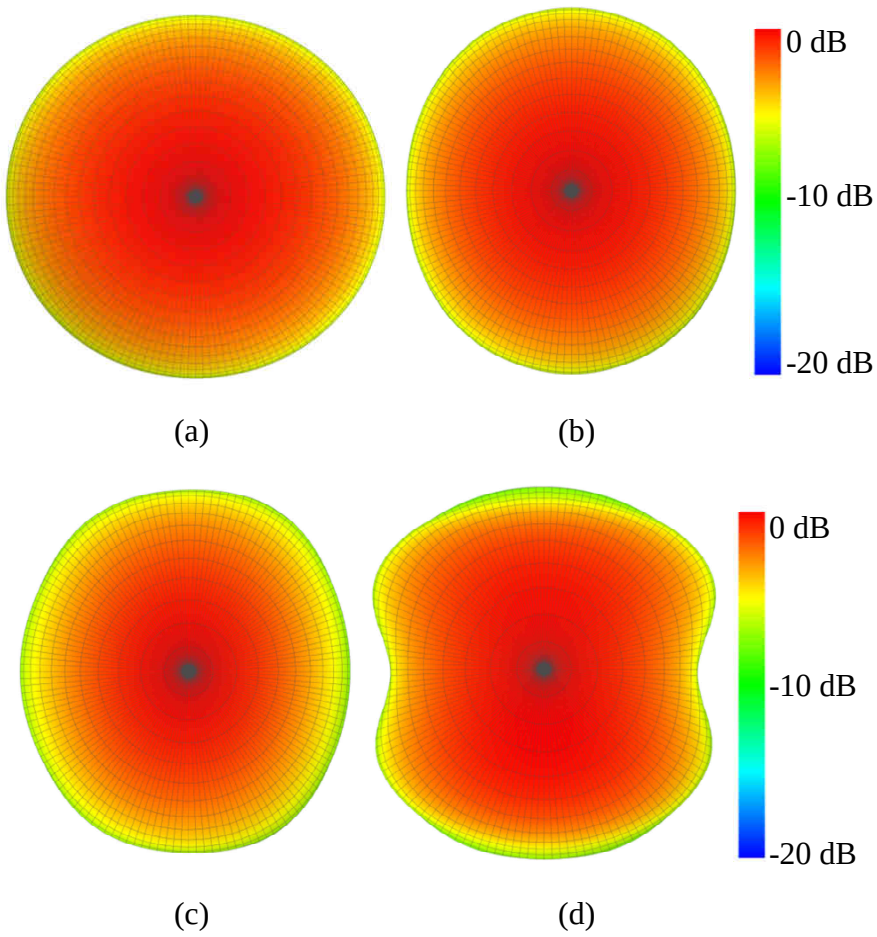

Figure 6.12. Simulated normalized 3D patterns to investigate the rotational symmetry of the antenna, (a) 0.75 GHz, (b) 1 GHz, (c) 2 GHz and (d) 3 GHz.

6.4 Conductive Loss

The conductive loss of the antenna is calculated using FEKO. As the structures are analysed using Method of Moments (MoM), the currents on the surface of the antenna are readily available. As the conductivity of the metal of the antenna is known, the conductive loss of the antenna can be estimated from the surface currents. When a material with finite directivity is specified and the currents output option is selected FEKO also calculates the conductive loss. The accuracy of this calculation was verified by comparing a structure with a known loss to one simulated in FEKO.

A rectangular waveguide was selected to validate the calculation of the loss as the loss can be calculated analytically. A sufficient length of waveguide was simulated to ensure that the loss is large enough to be observed. The waveguide was simulated at 15 GHz (the frequency and length of the waveguide can be scaled). The attenuation due to conductive loss in a section of rectangular waveguide for the TE_{10} mode can be calculated analytically by,

$$\alpha_c = \frac{R_s}{a^3 b\beta k\eta}(2b\pi^2 + a^3k^2) \tag{6.1}$$

where α_c is the attenuation in *Np/m*, R_s is the surface resistance of the waveguide wall, a and b are the width and height of the waveguide walls respectively, β is the propagation constant, η the wave impedance and k the wavenumber [63].

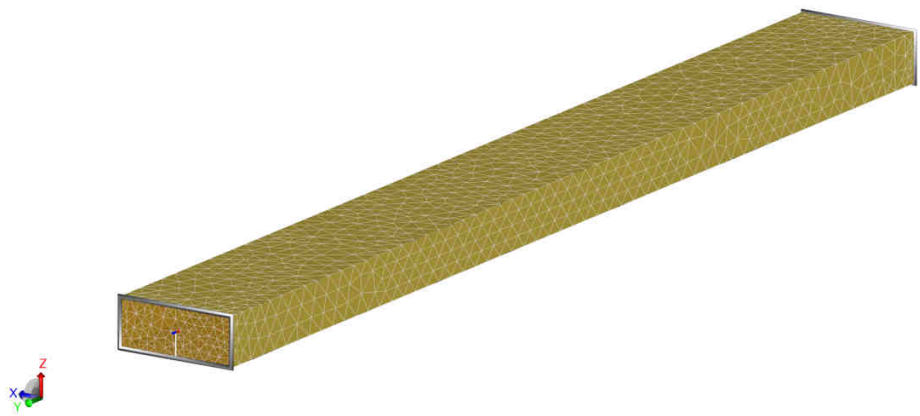

Figure 6.13. The FEKO model of the rectangular waveguide.

Equation 6.1 was used to calculate the attenuation in a section of air-filled waveguide with dimensions a = 10.7 mm and *b* = 4.3 mm at a frequency of 15 GHz. This is above the TE_{10} cut-off frequency of 14.01 GHz but below the next higher order mode cut-off of 28.02 GHz for the TE_{20} mode. The attenuation was calculated to be 0.8153 dB/m.

The FEKO model of the waveguide was filled with free space and fed on either side by a waveguide port as shown in Figure 6.13. The conductivity was set to that of copper – 5.8×10^7. The simulation was at 15 GHz with the waveguide meshed at a tenth of a wavelength, the waveguide was 100 mm long.

The calculation in FEKO obtained a power loss of 0.009385 W in the metallic elements for a source power of 1 W. This corresponds to a loss of 0.041 dB (0.41 dB/m), which is less than the expected loss. This is due to the way in which FEKO calculates the loss – there is an assumption in FEKO that the current is present on both sides of the metallic triangles. For the metallic sidewalls of the waveguide or for the horn antenna – where the electric field is present on only one side of the metal – this assumption is not valid and the loss is under-estimated (it should be noted that the loss calculation will be modified in future releases of FEKO). This assumption can be compensated for by reducing the conductivity of the metal by a factor of four (the power loss is estimated using the currents). Using this updated conductivity in the waveguide model the loss is calculated as 0.018672 W for a 1 W input – a loss of 0.08186 dB or 0.8186 dB/m, very close to the analytical value of 0.8153 dB/m.

This method was used to calculate the conductive loss of the antenna using FEKO. The conductivity was that of aluminium divided by four. The simulated conductive loss as a function of frequency is shown in Figure 6.14. It can be seen that the loss is significantly less than 0.1 dB over the band of interest (although the calculation excluded the effect of the SMA to air-line transition). This loss was regarded as sufficiently low that it could be neglected. The conductive loss would thus not contribute significantly to the noise temperature of the antenna.

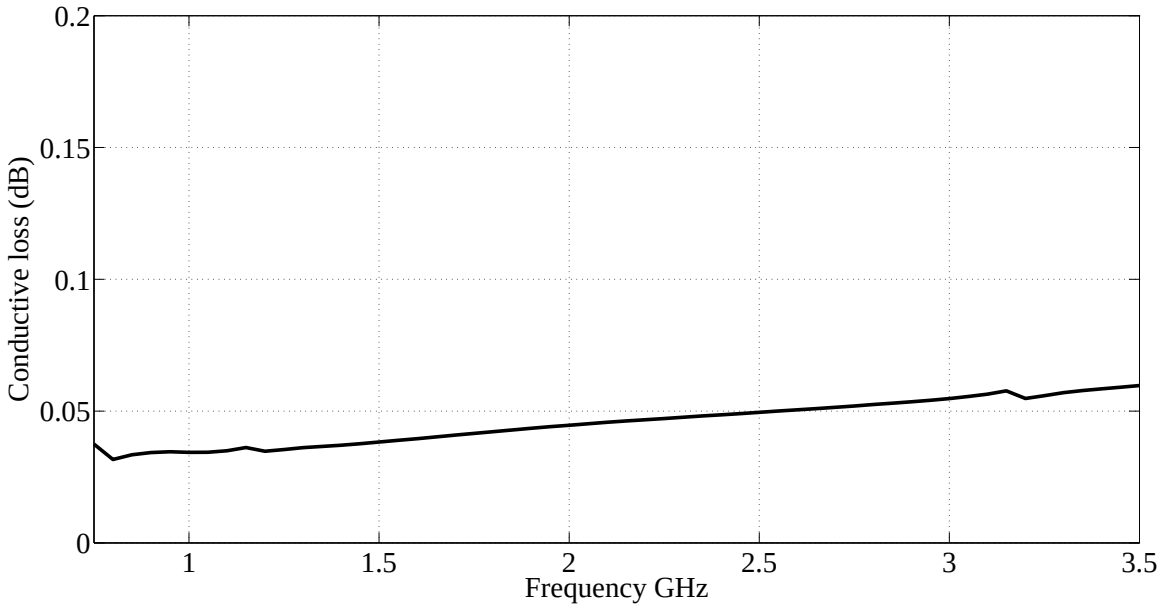

Figure 6.14. The simulated loss of the quad-ridge horn antenna, manufactured from aluminium.

6.5 Performance with a parabolic reflector

The performance of the antenna in a prime focus parabolic reflector is analysed. This is done by calculating the efficiency factors presented in Chapter 2. The antenna was designed for a reflector system with a shaped sub-reflector. Shaped sub-reflectors can improve the efficiency of reflector systems provided the beamwidth remains reasonably constant over the bandwidth. As this reflector system is currently under development the antenna was analysed for a prime focus feed with a half angle (and thus the *F*/*D* ratio) chosen to give high efficiency. This will give a good indication as to how the antenna will perform as a reflector feed. Analysis with a prime focus reflector is also more general than when applied for a specific shaped sub-reflector configuration. The prime focus reflector antenna configuration for which the performance of the feed antenna was evaluated is represented in Figure 6.15.

A half angle of 35° was found to give reasonable high efficiency over the band of interest. This half angle corresponds to an *F/D* ratio of 0.793. A 12 m diameter reflector antenna would thus have a focal point located at 9.515 m from the reflector. The large *F/D* ratio was required for high efficiency as the feed antenna has a very narrow beamwidth. Such a large *F/D* ratio might require a different reflector configuration to realise physically (with an effective focal length), for example a Cassegrain configuration.

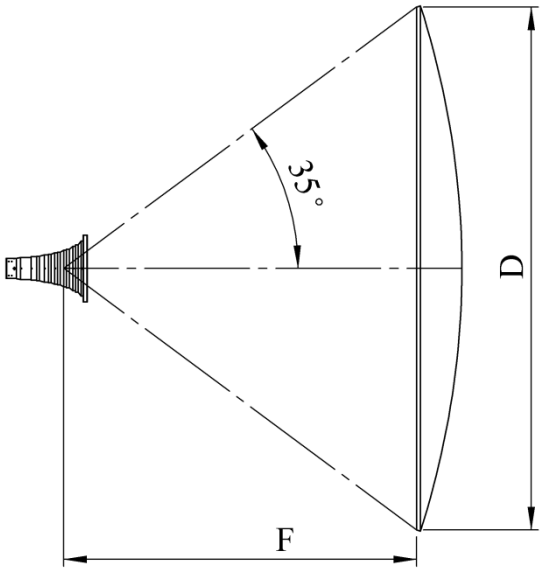

Figure 6.15. The prime focus reflector configuration for the analysis of the efficiency of the quad-ridge horn antenna when used as a reflector feed.

6.5.1 Efficiency calculation

The efficiency calculation was validated by first calculating the efficiency of a radiation pattern for which the efficiency is known. Such a pattern is the $cos^q\theta$ pattern which is often used to analyse reflector antennas as the results can be calculated analytically.

Such a radiation pattern was created in FEKO using EDITFEKO. The pattern is specified directly as a radiation pattern source (using the AR card) over a range of theta and phi angles. The far field is calculated from this $cos^q\theta$ pattern and exported to a .ffe (a far field data format) – the .ffe file is imported into Matlab. The spill-over, taper and illumination efficiencies are calculated from the imported pattern – using the equations below.

$$\eta_s = \frac{\int_0^{2\pi}\int_0^{\theta_0}|F(\theta,\phi)|^2 sin\theta d\theta d\phi}{\int_0^{2\pi}\int_0^{\pi}|F(\theta,\phi)|^2 sin\theta d\theta d\phi} \tag{6.2}$$

$$\eta_t = \frac{16F^2}{\pi D^2}\left(\frac{\left(\int_0^{2\pi}\int_0^{\theta_0}|F(\theta,\phi)|tan\frac{\theta}{2}d\theta d\phi\right)^2}{\int_0^{2\pi}\int_0^{\theta_0}|F(\theta,\phi)|^2 sin\theta d\theta d\,\phi}\right) \tag{6.3}$$

$$\eta_{ap} = \eta_t\eta_s \tag{6.4}$$

This is a special case of the efficiencies that have been discussed in Chapter 2. As the pattern is an ideal, analytically defined pattern it does not have any cross-polarization and has uniform phase. The phase and cross-polarization efficiencies are thus equal to unity and the aperture efficiency consists only of the spill-over and taper efficiencies.

The efficiencies of the $cos^q\theta$ can be expressed in terms of the angle from the reflector axis to the edge of the reflector θ_0. The spill-over efficiency and taper efficiencies can be expressed as below (where the taper efficiency is shown only for the case where q = 2) [3].

$$\eta_s = 1 - cos^{2q+1}\theta_0 \tag{6.5}$$

$$\eta_t = cot^2\frac{\theta_0}{2}\left(40\left[sin^4\frac{\theta_0}{2} + \ln\left(cos\frac{\theta_0}{2}\right)\right]^2\right) \tag{6.6}$$

The edge illumination of the $cos^q\theta$ pattern can be expressed as below.

$$EI = \frac{1 + cos\theta_0}{2}cos^q\theta_0 \tag{6.7}$$

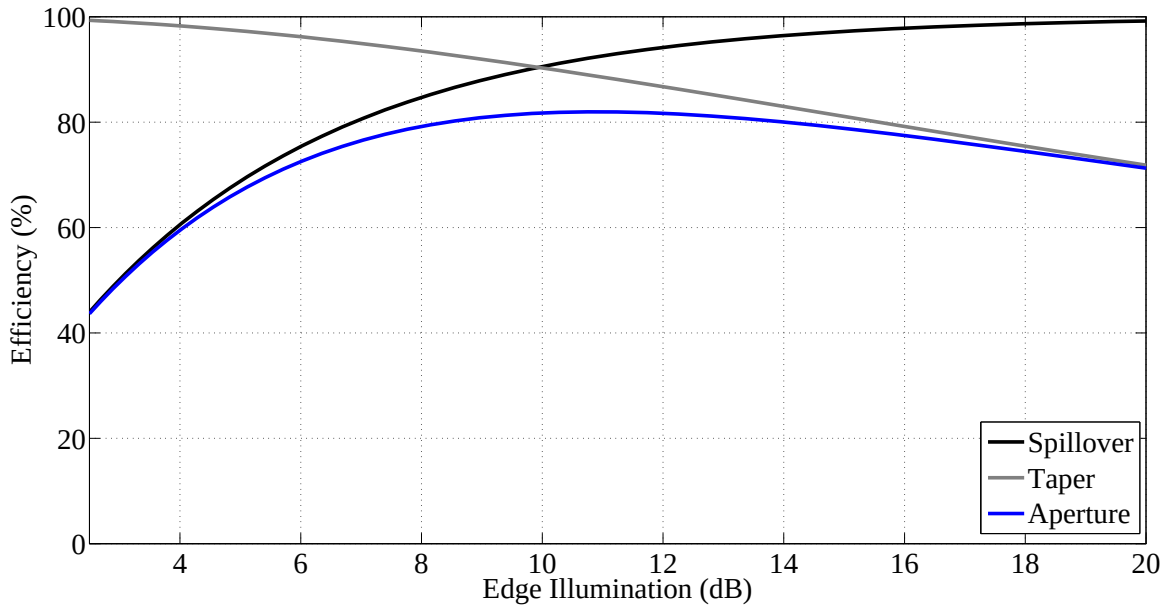

Figure 6.16. Efficiencies for various edge illuminations of the $cos^q\theta$ pattern.

The spill-over, taper and illumination efficiencies calculated using Matlab from the FEKO results can be compared to the values obtained using the analytical equations to validate that the efficiencies are being evaluated correctly. The efficiencies calculated for a $cos^q\theta$

pattern with q = 2 using FEKO and Matlab were nearly identical to the analytical results. Calculated results are shown in Figure 6.16, analytical results, if plotted on the same figure, would be indistinguishable. This validated the approach that was used.

6.5.2 Phase centre position

The determination of the phase centre is required if the antenna is to be correctly positioned in front of the reflector. The phase centre of the antenna was determined by finding the position at which the maximum phase efficiency is obtained for the reflector. The reflector antenna used is the prime focus reflector shown in Figure 6.15. The phase efficiency of the simulated pattern (over the full pattern solid angle) was calculated for a large number of feed positions. The phase reference position of the simulated pattern can be changed using:

$$F_{co-\delta} = F_{co} e^{-jk\delta cos\theta} \tag{6.7}$$

where the pattern with a new phase reference is denoted $F_{co\text{-}\delta}$ the wavenumber is k and the desired phase offset is δ. The position of the pattern's phase reference that resulted in maximum efficiency at each frequency is shown in Figure 6.17. The distance is with reference to the aperture of the antenna with positive distances corresponding to movement further into the antenna (towards the feed pins).

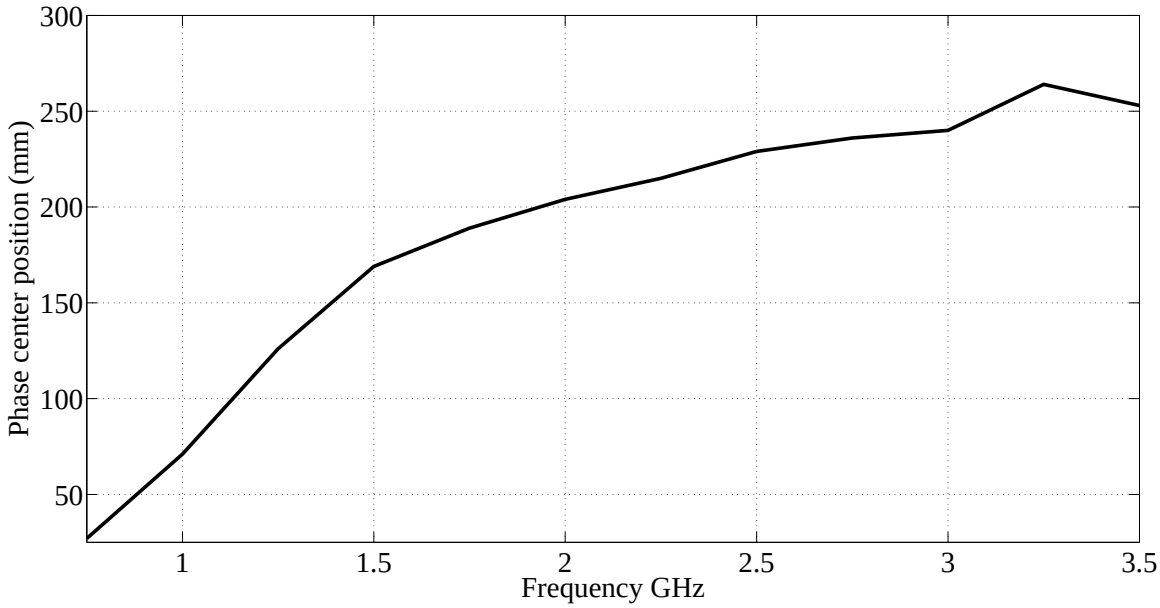

Figure 6.17. The distance of the simulated phase centre of the antenna from the aperture.

The phase centre of the antenna is located close to the aperture at low frequencies and moves into the antenna as the frequency increases. This is typical of horn type antennas. The phase centre is approximately 3 wavelengths from the aperture at 3.5 GHz. High phase efficiency can be obtained by positioning the antenna phase reference not at the aperture, but at a position that results in high phase efficiency throughout the band. The position of the phase reference was found by calculating the maximum average phase efficiency between 0.75 to 3.5 GHz. This maximum average occurred for a phase centre position 227 mm inside the antenna aperture. This calculation was based on patterns for port 1. The feed pin positions, however, differ by only 3 mm (3.5% of a wavelength at 3.5 GHz). The phase centre for maximum efficiency for both ports would thus be at 225.5 mm inside the aperture. At this position the phase centre of the antenna remains within half a wavelength of the position that gives maximum phase efficiency up to at least 3.75 GHz.

Although the phase efficiency is a maximum for only a single position it should be emphasized that reasonably high phase efficiencies can be obtained over a large range of phase reference positions. There is a 200 mm range of phase reference positions for which the mean phase efficiency is larger than 90% (0.75 GHz to 3.5 GHz). This indicates that even though there is phase centre movement the phase efficiency remains reasonably high throughout the band.

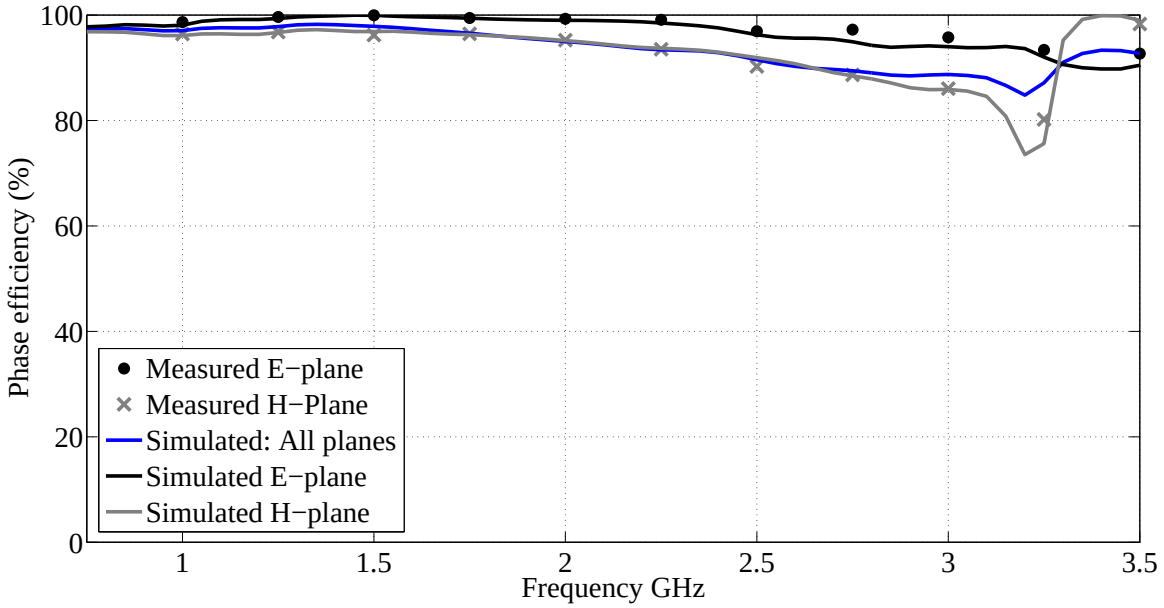

Figure 6.18. Measured phase efficiency compared to simulated efficiency.

The measured phase of the antenna was also compared to the simulated phase to determine the accuracy of the calculation. This was done by calculating the phase efficiency of the measured principal plane patterns and comparing it to the phase efficiency obtained for the simulated principal plane patterns. This comparison is shown in Figure 6.18. The phase efficiency decreases slightly as a function of frequency as the phase taper increases with frequency (the phase is less uniform) and there is some phase centre movement.

The simulated and measured phase efficiency show excellent agreement. The measurements were made with the antenna mounted in a support that placed the phase reference of the antenna close to the centre of mass to ensure stability during measurements. The antenna centre of mass is approximately 215 mm from the aperture (calculated using SolidWorks). The phase reference of the simulated patterns was modified to approximately coincide with the centre of mass. Deviation between the measured and simulated results in Figure 6.18 could thus possibly be due to slight alignment errors. Also shown in Figure 6.18 is the phase efficiency obtained when the full simulated pattern is integrated.

6.5.3 Reflector aperture efficiency

The reflector aperture efficiency is calculated using two methods. The simulated radiation patterns are integrated using the equations presented in Chapter 2. The reflector antenna is also analysed using hybrid Method of Moments – Physical Optics (MoM-PO) and the aperture efficiency of the reflector is calculated from the gain, comparison of the results serves as validation. Integration of the patterns allows the aperture efficiency to be separated into a number of efficiency factors that are detailed below.

- Spill-over efficiency. The power lost due to the part of the feed antenna radiation pattern that does not illuminate the reflector.
- Taper efficiency. The deviation of the feed antenna radiation pattern from a uniform amplitude distribution. Parts of the reflector that are not fully illuminated are under-utilised and cause the efficiency to drop.
- Phase efficiency. The deviation of the feed antenna radiation pattern from an equiphase distribution and defocusing loss due to phase centre variation.

- Cross-polarization efficiency. The power lost due to unwanted cross-polarization incident on the reflector aperture.

The simulated radiation patterns were used to calculate these efficiency factors. Measuring the 3D pattern of an antenna is a very time-consuming process and calculating the efficiency factors for an antenna based solely on the measured principal plane patterns can lead to inaccurate predictions of some efficiency factors, especially cross-polarization efficiency as cross-polarization is a minimum in the principal planes. The patterns are also not strictly rotationally symmetrical. Simulated results for a full pattern solid angle on the other hand can be obtained easily, and as measured and simulated efficiencies (on the principal plane) have shown good agreement, can be used to accurately estimate efficiency factors for radiation patterns that are not strictly rotationally symmetric

The taper efficiency was calculated using the measured principal plane patterns and compared to the simulated efficiency calculated using the same method to verify that using the simulated results would give an accurate estimation of the efficiency. The results are compared in Figure 6.19, also shown is the taper efficiency for the full simulated pattern (4π solid angle).

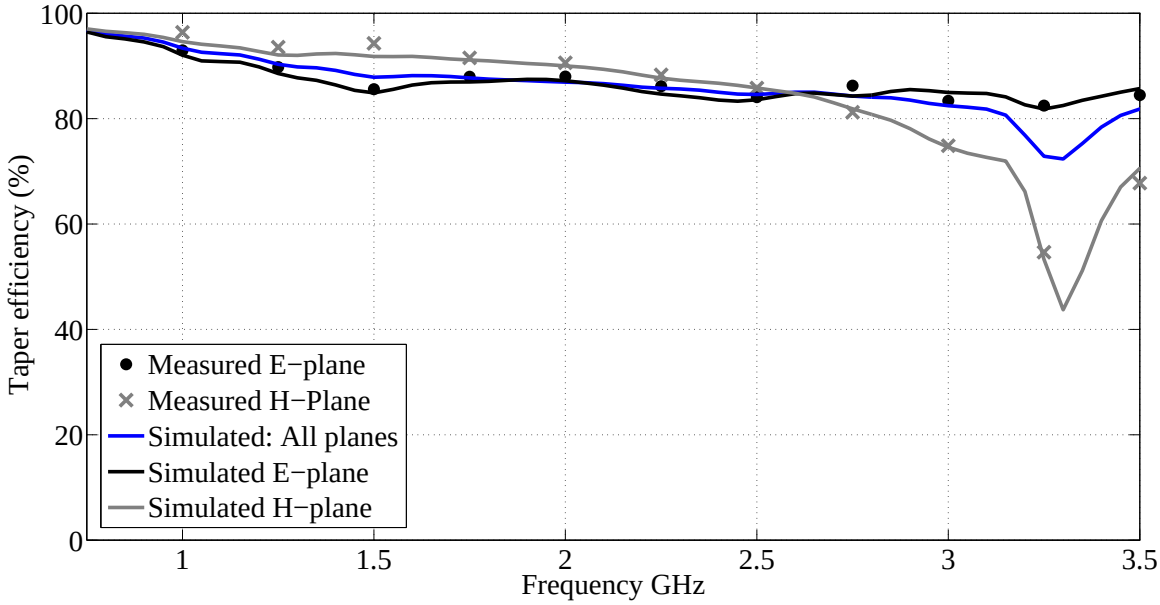

Figure 6.19. Calculated taper efficiency compared to simulated efficiency

It can be seen that excellent agreement is obtained between the measured and simulated results. This indicates that the calculation of the efficiency of the antenna using the simulated patterns would give an accurate estimation of the overall antenna efficiency.

The efficiency factors of the antenna when used as a feed for the 35° prime focus parabolic reflector antenna is shown in Figure 6.20. All four the efficiency factors as well as their product, the aperture efficiency is shown. The efficiency factors calculated from the simulated patterns are also compared to the aperture efficiency calculated using a hybrid MoM-PO approach to validate the calculation.

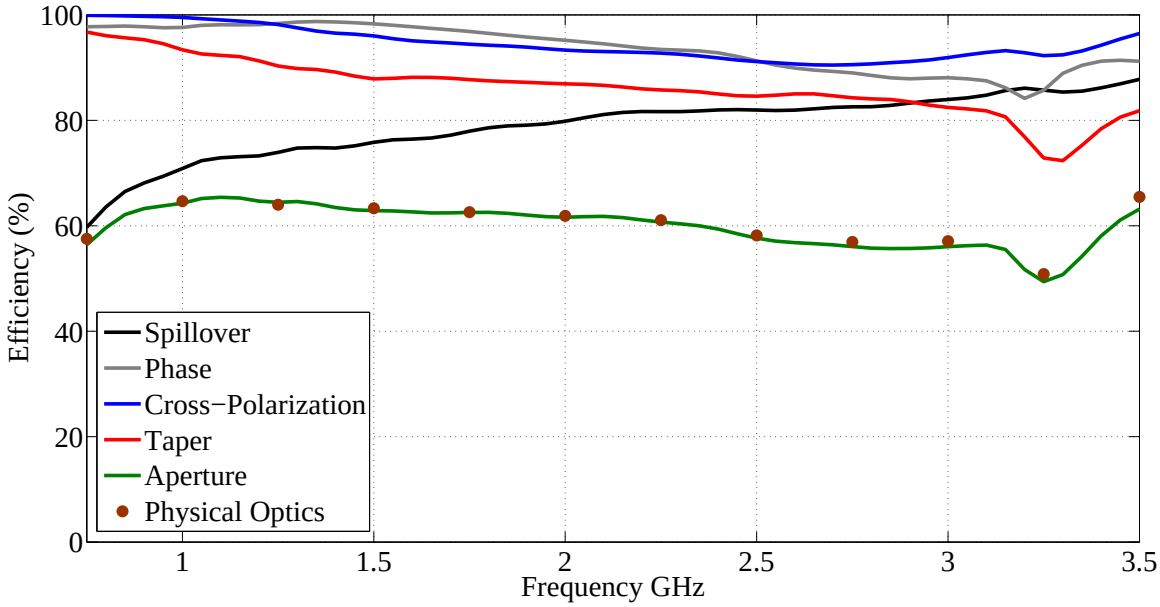

Figure 6.20. Efficiencies of the quad-ridge horn antenna in a 12 m 35° prime focus parabolic reflector antenna compared to a physical optics approximation.

The MoM and PO solutions were decoupled. The aperture efficiency was calculated from the maximum directivity obtained by simulating the feed and reflector antenna combination. It is seen that the aperture efficiencies obtained agrees very well with one another.

The antenna obtains reasonably high aperture efficiency up to approximately 3.5 GHz (larger than 50%) with the efficiency being more than 60% over a large part of the band. Beyond 3.5 GHz the efficiency drops off. The dip in efficiency just after 3 GHz can be seen to be caused by a reduction in taper efficiency. Figure 6.19 shows that this is due to a reduction in the taper efficiency in the H-plane – the radiation pattern in this plane narrows

beyond 3 GHz. The aperture efficiency reduces somewhat at higher frequencies. If only the taper, spill-over and cross-polarization factors are considered the efficiency remains reasonably constant throughout the band. The use of a shaped sub-reflector could result in increased efficiency.

6.6 Summary

The performance of the shaped sidewall quad-ridge horn antenna has been evaluated. The antenna was well matched over a wide bandwidth. The measured and simulated reflection coefficient showed good agreement. Port 1 achieved a reflection coefficient of less than -15 dB (VSWR < 1.405) over a frequency range of 0.75 GHz to 4.4 GHz while port 2 had a maximum reflection of -13.3 dB (VSWR < 1.552) over the same band. Coupling between orthogonal ports was less than 30 dB.

The measured and simulated radiation patterns showed excellent agreement. The beamwidth of the antenna was reasonably constant over the band and the patterns close to rotationally symmetrical. Radiation patterns at a number of frequencies were shown.

The antenna was also evaluated to determine its suitability for use as a reflector antenna feed. The phase centre of the antenna was determined. A position can be identified for the antenna over which the phase centre variation is less than half a wavelength in the frequency band of interest. The antenna is also shown to be able to achieve in excess of 55% aperture efficiency when used as a prime focus reflector antenna feed over a 4:1 bandwidth.

7. CONCLUSION

7.1 General conclusions

The goal of this study was the development of a wideband antenna suitable as a feed for radio astronomy reflector antennas. Radio astronomy reflector antennas require feeds that can give high efficiency and low spill-over over a broad bandwidth. This requires radiation patterns with a constant beamwidth and a sharp cut-off beyond the reflector edge. A quad-ridge horn antenna with elliptically shaped sidewalls was developed that proved capable of achieving these requirements reasonably successfully.

The quad-ridge horn antenna was modelled using Method of Moments (MoM). The antenna model was used to conduct a parametric study that identified parameters of the quad-ridge horn antenna that affected the radiation pattern and how these parameters could be manipulated to obtain radiation patterns more suited for radio astronomy reflector antenna feeds. A quad-ridge horn antenna with elliptically shaped sidewalls was shown to have near constant radiation patterns. The beamwidth of the antenna could be manipulated over a wide range by changing the sidewall parameters.

A quad-ridge horn antenna with elliptically shaped sidewalls was developed for use as a reflector antenna feed using the results of the parametric study. Elliptically shaped sidewall quad-ridge horn antennas were compared to conventional quad-ridge horn antennas and were shown to have radiation patterns that are reasonably constant as a function of frequency, close to being rotationally symmetrical and with low side lobes. A simple design approach has been presented that allows these antennas to be designed for a wide range of beamwidths. The design and mechanical implementation of a prototype antenna was presented.

The performance of the quad-ridge horn antenna with elliptically shaped sidewalls has been comprehensively evaluated. Good agreement between measured and simulated results was obtained for the prototype. The antenna was well matched to the source over a bandwidth exceeding the original goal of 4:1 (0.75 GHz to 4.4 GHz). Good radiation patterns that were reasonably constant and rotationally symmetrical were obtained. Measured co- and cross-polarization radiation patterns in the 45° degree plane have been

presented. Analysis of the antenna with a reflector antenna, using both pattern integration with 3D simulated patterns and Physical Optics (PO) indicated that the antenna would be capable of achieving high aperture efficiencies (larger than 55 %) over at least a 4:1 bandwidth (0.75 GHz to 3 GHz). The variation in phase centre was found to be less than half a wavelength to either side of the phase reference and the conductive loss was calculated to be less than 0.06 dB. The quad-ridge horn antenna was thus successfully developed to be suitable for radio astronomy applications.

7.2 Future research

Possible future work that was identified during the course of this study is detailed below:

- Modifications to the feed of the antenna. The manufacturing of the antenna indicated that this section had a large effect on the impedance characteristics. Careful assembly and design of this section can result in improved impedance characteristics. Using alternative feed pins and connectors could also be investigated.
- Improvement of the back lobe of the antenna. The back lobe at low frequencies of the antenna is relatively high. Modifications to improve this can be investigated. Aperture matching could be used but would increase the size of the antenna. Placing the antenna in a cylindrical housing (with the housing having the same diameter as the antenna) could result in some improvement with little effort or cost.
- Alternative manufacturing, suitable for cryogenic cooling of receivers. Manufacturing techniques suitable for cryogenic cooling of the receiver would have to be investigated for radio astronomy applications.
- Investigation of higher order mode suppression. The bandwidth of the antenna is limited by higher order mode propagation. Suppressing these modes would extend the bandwidth of the antenna.
- Investigation of phase error over the aperture. An investigation into the effect that the shaped sidewalls have on the aperture phase error of quad-ridge horn antennas and how modification to the phase error can be used to improve the radiation patterns.
- Investigate methods to decrease the cross-polarization level in the 45° plane.

REFERENCES

[1] SKA. (2010, March). The Square Kilometer Array: The International Radio Telescope for the 21st Century. [Online]. Available: http://www.skatelescope.org /PDF/brochure/ SKA_Brochure_2009.pdf

[2] G.L. James, "Wideband Feed Systems for Radio Telescopes," *IEEE International Microwave Symposium Digest*, 1992, vol. 3, pp. 1361 – 1363.

[3] W.L. Stutzman and G.A. Thiele, *Antenna Theory and Design*, 2nd ed., Hoboken, NJ: Wiley, 1998.

[4] P.J. Napier, A.R. Thompson and R.D. Ekers, "The very large array: design and performance of a modern radio telescope," *Proc. IEEE*, vol. 71, no. 11, pp. 1295-1322, Nov. 1983.

[5] G. Engargiola, "Non-planar Log-periodic Antenna Feed for Integration with a Cryogenic Microwave Amplifier", *Antennas and Propagation Society International Symposium*, 2002, vol. 4, pp. 140 – 143

[6] J. Welch, D. Backer, L. Blitz, et al, "The Allen Telescope Array: The First Widefield, Panchromatic, Snapshot Radio Camera for Radio Astronomy and SETI," *Proc. IEEE*, vol. 97, no. 8, pp. 1438-1447, Aug. 2009.

[7] R. Olsson, P. Kildal and S. Weinreb, "The Eleven Antenna: A Compact Low-Profile Decade Bandwidth Dual Polarized Feed for Reflector Antennas," *IEEE Trans. Antennas Propag.*, vol. 54, no. 2, pp. 368 – 375, Feb. 2006.

[8] P. Kildal, "Broadband Multi-Dipole Antenna with Frequency Independent Radiation Characteristics," International Patent Publication Number WO 2005/015686, Feb. 17, 2005.

[9] J. Yang, X. Chen, N. Wadefalk and P. Kildal, "Design and Realization of a linearly Polarized Eleven Feed for 1–10 GHz," *IEEE Antennas Wireless Propag. Lett.*, vol. 8, pp. 64 – 68, 2009

[10] J. Yang and P. Kildal, "Optimization of Large Log-Periodic Dual-Dipole Antenna by Using Genetic Algorithm on Embedded Element in Small Log-Periodic Array," *3rd European Conference on Antennas and Propagation*, 2009, pp. 1308 – 1311.

[11] G. Cortés-Medellín, "Novel non planar ultra wide band quasi self-complementary antenna," *Antennas and Propagation Society International Symposium*, 2007, pp. 5733 – 5736.

[12] G. Cortés-Medellín, "Input impedance characterization of the QSC ultra wide band feed," *Antennas and Propagation Society International Symposium*, 2008, pp. 1 – 4.

[13] G. Cortés-Medellín, "Measured Pattern Characteristics and Optics Design with the Ultra Wide Band QSC Feed for the SKA," *Antennas and Propagation Society International Symposium*, Charleston, 2009, pp, 1 – 4.

[14] W.A. Imbriale, S. Weinreb and H. Mani, "Design of a Wideband Radio Telescope," NASA, IPN Progress Report 42 – 168, Feb. 2007.

[15] W.A. Imbriale and A. Akgiray, "Performance of a quad-ridged feed in a wideband Radio Telescope," *Proceedings of the 5th European Conference on Antennas and Propagation*, 2011, pp. 662 – 665.

[16] R.H. DuHamel and D.E. Isbell, "Broadband Logarithmically Periodic Antenna Structures," *IRE International Convention Record*, 1957, vol. 5, no. 1, pp. 119 – 128.

[17] R.B. Dybal, "Defocusing Loss for a Log Periodic-Fed Reflector," *IEEE Trans. Antennas Propag.*, vol. 33, no. 7, pp. 809 – 812, Jul. 1985.

[18] V. Rodriguez, "A multi-octave, open-boundary, quad-ridge horn antenna for use in the S- to Ku-bands," *Microwave Journal*, vol. 49, no. 3, Mar. 2006.

[19] S.J. Skinner and G.L. James, "Wide-band orthomode transducers," *IEEE Trans. Microw. Theory and Tech.*, vol. 39, no. 2, Feb. 1991.

[20] Z. Shen and C. Feng, "A New Dual-Polarized Broadband Horn Antenna," *IEEE Antennas Wireless Propag. Lett.*, vol 4., pp. 270 – 273, 2005.

[21] C.F. Parker and R.J. Anderson, "Constant Beamwidth Broadband Antennas," *IRE International Convention Record*, 1957, vol. 5, pp. 87-98.

[22] M. Gilbert, K. Higgins and L. Romero, "Quad-ridge Horn Utilizing Resistive Films to Reduce Sidelobes," *IEEE Antennas and Propagation Society Int. Symp.*, 2007. pp. 5684-5687.

[23] R.J. Bauerle, R. Schrimpf, E. Gyorko and J. Henderson, "The use of a dielectric lens to improve the efficiency of a dual-polarized quad-ridge horn from 5 to 15 GHz," *IEEE Trans. Antennas Propag.*, vol. 57, no. 6, pp. 1822–1825 June 2009.

[24] J.A.G Malherbe and Y. Katcondia, "An elliptically flared waveguide horn," *Microwave and Optical Technology Letters*, vol. 52, no. 9, Sept. 2010.

[25] J.L. Jonas, "MeerKAT – the South African array with composite dishes and wide-band single pixel feeds," *Proc IEEE*, vol. 97, no. 8, pp. 1522-1530, Aug. 2009.

[26] O.B. Jacobs, J.W. Odendaal and J. Joubert, "Elliptically shaped quad- ridge horn antennas as feed for a reflector," *Antennas Wireless Propag. Lett.*, vol. 10, pp. 756 – 659, Jul. 2011.

[27] G.L. Verschuur, *The Invisible Universe Revealed: The Story of Radio Astronomy*, New York: Springer Verslag, 1987.

[28] J.L. Steinberg and J. Lequeux, *Radio Astronomy*, New York: McGraw-Hill, 1963.

[29] J.L. Spradley, "The First True Radio Telescope", *Sky and Telescope*, vol. 76, no. 1, pp. 28 – 30, Jul. 1988.

[30] IEEE Standard Definitions of Terms for Antennas, IEEE Std 145-1993, 18 March 1993.

[31] M. Arts, R. Maaskant, E. de Lera Acedo and J.G. bij de Vaate, "Broadband differentially fed tapered slot antenna array for radio astronomy applications," *3rd European Conference on Antennas and Propagation*, 2009, pp. 566 – 570.

[32] C.A. Balanis, *Antenna Theory Analysis and Design*, 3rd ed., Hoboken, NJ: Wiley, 2005.

[33] Y. Huang, K. Boyle, *Antennas from Theory to Practice*, United Kingdom: Wiley, 2008.

[34] W.V.T. Rusch, A.P.Y Rahmat-Samii and R.A. Shore, "Derivation and application of the equivalent paraboloid for classical offset Cassegrain and Gregorian antennas," *IEEE Trans. Antennas Propag.*, vol. 38, no. 8, Aug. 1990.

[35] R. Lehmansiek and I.P. Theron, "L-Band Feed Horn and Ortho-Mode Transducer for the Kat-7 Radio Telescope," *IEEE Trans. Antennas Propag.*, vol. 59, no. 6, pp. 1894-1901, Jun. 2011.

[36] P. Kildal, "Factorization of the Feed Efficiency of Paraboloids and Casegrain Antennas," *IEEE Trans. Antennas Propag.*, vol. 33, no. 8, pp. 903 – 908, Aug. 1985.

[37] P. Kildal, S.A. Skyttemyr and A.A. Kishk, "G/T Maximization of a Paraboloidal Reflector Fed by a Dipole-Disk Antenna with Ring by Using the Multiple-Reflection Approach and the Moment Method," *IEEE Trans. Antennas Propag.*, vol. 45, no. 7, pp. 1130 – 1139, Jul. 1997

[38] P. Kildal, "Combined E- and H-Plane Phase Centers of Antenna Feeds," *IEEE Trans. Antennas Propag.*, vol. 31, no. 1, pp. 199 – 202, Jan. 1983.

[39] Y.Y. Hu, "A method for determining phase centers and its application to electromagnetic horns," *Journal of the Franklin Institute*, vol. 271, no. 1, pp. 31-39, Jan. 1961.

[40] P. Kildal and S. A. Skyttemyr, "Dipole-Disk Antenna with Beam-Forming Ring," *IEEE Trans. Antennas Propag.*, vol. 30, no. 4, pp. 529 – 524, Jul. 1982.

[41] P. Kildal, "A Small Dipole-Fed Resonant Reflector Antenna with High-Efficiency, Low Cross Polarization, and Low Side Lobes," *IEEE Trans. Antennas Propag.*, vol. 33, no. 12, pp. 1386 – 1391, Dec. 1985.

[42] K. L. Walton and V. C. Sundberg, "Constant-Beamwidth Antenna Development," *IEEE Trans. Antennas Propag.*, vol. 16, no. 5, pp. 510 – 513, Sept. 1968.

[43] B. M. Thomas, G.L. James and K.J. Greene, "Design of Wide-Band Corrugated Conical Horns for Cassegrain Antennas," *IEEE Trans. Antennas Propag.*, vol. 34, no. 6, pp. 750 – 757, Jun. 1986.

[44] G.L. James, "Design of Wide-Band Compact Corrugated Horns," *IEEE Trans. Antennas Propag.*, vol. 32, no. 10, pp 1134 – 1138, Oct. 1984.

[45] C. Granet, "Profile Options for Feed Horn Design," *Asia-Pacific Microwave Conference*, 2000, pp 1448 – 1451.

[46] R. Lehmansiek and I.P. Theron, "On the design of the feed horns for the Karoo array telescope dish antennas," *Africon*, 2007, pp. 1-5.

[47] W. Sun and C.A. Balanis, "Analysis and design of quadruple-ridged waveguides," *IEEE Trans. Microw. Theory Tech.*, vol. 42, no. 12, Dec. 1994.

[48] D.I.L. de Villiers, P. Meyer and K.D. Palmer, "Broadband offset quad-ridged waveguide orthomode transducer," *Electronics Letters*, vol. 45, no.1, Jan. 2009.

[49] Z. Zhuang, B. Li and Q. Fan, "Design of improved quad-ridged orthomode transducer," *International Conference on Microwave and Millimeter wave technology*, 2010, pp. 867-870.

[50] E. Lier, "A Dielectric Hybrid Mode Antenna Feed: A Simple Alternative to the Corrugated Horn," *IEEE Trans. Antennas Propag.*, vol. 34, no. 1, pp. 21 – 29, Jan. 1986.

[51] P.R. Clark, "Ultra-Wideband Hybrid-mode Feeds," *Electronics Letters*, vol. 31, No. 23, pp. 1968 – 1969, Nov. 1995.

[52] K. Lee, C. Chen and R. Lee, "UWB Dual-Linear Polarization Dielectric Horn Antennas as Reflector Feeds," *IEEE Trans. Antennas Propag.*, vol. 55, no. 3, pp. 798 – 804, Mar. 2007.

[53] M.V. Ivashina, M.N.M. Kehn, P. Kildal and Maaskant, "Decoupling Efficiency of a Wideband Vivaldi Focal Plane Array Feeding a Reflector Antenna," *IEEE Trans. Antennas Propag.*, vol. 57, no. 2, pp. 373 – 382, Feb. 2009.

[54] J.W.M Baars, L.R. D'Addario and A.R. Thomson, "Radio Astronomy in the Early Twenty-First Century," *Proc. IEEE*, vol. 97, no. 8, pp. 1377 – 1381, Aug. 2009.

[55] R. Kindt and R. Pickles, "12-to-l Bandwidth All-Metal Vivaldi Array Element," *Antennas and Propagation Society International Symposium*, 2009, pp 1 – 4.

[56] J.P. Weem and Z. Popovic, "Vivaldi Antenna Arrays for SKA," *Antennas and Propagation Society International Symposium*, 2000, pp 174 – 177.

[57] D. Ericsson, P. Kildal and S. Weinreb, "Study of Efficiencies and Phase Centers of Broadband Log-periodic Feeds for Large Offset Dual-reflector Antennas Using Formulas for Bodies of Revolution (BOR_1 extraction)," *Antennas and Propagation Society International Symposium*, 2003, vol. 1, pp. 241 – 244.

[58] Y. Mushiake, "A Report on Japanese Development of Antennas: From the Yagi-Uda Antenna to Self-Complementary Antennas," *IEEE Antennas Propagat. Mag.*, vol. 46, no. 4, pp 47 – 60, Aug. 2004.

[59] G. Cortés-Medellín, (2007, August), *Wide band Feed Technologies for Arecibo*, [Online]. Available: http://www.naic.edu.

[60] R. S. Gawande, R. F. Bradley, "G/T Sensitivity Comparison of DifferentTopologies Using Ultra Wide Band, Active, Conical Sinuous Antenna," Proceedings of IEEE APSURSI, 2009.

[61] G. Grekou, G. Dubost and A. Madani, "Plane Equiangular 4-Arm Spiral Antenna with Conical Reflector Isolated or Fitted into a Structure," *5th European Microwave Conference*, 1975, pp 116 – 120.

[62] S. Joardar and A. B. Bhattacharya, "Two New Ultra Wideband Dual Polarized Antenna-Feeds Using Planar Log Periodic Antenna and Innovative Frequency Independent Reflectors," *J. of Electromagn. Waves and Appl*, vol. 20, no. 11, pp. 1465 – 1479, 2006.

[63] D.M. Pozar, *Microwave Engineering*, 3rd ed. Hoboken, NJ: Wiley, 2005, pp. 154 – 155.

[64] J.L. Kerr, "Short Axial Length Broad-Band Horns," *IEEE Antennas Propagat.*, vol. 21, no. 5, pp. 710 – 714, Sept. 1973.

[65] C. Bruns, P. Leuchtmann and R. Vahldieck, “Analysis and Simulation of a 1–18-GHz Broadband Double-Ridged Horn Antenna,” *IEEE Trans. Electromagn. Compat.*, vol. 45, no. 1, pp. 55 – 60, Feb. 2003.

[66] B. Jacobs, J.W. Odendaal and J. Joubert, “The effect of manufacturing and assembly tolerances on the performance of double-ridged horn antennas,” *J. of Electromagn Waves and Appl.*, vol. 24, pp. 1279 – 1290, 2010.

[67] J.S. Shimizu, “Octave-bandwidth feed horn for a paraboloid,” *IRE Trans. on Antennas and Progap.*, vol. 9, no. 2, pp. 223-224, Mar. 1961.

[68] H. Lai, R. Franks, D. Kuck and T. Gackstetter, “A broad band high efficient quad ribbed horn,” *Antenna and Propagation Society International Symposium*, Jun. 1987, pp. 676 – 697.

[69] D.B. Davidson, *Computational Electromagnetics for RF and Microwave Engineering*, Cambridge University Press, 2005.

[70] FEKO, Users Manual Suite 6, Sept. 2010. EM Software and Systems, 32 Techno Avenue, Technopark, Stellenbosch, South Africa.

[71] S.B. Cohn, “Properties of ridge wave guide,, *Proceedings of the IRE*, vol. 35, no. 8, pp. 783 – 788, Aug. 1947.

[72] Y. Tao, Z Shen and G. Liu, ”Efficient analysis of quadruple corner cut ridged circular waveguide by hybrid mode-matching boundary element method,” *IEEE Trans. Magnetics*, vol. 43, no.3, pp. 1076 – 1079, Mar. 2009.

[73] F. King, J.S. Yee and D.R. Erbach, “A broadband quadruple-ridged waveguide radiator,” Army Missile Research, Development and Engineering Laboratory, Alabama, RE-74-7, Jun. 1974.

[74] A.R. Mallahzadeh, A.A. Dastranj and F. Karshenas, “Pattern squint elimination for quad-ridged conical and pyramidal horn antennas using bended probes,” *International Journal of RF and Microwave Computer-Aided Engineering*, vol. 20 no. 1, pp. 94 – 102, Jan. 2010.

[75] R. Dehdasht-Heydari, H.R. Hassani and A.R. Mallahzadeh, “A new 2-18 GHz quad-ridged horn antenna,” *Progress in Electromagnetics Research*, vol. 81, pp. 183 – 195, 2008.

[76] R. Dehdasht-Heydari, H.R. Hassani and A.R. Mallahzadeh, “Quad ridged horn antenna for UWB applications,” *Progress in Electromagnetics Research*, vol. 79, pp. 23-38, 2008.

[77] A.R. Mallahzadeh, A.A. Dastranj and S. Akhlagi, "Quad-ridged conical horn antenna for wideband applications," *International Journal of RF and Microwave Computer-Aided Engineering*, vol. 20 no. 1, pp. 519 – 528, Jan. 2010.

[78] J. Qiu, Y. Suo and W. Li, "Design and simulation of ultra-wideband quad-ridged horn antenna," *International Conference on Microwave and Millimetre Wave Technology*, 2007.

[79] K.L. Walton and V.C. Sundberg, "Broadband ridged horn design," *The Microwave Journal*, pp. 96 – 101, Mar. 1964.

[80] J.A.G Malherbe, "Frequency-independent performance of elliptic profile TEM horns," *Microwave and optical technology letters*, vol. 51, no. 3, pp. 607 – 612, Mar. 2009.

[81] D.H. Schaubert, "Wide-band phased arrays of Vivaldi notch antennas," *10th International Conference on Antennas and Propagation*, 1997, pp. 1.6 – 1.12,

[82] K. Liu, "Diagonal dual-polarized broadband horn antenna", United States Patent Number US006489932B2, Dec. 3, 2002.

[83] Huber+Suhner, "Data Sheet Coaxial panel connector: 23_SMA-50-0-167/199_N", Document number: DOC-0000188276I, Oct. 2010.